30.09.2019

Measurements of shipping emissions in the marine troposphere - Phase 2: Further development of remote sensing methods and implementation into an operational network

MeSmarT-II

MeSmarT-II – Final report

BUNDESAMT FÜR SEESCHIFFFAHRT UND HYDROGRAPHIE

Institut für Umweltphysik

Universität Bremen

TABLE OF CONTENTS

Introduction 7

Work Package 1 - Open Path DOAS System 8

Suitability study of Open Path-Differential Absorption Spectroscopy for measurements of SO_2 and NO_2 in ship emission plumes 8

Motivation 8

Campaign description 8

Instrument and retrieval description 8

Exemplary Results from the campaign 14

Conclusions 16

The new airyx open path DOAS system for monitoring shipping emissions 17

Technical Description of the newly developed Open Path DOAS 17

Comparison between Heidelberg Open Path DOAS and airyx Open Path DOAS 19

Results: SO_2/NO_2 ratios 23

Calculation of absolute emission factors for SO_2 and NO_2 from open path DOAS observations 25

Work package 1 summary 29

Work Package 2 – in situ measurements and passive remote sensing 31

In situ observations 31

Quality control 31

Analysis of NO_x emissions 32

Passive Remote Sensing 34

MAX-DOAS Neuwerk: Measurement geometry and acquired database 34

MAX-DOAS Neuwerk: SO_2 / NO_2 ratios in ship plumes 36

MAX-DOAS Neuwerk: onion peeling MAX-DOAS approach 41

O_4 scaling method 41

Onion peeling approach 41

Plume light path geometry 43

Plume trajectories 45

Comparison to airborne imaging DOAS measurements 49

MAX-DOAS Wedel 52
Satellite-DOAS 53
Potential and limitations of satellite observations 54
Summary of satellite measurements of ship emissions in the literature 55
The TROPOMI instrument on Sentinel-5 precursor 56
Some TROPOMI NO_2 results 56
Summary of satellite measurements 58
Work Package 3 – Network for compliance monitoring 60
Transformation to operational FSC Monitoring stations 60
Automation of non-compliant ship identification 60
New Measurement sites 61
Site Assessment 64
Summary and Outlook 66
Work Package 1 66
Work Package 2 66
Work Package 3 66
Outreach 68
Poster presentations 68
Talks 68
Website 69
Peer-reviewed publications 69
PhD, Bachelor and master thesis 70
Bibliography 70
ACKNOWLEDGMENTS 78
Acronyms and abbreviations 79

MEASUREMENTS OF SHIPPING EMISSIONS IN THE MARINE TROPOSPHERE - PHASE 2: FURTHER DEVELOPMENT OF REMOTE SENSING METHODS AND IMPLEMENTATION INTO AN OPERATIONAL NETWORK

MESMART-II

The project **MeSmarT** (***Measurements of shipping emissions in the marine troposphere***) has been established as a cooperation between the **University of Bremen** and the German **Bundesamt für Seeschifffahrt und Hydrographie** (Federal Maritime and Hydrographic Agency, BSH) to estimate the influence of ship emissions on the chemistry of the atmospheric boundary layer and to provide methods for routine emission monitoring of individual ships. It aims to monitor background concentration as well as elevated signals of gases and particles related to ship emissions with various methods to cover a wide range of relevant pollutants and their spatial and seasonal distribution.

This report gives an overview on the results of the second phase of the project: MeSmarT-II (2015 to 2019). Major aims of this phase was the setup of an open path DOAS (active remote sensing) system to monitor emissions of single ships in harbor areas (work package 1), the further development of passive remote sensing and in situ techniques and their retrieval methods (work package 2), and the deployment of an operational network for compliance monitoring (work package 3).

Following authors have contributed to this report:

Lisa Behrens, Lisa Kattner, Barbara Mathieu-Üffing, Kai Krause, Andreas Meier, Sebastian Ochmann, Mareike Ostendorf, Enno Peters, Andreas Richter, Anja Schönhardt, André Seyler, and Folkard Wittrock
Institute of Environmental Physics, University of Bremen

Annika Grage, Simone Griesel, Stefan Schmolke, Andreas Weigelt
Bundesamt für Seeschifffahrt und Hydrographie, Hamburg

Denis Pöhler, Johannes Lampel, Stefan Schmitt
Institute of Environmental Physics, University of Heidelberg

INTRODUCTION

Over the last decades, there has been a strong increase in ship traffic and shipping emissions of gas-phase and particulate pollutants. The total global transport work by ships (in ton miles) has been tripled since the mid-1980s (Smith et al., 2014), corresponding to an average growth rate of 4 % p.a.. But at least in case of Sulphur and NOx emissions there was a reduction in their land sources in much of Europe (EEA report, No. 08/2019). This has led to an increasing relative contribution of shipping emissions to air pollution particularly in coastal regions. Consequently, emission reduction measures have been introduced by the International Maritime Organization (IMO) in the International Convention for the Prevention of Pollution from Ships (MARPOL 73/78 Annex VI) globally as well as, more stringently, locally in so-called emission control areas (ECAs) like the North and Baltic seas (IMO, 2009). To reduce sulfur oxide (SOx) emissions, at the time of the project MeSmarT phase I, the allowed sulfur content in shipping fuel is limited to 0.10 % m/m in ECAs (since 2015, before it was 1.0 % m/m) and to 3.5 % m/m globally, which is reduced to 0.50 % m/m by 2020. For NOx , the allowed emission rate depends on the rated rotational speed of the engine crankshaft (engine power and fuel efficiency) and is implemented in three different levels (Tiers): Tier I (globally) for ships keel laid between 2000 and 2010, Tier II (globally) for ships keel laid from 2011 onwards, and Tier III (locally in ECAs) for ships keel laid from 2016 onwards, with the last one not yet implemented in the North and Baltic seas, but shifted to 2021 (IMO, 2017). In order to monitor the effectiveness of these measures as well as the overall impact of ship emissions on air quality, measurements of air pollution from ships are required. These measurements have been introduced in Germany with the project MeSmarT-I in 2013. MeSmarT-II is the follow-up developing new methods to monitor and quantify shipping emissions as well as to develop an effective operational method to support the prosecution of violations according MARPOL VI. This report summarizes the findings of this project.

WORK PACKAGE 1 - OPEN PATH DOAS SYSTEM

MAIN AUTHORS: KAI KRAUSE, STEFAN SCHMITT, FOLKARD WITTROCK

SUITABILITY STUDY OF OPEN PATH-DIFFERENTIAL ABSORPTION SPECTROSCOPY FOR MEASUREMENTS OF SO_2 AND NO_2 IN SHIP EMISSION PLUMES

MOTIVATION

Within MeSMarT, ship emissions have been monitored since 2013 by using in situ and passive remote sensing instruments. While in situ measurements rely on favorable wind conditions to identify emission peaks from ships (Kattner et al. (2015)), passive remote sensing instruments (MAX-DOAS) have a limited sensitivity to SO_2 in particular in wintertime, since the absorption of SO_2 takes place in the UV, where only a few scattered photons are available in particular for high solar zenith angles (see e.g. report on MeSmarT-I). Moreover, passive remote sensing instruments cannot measure during night and twilight, because of the missing light source (sun).

Similar to MAX-DOAS, the long path or open path DOAS (LP- or OP-DOAS) technique exploits the unique spectral absorption of molecules to retrieve their volume mixing ratios in the atmosphere. Practically, this is accomplished by coupling the light of an artificial light source, here a laser driven xenon arc lamp, into a telescope and sending it through the atmosphere on a mirror. The mirror, a so-called retro reflector, reflects it back to the telescope where it gets analyzed by a spectrometer. By knowing the spectrum of the used lamp, the spectral analysis of the reflected light yields absorption features of trace gases and therefore averaged mixing ratios along the measurement path. Thus, like for other DOAS techniques a wide range of trace gases like NO_2, O_3, SO_2 and HCHO can be detected simultaneously.

The OP-DOAS technique represents a promising complement to the MeSmarT project. By using an artificial light source which provides high intensities in the UV, SO_2 can be measured with high precision and time resolution. Due to the measurement geometry of open path DOAS, emission peaks can be directly assigned to specific ships. In contrast to MAX-DOAS, measurements are also provided during nighttime.

CAMPAIGN DESCRIPTION

Within a six-week measurement campaign in July and August 2016, ship emissions were measured in Wedel, Hamburg using the OP-DOAS technique. For the campaign a scientific instrument was set up by the IUP Heidelberg. In total, signatures of more than 5000 passing ships were measured during this time. A software algorithm was developed to merge the OP-DOAS data with AIS data to assign measured NO_2 and SO_2 peaks to individual ships. The measurements serve as a feasibility study of the OP-DOAS technique to monitor emission plumes of individual ships.

INSTRUMENT AND RETRIEVAL DESCRIPTION

A detailed description of the IUP Heidelberg OP-DOAS instrument and the general trace gas retrieval is given in the report by Stefan Schmitt (2017). Briefly the OP-DOAS instrument which was used for the measurements is based on optical fibers, described by Merten (2008). The telescope unit consists of a single spherical mirror and a fused silica Y-fiber bundle. The main hardware components are listed in table 1. The light of a laser-driven xenon arc lamp is focused on a single fused silica optical fiber. This 200 µm fiber is part of a multifiber bundle consisting of six additional single fibers with 200 µm diameter arranged in a circular way around the center fiber in which the light of the lamp is coupled in. The seven-fibered end is positioned near the focal point of the telescope mirror. The mirror parallelizes the light and sends it through the atmosphere to a retro reflector array. The light is reflected back to the telescopes mirror and focused on the circle of six 200 µm fibers, which are coupled to a big 800 µm fiber bringing the light into the spectrometer for spectral analysis.

The OP-DOAS data was acquired using the software COS developed at the Institute for Environmental Physics, Heidelberg. One measurement sequence consists of 1 lamp reference spectrum followed by 4 blocks of 32 atmospheric spectra and one atmospheric background spectrum each. Prior to each run the exposure time for each single spectrum was adapted to a fixed saturation to account for changing meteorological conditions. The time resolution was around 1 second. Between the measurement sequences the software checks, whether sufficient intensity is received. At insufficient intensity the alignment of the telescope is optimized with respect to received intensity using stepper motors.

The OP-DOAS instrument was positioned close to the other equipment (Figure 1-2). All components of the instrument were placed inside a sea container. The height of the telescope was approximately 7 meters above water level. The retro reflector of the OP- DOAS instrument was mounted at a light house in Lühe at the southern coastline of the river at an altitude of approximately 35 m above water level. The distance between instrument and reflector was measured with GPS to be 2.87 km leading to a total absorption path of 5.74 km (Figure 1-1).

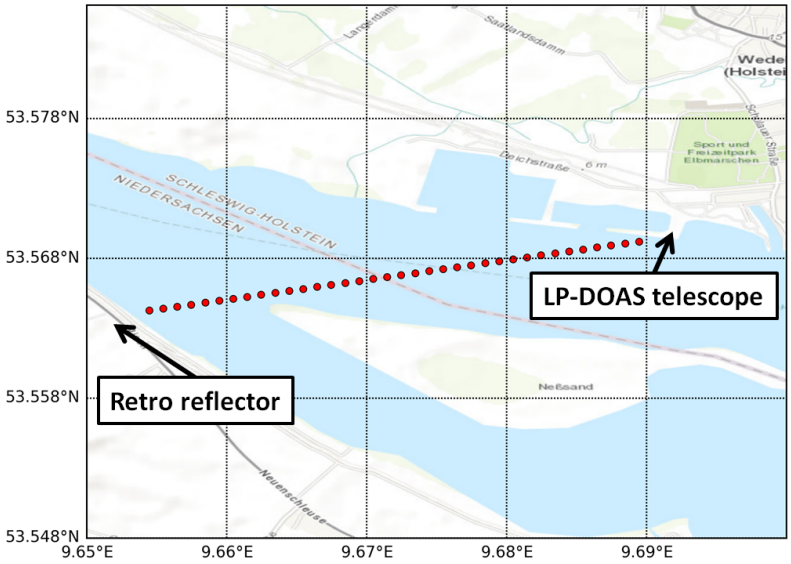

Figure 1-1: Geometry of the OP-DOAS measurement setup at Wedel. The red dots represent the light path across the Elbe river. Telescope and mirror are positioned at the northern and southern end of the light path, respectively. Basemap taken from arcGIS (courtesy by Esri).

Figure 1-2: Left: View from retro reflector on the light house towards the measurement site in Wedel. Middle: Light house at Lühe with mounted retro reflector. Right: The container which inhibited the OP-DOAS instrument next to the weather station and the in situ instruments.

The OP-DOAS data was analyzed using the software DOASIS developed at the Institute or Environmental Physics Heidelberg by Kraus (2006). The wavelength calibration was done using a spectrum of a mercury lamp which were recorded at the beginning and at the end of the measurement period. Additionally, the calibrated mercury lamp spectrum was fine-tuned by performing a Fraunhofer calibration on a recorded atmospheric background spectrum using a convoluted high-resolution solar spectrum by Chance and Kurucz (2010). To adapt high spectral resolution of the reference absorption cross sections to the resolution of the OP-DOAS spectrometer, a convolution with the mercury peaks at 296.7 nm and 334.5 nm is performed for the SO_2 and NO_2 retrieval, respectively. The measured atmospheric and lamp spectra were corrected with their corresponding background spectra. Since the background spectra were recorded with the same conditions as the atmospheric spectra (same exposure time and number of scans), the background correction also corrects for detector offset and dark current signal. Optical densities were calculated using the atmospheric spectra and the single

lamp spectrum from each measurement sequence. After applying a high pass filter to both the optical density and the convoluted absorption cross sections, the DOAS fit is applied. Two different fit windows are used to retrieve SO_2 and NO_2 with wavelength ranges optimized with respect to the corresponding absorption strength. Assuming that the DOAS fit respects all necessary fit constituents, the RMS signal is dominated mainly by photon and instrument noise. Filtering the data with respect to intensity, results in a RMS cutoff of about 1.2e-3 for the SO_2 retrieval and 9e-4 for the NO_2 retrieval. The detection limit for SO2 and NO_2 is defined as twice the DOAS fit error (2 σ). Applying the RMS filtering described above yields a median detection limit of 77 ppt_v and 427 ppt_v for SO_2 and NO_2, respectively.

To identify trace gas peaks in the OP-DOAS data and to assign those peaks to single ships, OP-DOAS and AIS data are processed using a software written in Python. The software was used to re-sample the OP-DOAS to constant time resolution of one second, which was achieved by interpolation (Phython/Pandas "interpolate" function). Further, the AIS data was reduced by filtering with respect to distance between ships and OP-DOAS instrument and finally binned to a single data point for each ship. After filtering the OP-DOAS data with respect to changing light intensity e.g. due to bad viewing conditions to exclude bad data points, the algorithm identifies and assigns trace gas peaks to single ships.

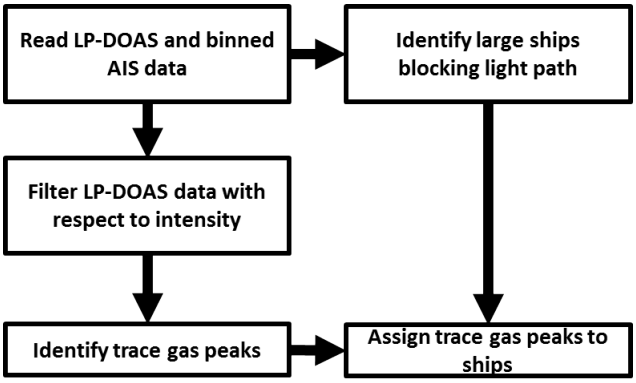

Figure 1-3: Scheme of the filter operations applied on the data set to assign trace gas peaks to ship emission plumes.

Depending on their course and speed, ships send AIS information in short intervals of a few seconds. Thus, a single ship is described by multiple data points while approaching and passing the measurement path of the OP-DOAS instrument. To obtain the exact time the ship passes the light path and to assign potential increases in observed trace gas concentrations to a specific ship, the AIS data has been processed. First, all data with speed equal zero is removed from the data set to exclude moored or stationary ships. Further, the distance between ships and the light path of the OP-DOAS instrument is calculated using the ship coordinates from the AIS data. The position of the light path is approximated by a set of coordinates in intervals of 0.001 degrees between the positions of the telescope and the retro reflector. The distance between ship and light path is then defined by the minimum of the distances between the ship and all points representing the light path. In the next step all AIS data points with a distance to the light path larger than 100 m are removed. With an average ship speed between 3 and 10 m/s, ships are near the light path for 20 to 60 seconds. Since AIS

data is sent with in periods of 2 to 10 seconds, a single ship passing the light path is represented by multiple AIS data points. To correlate single ship passing events with the OP-DOAS data, the AIS data is binned with respect to the ship name to obtain only one single data point per passing ship. Therefore, the timestamps and coordinates from the AIS data points from a single ship passing the OP-DOAS instrument are averaged. To exclude averaging over regularly passing ships (e.g. ferries which pass multiple times a day) the time window for binning AIS data is restricted to 15 minutes.

To identify the trace gas peaks, a smoothed copy of the trace gas data is created using a running mean with a window size of 300 seconds. It is crucial that the window size is chosen in a way that diurnal variations of ambient pollution and meteorological induced variations (in the range of hours to minutes) are still resolved and not lost during the smoothing. Further, the smoothing window must be large compared to fast variations caused by ship emissions, which are usually in the order of a few seconds. All trace gas concentration data whose difference between original time series and smoothed time series is smaller than the corresponding detection limit (which is defined as two times the DOAS fit error) was defined as "trace gas background". It represents the ambient trace gas abundance which is influenced by old, diluted ship plumes or emissions from motor traffic near the riverside or industry and has a smooth temporal behavior. To close the gaps caused by the threshold criteria, the background data is linearly interpolated. All data with a difference to the background larger than the corresponding detection limit are defined as trace gas peaks. Finally, the absolute strength of the trace gas peaks is calculated by subtracting the interpolated background from the peak values.

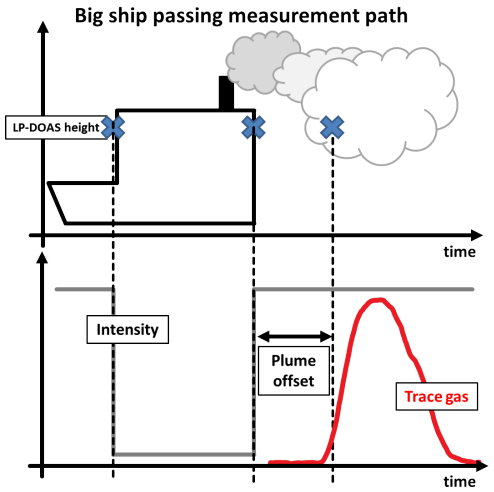

Figure 1-4: Example of a big ship passing and blocking the light path (blue crosses) leading to a drop in intensity (gray curve). Since the measurement path is below the exhaust, emission plumes may be detected with a temporal offset and temporally smoothed (red curve) compared to smaller ships.

Due to the relatively low height of the light path (approximately 10 m above the water surface at the position of the main shipping channel), large ships block the light path resulting in sharp and strong decreases in relative intensity. Usually the exhaust pipes are positioned on top of ships. Besides the impact of wind direction and wind speed, the position of the exhaust pipe

may lead to different trace gas signatures for small and large ships. Therefore, plumes of large ships may be observed with temporally smoothed slopes and with a time delay with respect to the time they cross the measurement path. This time-delay is assumed to be influenced by turbulence caused by the ship itself as well as wind direction and speed. By knowing if a ship blocks the light path, the algorithm to assign trace gas peaks to single ships can be optimized by adjusting the size and the offset of a valid time window close to a ship pass. To identify ships blocking the light path, the time series of the OP-DOAS measurement intensity is compared with a temporally smoothed copy of itself. The intensity drops were identified and assigned to large ships passing the measurement path by correlation with AIS data. The allowed time window, in which intensity dips were assigned to a ship is calculated for each individual ship by dividing its length in meter by its speed (equal to the time the ship passes the light path). The absolute temporal position of the time window is defined by the averaged AIS time stamp. For example, for a ship of 300 m length and a speed of 5 m/s, the time window yields 60s.

The assignment of trace gas peaks to ships is similar to the assignment of intensity dips. However, the allowed time window is dynamic and depends on the ship length, its speed and whether it blocks the light path or not. For small ships (length below 100 m) the allowed forward time window is one minute. For ships with lengths above 100 m, peaks with in the following 2 minutes are valid. Ships with lengths above 100 m and widths above 30 m (large tanker and cargo ships) have a forward time window of 15 minutes since plumes are most likely emitted above the instrument and may be detected after a large delay (as discussed above). The backward time window for all ships is 1 minute to cover the case of heavy tailwind were the plume might be detected shortly before the ship passes the OP-DOAS instrument. Since exhaust pipes are usually at the back end of the ship and to respect the length and ship movement, a dynamic delay of the forward time window is applied. This delay is calculated by division of the half ship length by its speed. Further, if a ship is identified to block the light path, the forward time window is delayed by an additional minute.

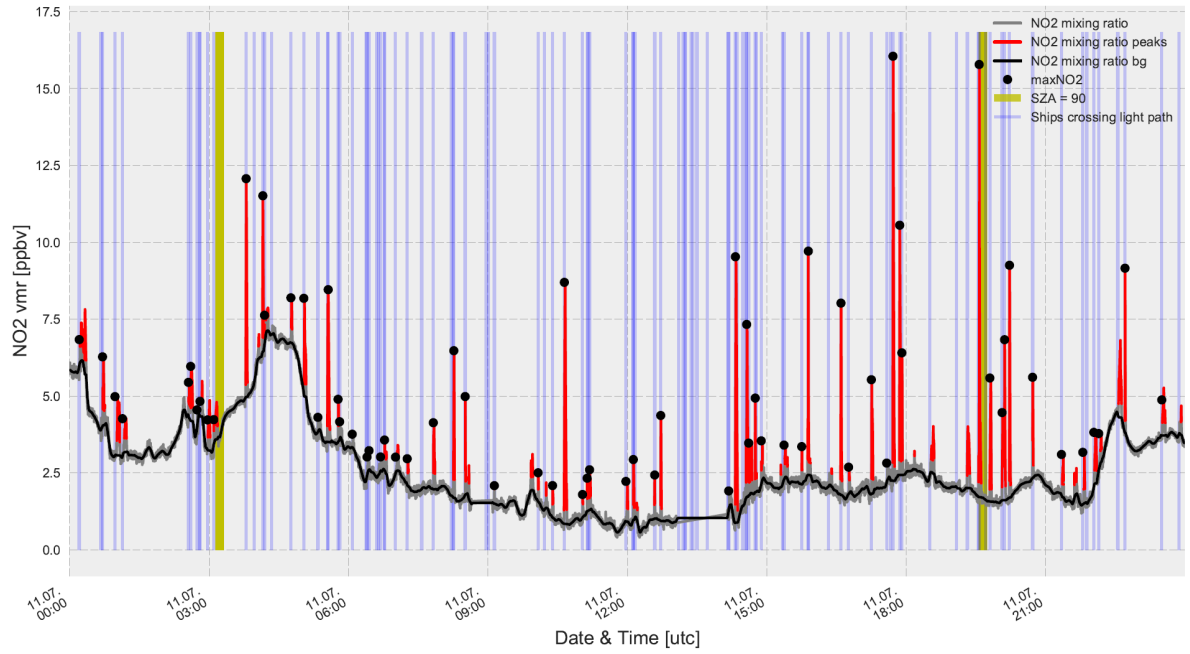

Figure 1-5: Exemplary time series of NO2 mixing ratios measured by the OP-DOAS instrument. Raw data is represented by the gray line, while the black and red lines represent NO_2 background and peak values after applying the peak identification algorithm. The vertical blue lines are ships passing the measurement path of the OP-DOAS instrument. NO_2 peaks (without background correction) assigned to ships are represented by black dots drawn on the respecting ship line. Additionally, sunrise and sunset are marked by yellow bars representing an solar azimuth angle (SZA) of 90°.

EXEMPLARY RESULTS FROM THE CAMPAIGN

Here only a few findings from the six weeks campaign are reported, most of them taken over from the detailed study in Schmitt et al., 2020.

During the time period between July 6th and August 17th 2016, the OP-DOAS instrument acquired atmospheric absorption spectra from which mixing ratios of SO_2, NO_2, O_3, HCHO, and HONO where retrieved by spectral analysis based on the method of Differential Optical Absorption Spectroscopy (DOAS, Platt et al. (1979)). Figure 1-6 shows histograms of mixing ratios (averaged along the measurement path) and corresponding detection limits of the different trace gas species as well as root mean square (RMS) values of the residual spectra from the DOAS analysis representing the overall analysis quality. Observed NO_2 mixing ratios ranged from several ppbv to maximum values of up to 20 ppbv (maximum values caused by ship emissions) with an average of 4.2 ppbv and an average detection limit of 0.44 ppbv (variance σ = 65 pptv). Considering SO_2, mixing ratios of up to 20 ppbv (also caused by ship emissions) where observed with an average value of 400 pptv and an average detection limit of 80 pptv (variance σ = 0.2 pptv). Mixing ratios of O_3 ranged from below the detection limit to up to 100 ppbv with an average value of 32 ppbv at average detection limit of 4.9 ppbv (σ = 0.9 ppbv). Further, the OP-DOAS spectra were analysed for absorption features of HCHO and HONO. While HCHO mixing ratios ranged from below the detection limit (average 1.4 ppbv, σ = 70 pptv) to approximately 8 ppbv, no significant mixing ratios of HONO could be observed

(detection limit of 230 pptv, σ = 18 pptv). Furthermore, there was no identification of ship emission signatures in the time series of HCHO data. Consequently, a correlation of HCHO and emissions from ship traffic cannot be draw given the sensitivity of the instrument used in this study.

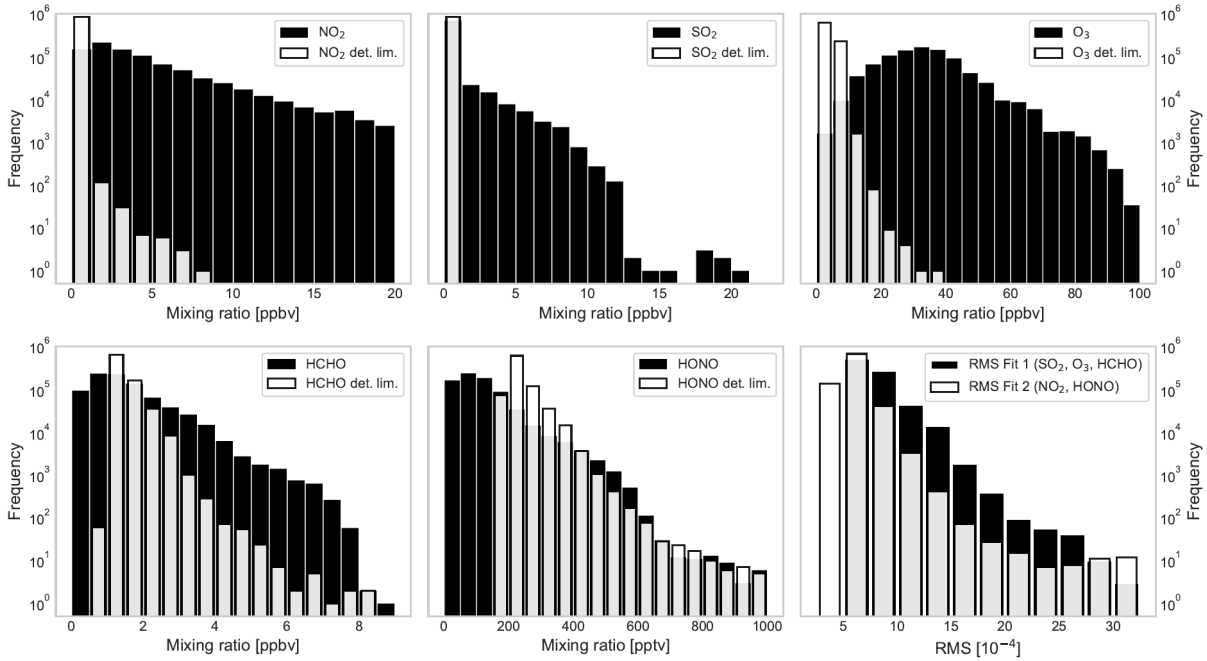

Figure 1-6: Histograms of measured trace gas mixing ratios (given in units of parts per billion (ppbv, 10^{-9}), except for HONO, given in units of parts per trillion (pptv, 10^{-12}), corresponding detection limits and RMS values of the residual spectra from the OP-DOAS analysis for two different fit ranges obtained during six weeks of continuous ship plume measurements along a total absorption path of 5.74 km (2.87 km one way) and a time resolution between 1 to 3 seconds. Note that the ordinate scale is logarithmic for the sake of readability.

The robustness of the measurement technique as well as the performance of the algorithm which identifies and assigns trace gas peaks can be quantified by a separate analysis of the data of ships which pass the instrument multiple times a day like passenger ferries, law enforcement vessels and dredging vessels which transport sediments out of the harbour basin regularly. Therefore, the seven ships with the highest number of passes were used as so-called benchmark ships. The yield (probability) of whether a CO_2 (for the case of in situ) or NO_2 (OP-DOAS) peak is assigned to a ship is calculated by dividing the total number of detected peaks for each ship with the total number of passes for each ship. The resulting peak yields for the benchmark ships show that for the in situ instrument, plumes of smaller ships with lengths of up to 50 m are detected with a yield between zero and 7 % while the OP-DOAS detects plumes with a probability between 27 % and 36 %. For larger ships (length above 50 % to 150 m) the in situ yield is between 27 % and 30 % and for OP-DOAS 55 % and 69 %. The higher yield for larger ships is most likely caused by larger engines and thus stronger emission signatures leading to a higher detection probability even for plumes at advanced dilution. Detection yields for all ship types of all ships passing the instruments during the measurement period are shown in Figure 1-7. It should be noted that in addition to the dependence on meteorological transport, the in

situ technique peak yield might also be limited by well-advanced plume dilution at the point of detection leading to less significant peak signals and thus, a less number of successful peak to ship assignments even during suitable wind directions.

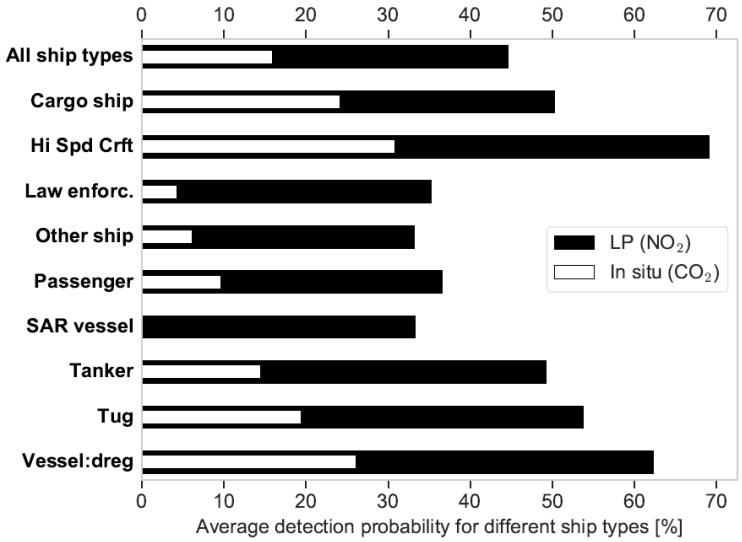

Figure 1-7: Detection yields for different ship types and for all ships combined (first row) for the complete dataset acquired during six weeks of plume monitoring by OP-DOAS (black) and in situ (white). Note that the total number of ship types varies from one to several hundreds.

CONCLUSIONS

NO_2 and SO_2 contents of ship emission plumes of more than 5000 passing ships have been measured with OP-DOAS across the river Elbe. An algorithm was developed to combine AIS data and OP-DOAS data. Thus, sharp NO_2 peaks were used as a proxy for air masses containing ship emissions and to assign these emissions to single ships. High SO_2 to NO_2 ratios between 1 and 6.7 have been observed for single ships while median values for the most common ship types Cargo, Tanker and passenger lie between 0.13, 0.15 and 0.08 respectively. With respect to in situ instruments and passive remote sensing techniques, the OP-DOAS technique represents a promising tool for the monitoring of ship emissions. However, since it relies on two components, the telescope on one end of the light path and the retro reflector on the other end, its application demands appropriate infrastructure to ensure an optimal position of the measurement path. On the other hand, the assignment of trace gas peaks to single ships does not rely on calculation of trajectories or favorable wind conditions since trace gas emissions are detected close to the ship exhausts. Thus, the impact of meteorology on the OP-DOAS measurements is negligible and therefore the detection probability for ship plumes is much higher than for all other methods. The major limitation for the OP-DOAS was found to be due to the high traffic density and, thus, the difficulty to unambiguously assign recorded plumes to particular vessels, rather than to the sensitivity to the emission strength.

Since the OP-DOAS-instrument used in this suitability study is difficult to operate, quite expensive and space-consuming, parameters for a new system have been defined. The

realization of the hardware of this OP-DOAS setup dedicated to monitor shipping emission was carried out by the company Airyx GmbH. The new setup, retrieval methods and first results of this system will be described in the next sections.

THE NEW AIRYX OPEN PATH DOAS SYSTEM FOR MONITORING SHIPPING EMISSIONS

TECHNICAL DESCRIPTION OF THE NEWLY DEVELOPED OPEN PATH DOAS

The airyx Open Path DOAS is a newly developed Open Path DOAS system which has been specifically designed to detect trace gases emitted by ships based on the experiences from the measurement campaign described in the last section, with a special focus on NO_2, SO_2, O_3, HCHO and HONO. The system comprises a telescope unit, which is connected to a spectrometer and an artificial light source via optical fibres, and an array of retro reflectors. A schematic representation of the whole setup is shown in Figure 1-8.

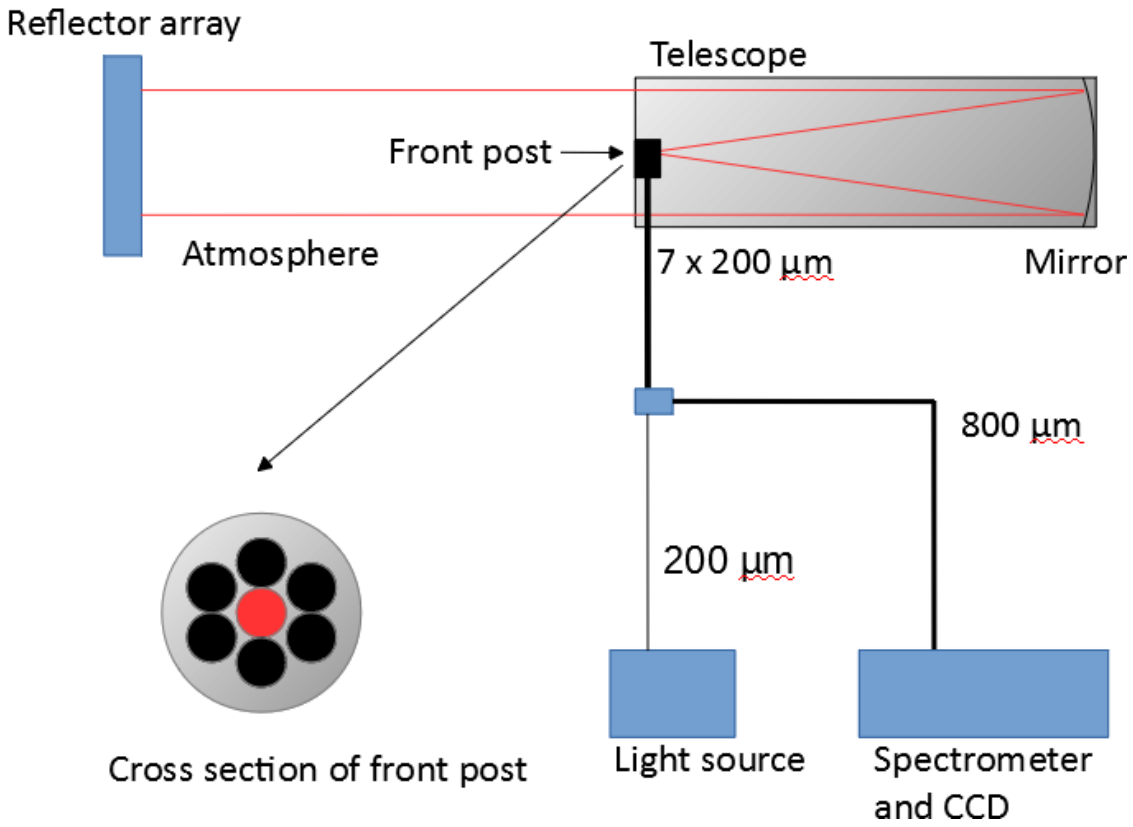

Figure 1-8: Schematic representation of the airyx Open Path DOAS system. The system itself consists of a telescope, a y-shaped fibre bundle, a light source, a spectrometer, and a reflector array. The emitting fibre is shown in red, while the receiving fibres are shown in black.

The artificial light source is a commercially available Laser-Driven Light Source (Energetiq EQ99) which supplies energy to a xenon plasma with an infra-red laser, which results in a high brightness across the whole generated spectrum (280 -500 nm) with a high spatial and power

stability. The light source is coupled to an optical fibre with a diameter of 200 µm which leads to the telescope.

The telescope is a fully enclosed box (see Figure 1-9), which is fixed in position and contains a small heater and a drying agent to prevent condensation of water vapor inside the telescope. Light is only able to enter the telescope through a fused silica window. The telescope itself consists of a spherical mirror with a diameter of 20 cm width a focal length of 80 cm. Close to the focal point there is a smaller angled mirror, which reflects the light coming from the light source onto the main mirror. The position of the smaller mirror can be adjusted so that the telescope can be aimed directly at the retro reflectors while the telescope box itself stays in a fixed position. Additionally, there is a video camera, which allows to survey the light path during the measurements.

The light, which enters the telescope, is transmitted to the spectrometer by six 200 µm optical fibres, which are coupled to the telescope in such a way that they surround the emitting fibre in circular manner. These six optical fibres are coupled to a single 800 µm optical fibre, which is used for mode mixing and thus increases the quality of the derived spectra. The optical fibre is also connected to the spectrometer. The spectrometer is an Avantes UV-VIS spectrometer covering the wavelength-interval from 280 to 445 nm with an average resolution of 0.76 nm (FWHM of the slit function). The spectrometer is equipped with a two-dimensional 2048x64 pixel Hamamatsu back thinned CCD, where the 2048 pixels are used for the wavelength axis. The whole spectrometer can be temperature regulated to a certain degree to decouple the spectrometer temperature from temperature changes in the ambient air and thus increases the quality of the measured spectra.

Figure 1-9: Picture of the telescope of the airyx Open Path DOAS system.

COMPARISON BETWEEN HEIDELBERG OPEN PATH DOAS AND AIRYX OPEN PATH DOAS

The Heidelberg Open Path DOAS used in the suitability study has been used for several months as a reference system to evaluate the performance of the airyx Open Path DOAS. Both generally use the same measurement principle but there are some differences in the actual hardware used. First of all the airyx system uses a smaller telescope which in general results in less light received. Furthermore, the airyx system has a smaller spectrometer and CCD and covers a larger wavelength range than the Heidelberg reference system. Therefore, both systems use slightly different wavelength regions to calculate the DOAS fit for the specific trace gases. The hardware components of both systems are shown in table 1.

Table 1: Hardware components of the airyx and the Heidelberg Open Path DOAS systems.

Component	Heidelberg campaign instrument	Airyx instrument
Light source	Energetiq EQ99	Energetiq EQ99
Optical fibres	200 µm, 800 µm	200 µm, 800 µm
Telescope Mirror	Diameter 0.3 m, focal length 1.5 m	Diameter 0.2 m, focal length, 0.8 m
Spectrometer	Acton Spectra 300i	Avantes UV-Vis
CCD	2048×512 pixel Roper scientific back-illum.	2048×64 pixel Hamamatsu back thinned
Measured wavelengths	280 – 362 nm	280 – 445 nm

A first comparison between both systems for a single day is shown in Figure 1-10. In general, both system match quite well both in SO_2 and NO_2. The general shape of the trace gas time series is the same for both systems and even the finer peak structures are similar. The negative values in the NO_2 time series of the airyx system are caused by spectra with a low intensity (e.g. times where ships blocked the light path across the river) which were not automatically filtered out before the DOAS fit and are not caused by the instrument itself.

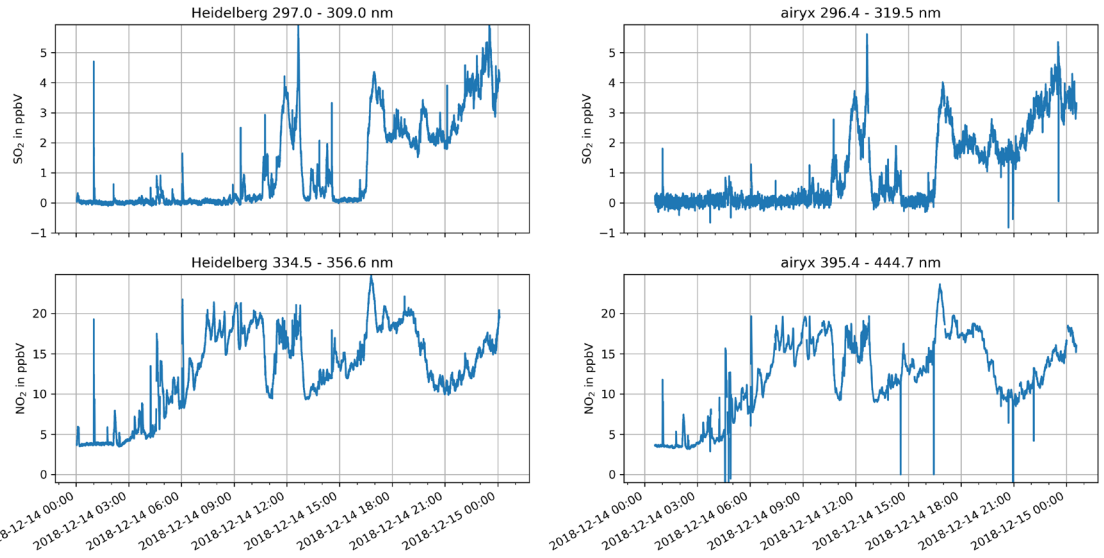

Figure 1-10: Comparison of derived SO_2 and NO_2 mixing ratios for both systems for a single day. Left Column shows the results of the Heidelberg Open Path DOAS, right column the respective results of the airyx system.

The noise level for SO_2 is bigger than for NO_2, due to several reasons. First of all the airyx system uses a smaller telescope and therefore catches less light compared to the Heidelberg instrument. This leads to a smaller signal to noise ratio especially within the UV wavelength regions which are used to fit SO_2. Second, the airyx system uses a fully enclosed telescope with a fused silica window while the Heidelberg telescope is not fully enclosed. The fused silica window further decreases the amount of light that ultimately reaches the spectrometer and thus also decreases the signal-to-noise ratio. The third influence is the way the telescope of the airyx instrument is currently mounted, which leads to stray light that is reflected onto the optical fibres leading towards the spectrometer. The intensity of this stray light can reach up to 12% of the total received intensity in the UV wavelengths, depending on the lighting conditions. The stray light increases the errors for the derived trace gas concentrations, especially when the fits are applied in the UV. For example, the errors in SO_2 are in the range of 0.05 to 0.1 ppb, which is approximately 40% larger than for the Heidelberg instrument.

For NO_2 there are less deviations in the results between both instruments. First of all the NO_2 fit for the airyx system uses a completely different fitting window which is in the visible wavelength region of the spectrum, where more light is available, which enhances the signal-to-noise-ratio and also reduces possible stray light within the telescope. Furthermore, NO_2 has stronger absorption features in the visible wavelengths than in the UV, which also results in lower detection limits of NO_2 compared to the Heidelberg instrument.

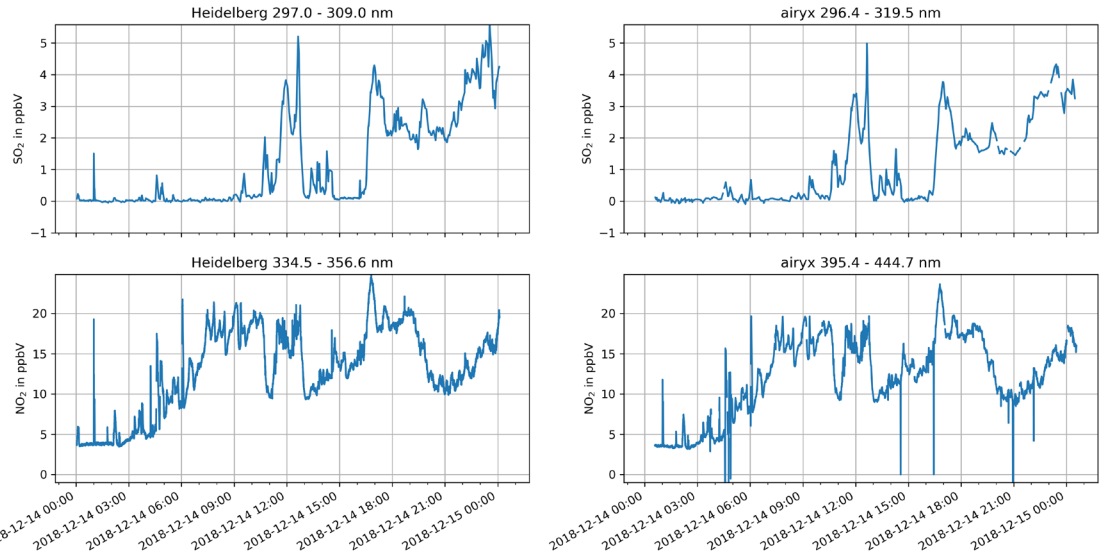

Figure 1-11:Same as figure 10 but for SO2 the 12 spectra have been averaged before the DOAS fit has been applied.

Errors can be further decreased by temporal averaging of the individual spectra before the DOAS fit is applied, which ultimately results in lower errors and decreases the detection limit. An example for temporal averaging is shown in Figure 1-11, where 12 spectra were averaged before the DOAS fit has been applied. Due to the loss of temporal resolution, the peaks within the time series caused by small emission events such as passing ships are also reduced, but still recognizable.

A regression analysis has been carried out for data collected between 16th November 2018 and 29th January 2019 and the resulting scatter plots can be seen in Figure 1-12. For the regression, the DOAS fit has been applied to single spectra, so there was no temporal averaging. The figure shows a good match between both instruments and the R^2 of the linear regressions is 0.97 for SO_2 and 0.96 for NO_2, respectively. The slope of the fitting line is not exactly one but relatively close in both cases. Deviations can be explained by a small miscalibration within the telescope unit which has been solved in the meantime. Standard error of slope and offset are several magnitudes smaller than the estimated value itself and are therefore not shown for both cases. The scatter plot of NO_2 shows several single data points where the airyx instrument detected very small NO_2 mixing ratios, while the reference system did not. This is caused by the already mentioned spectra with low intensity that have not been filtered out properly.

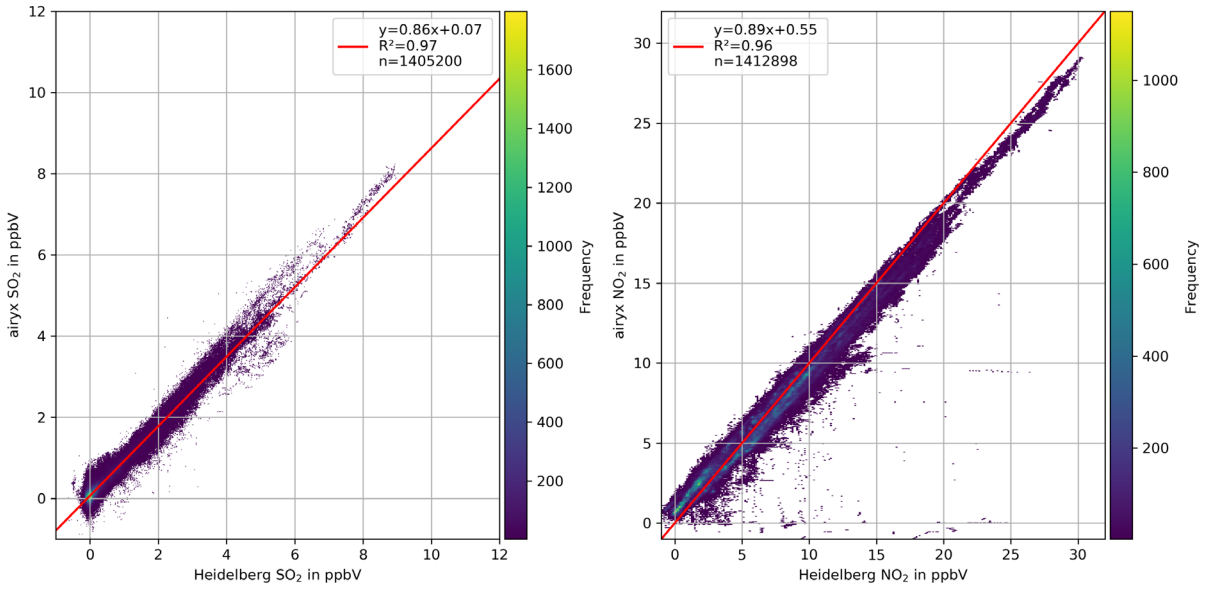

Figure 1-12: Scatter plots of derived SO2 and NO2 between both instruments. Red line shows the result of the linear regression, equation number of measurements and R^2 are shown in the figure.

Detection limits are tied to the respective measurement error of the trace gas and can be estimated by multiplying the measurement error with a constant (Stutz and Platt, 1996). The resulting detection limits of the airyx DOAS instrument are then on the order of 0.5 ppb for SO_2 and 0.3 ppb for NO_2, respectively. These detection limits are expected to decrease once the mounting position of the telescope has been changed to eliminate the stray light within the telescope.

In conclusion the airyx Open Path DOAS is comparable to the Heidelberg Open Path DOAS instrument and both systems show results of similar quality. Differences are small and can be explained by the differences in the hardware used. The quality of the derived trace gas time series of the airyx system can be further increased once the telescope position has been adjusted to fix the current stray light issues. At the same time the airyx system is much smaller and therefore easier to set up and easier to maintain.

RESULTS: SO_2/NO_2 RATIOS

To monitor the influence of ship emissions, individual plumes of ships have to be analyzed. The first step of this analysis is to combine the trace gas time series with the information about the ships that pass the measurement site. The ship positions and information about them is taken from AIS data. First of all a high pass filtered time series has been calculated for each trace gas using a running median window with a window size of 5 minutes. This high pass filtered time series represents the background concentration which still includes differences due to meteorological factors but excludes the small peaks caused by emissions from passing ships. This high pass filtered time series has been subtracted from the original time series, resulting in a time series that in average is close to zero but contains a lot of small peaks. If those peaks

exceed a set threshold, for example two times the measurement error, then the peak is classified as a valid peak caused by some sort of emission within or close to the light path. The next step checks for each peak whether there was a ship close or within the light path. This check includes all ships within a certain time frame, usually roughly one or two minutes. If there are several ships, the ship with an AIS signal closest in time to the peak and closest in space to the light path is chosen as the pollution source. If there are several ships within a similar time frame, the peak is excluded and is not evaluated further, because it may be actually caused by the combined emissions of several ships. This analysis is then carried out for all relevant trace gases.

Even though the analysis is carried out for all trace gases which are all measured at the same time and by the same instrument, there are differences for each trace gas. The peak in NO_2 is found for every ship that passes the measurement site, however sometimes SO2 peaks are too low to be detected. An observed delay from the NO_2 peak and SO_2 is caused by conversion of NO to NO_2 (see below) within the atmosphere, so that the NO_2 peak might be measured after the SO_2 peak. When there is no peak in SO_2 but one in NO_2 the fuel sulfur content might be too small to cause a significant increase in SO_2 within the plume.

It has to be kept in mind that this kind of analysis implies that each plumes crosses through the light path and causes a signal, which is larger than the deviations caused by other factors, so it can be distinguished from the background values. For smaller ships, this requires the plume to rise from the water surface upwards through the light path, while for larger ones, where the emission takes place above light path, a downward mixing is required, for example caused by turbulence generated by the movement of the ship itself.

Width and height of the measured peaks are dependent on several factors and it is therefore challenging to derive the absolute amounts of each emitted species. First of all, the width and height are dependent on the viewing geometry; largest peaks are found if plume and light path are alongside each other and smallest are found when the peak is orthogonal to the light path. Furthermore, for NO_2 the height is also dependent on the age of the plume, since mainly NO is released during the combustion process and is then converted to NO_2 via reaction with ozone within the atmosphere. The light path of the Open DOAS instruments also include larger volumes of air, which are not part of the plume itself, which also lowers the peak intensity. Using additional assumptions, the emission rates for the emitted gases can be determined which is explained in the next section.

To get a first impression about the emissions of a single ship the calculation of SO_2/NO_2 ratios is useful. In first order the assumption is valid, that the amount of nitrogen oxides produced by burning shipping fuel is more or less constant independent of the type of fuel. Therefore, the amount of SO_2 determines the value of this ratio. Fuels with larger sulfur content should lead to larger SO_2 emissions and thus increase the ratio. However, it is still not possible to derive the sulfur content of the shipping fuel in absolute units.

This kind of analysis has been carried out for all days where there were trace gas time series measured by one of the Open Path DOAS systems and AIS data about the passing ships. In total roughly 10.000 ships have been detected over a time frame of 147 days by each system.

The respective SO_2/NO_2 ratios have been calculated by calculation of the peak integrals for each trace gas. Peaks have been assigned for each trace gas individually. If there was no SO_2 peak, the width of the respective NO_2 peak has been used for the calculation of the SO_2 integral within this limits. The resulting SO_2/NO_2 ratios are shown in Figure 1-13 and are classified by ship length. The histogram shows a normal distribution of SO_2/NO_2 ratios with a median of about 0.045. Negative values are caused by low SO_2 peak values. These low SO_2 values are usually close to the detection limit and result in negative values if the respective background values have been subtracted.

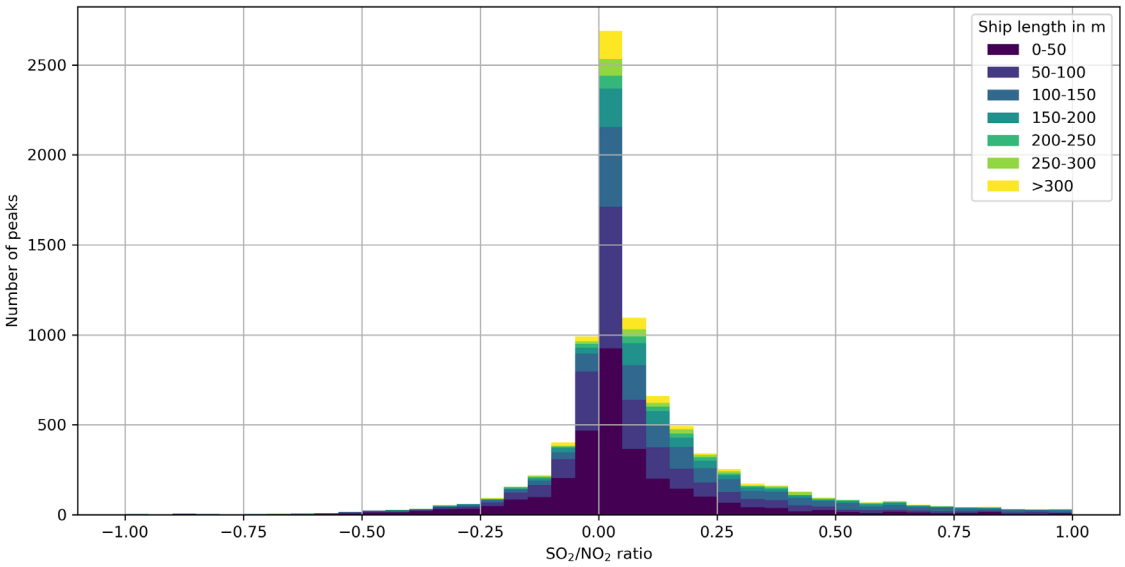

Figure 1-13: Histogram of SO_2/NO_2 ratios from data derived from the Open Path DOAS instrument. Data from 27th April 2018 to 29th January 2019 has been processed. Total number of detected ships was 10047. Data has been classified according to the length of the according ship.

CALCULATION OF ABSOLUTE EMISSION FACTORS FOR SO_2 AND NO_2 FROM OPEN PATH DOAS OBSERVATIONS

In principle the information of the horizontal plume extent caused by shipping emissions can be utilized to calculate absolute emission factors for single ships passing the measurement site. In the following, we briefly describe a method for the estimation of emission source strengths using a simple Gaussian plume dispersion model.

The Gaussian dispersion model developed by Sutton and Simpson (1932) describes the concentration C(x,y,z) of a substance being emitted by a point source into the atmosphere at a constant emission rate Q with x representing the distance from the emitting source along the ground, while y and z represent horizontal and vertical distance from the center line perpendicular to the wind direction (Figure 1-14).

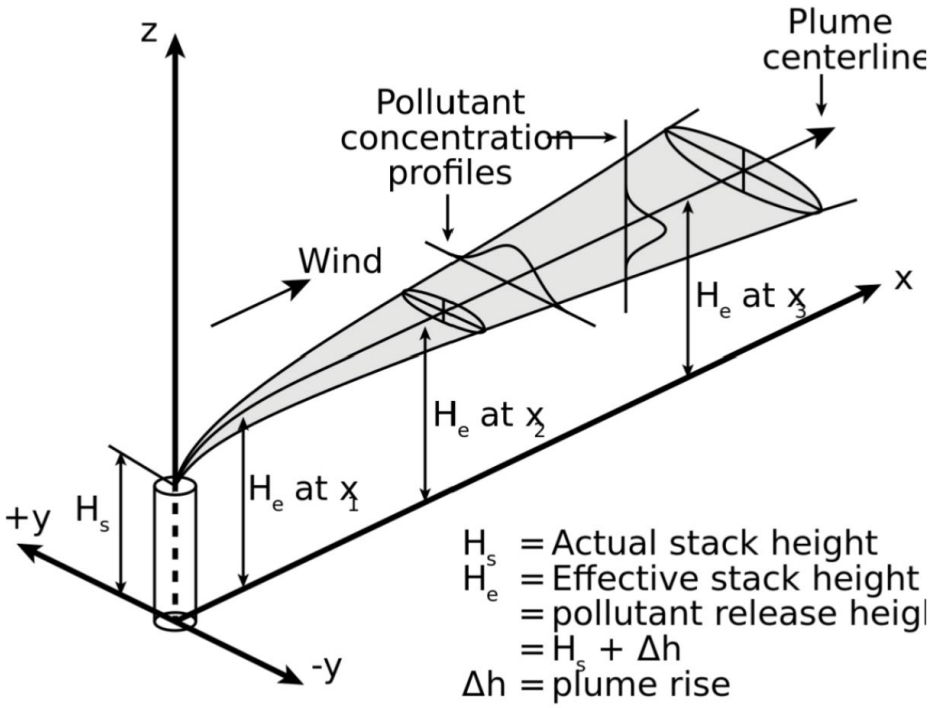

Figure 1-14: Illustration of the Gaussian plume dispersion model.

Since a ship is a moving point source, apparent wind speed and direction have to be calculated according to Lööv et al., 2013. Vertical and horizontal dispersion parameters are depending on the atmospheric stability. This is estimated by using local meteorological observations. Since the OP-DOAS is measuring in a fixed geometry through the plume, the measured concentration can be simply used as a proportionality factor to a modeled concentration with a randomly chosen source strength to calculate the actual source strength or absolute emission rate. Due to the fact, that several simplifications have to be made, the error for a single measurement (ship) is quite large. Nevertheless, by applying this method to many ships valuable information on the emission patterns e.g. depending on ship size, speed, current and others can be derived.

Figure 1-18 illustrates the OP-DOAS light path through a modeled ship plume. For clarification, the plume is shown in slides for every five meters in altitude.

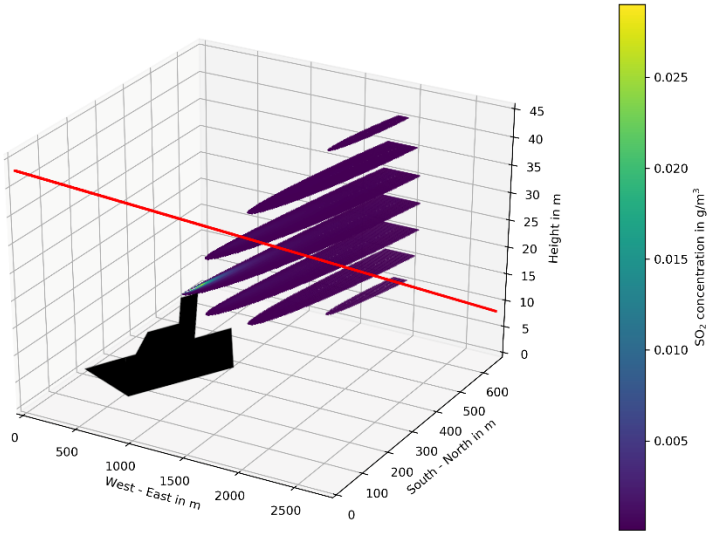

Figure 1-15: Illustration of the OP-DOAS light path (red line, from Wedel to the right towards the light house Lühe to the left) going through a modeled ship plume. Only very close to the chimney very high values can be found.

The following Figure 1-16 shows the calculated NO_X emission ratios for the local ferry "Dat Ole Land 2" passing on a regular basis. The ship was constructed in 2012 with an engine power of twice 331 kW. Assuming a typical fuel rate of 0,25l/kWh and an emission behavior according to the BinSchAbgasV, ships of this type should emit less than 8.7 g/kWh of NO_x plus HC. This can be transferred to an absolute emission rate of 1.6 g/s for this ship. OP-DOAS observations show slightly higher values but still in a reasonable range. Slightly smaller values downstream the Elbe river (West direction) are also expected due to a lower load of the engine (please note, that the actual flow is modulated by the tide). Since the OP-DOAS cannot measure NO, the NO_x value has been converted from the NO_2 applying the method by Kurtenbach et al., 2016 to calculate the NO/NO_x-ratio. A conversion factor of 0,083 has been derived from local in situ data.

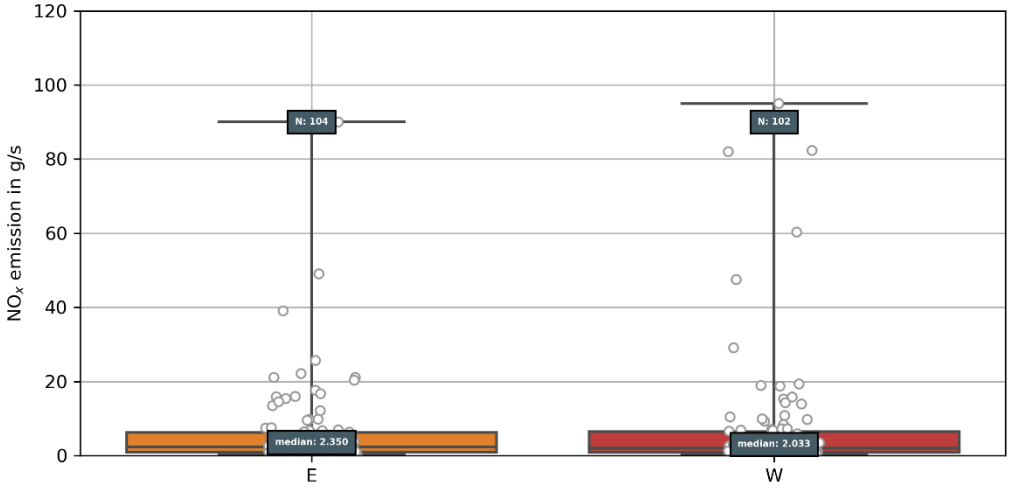

Figure 1-16: Calculated absolute emission rates for NO_x for the local ferry "Dat Ole Land 2". E means East direction (upstream), W West direction, downstream. Each dot represents a single measurement, the box the range between the 9th and 91th percentile of the data.

Figure 1-17 and Figure 1-18 show the results for all observed ships depending on the ship size for SO_2 and NO_2 respectively. In general, the results show the expected behavior with increasing emission rates for bigger ships (engines). A more detailed study is in preparation (Krause et al., 2020).

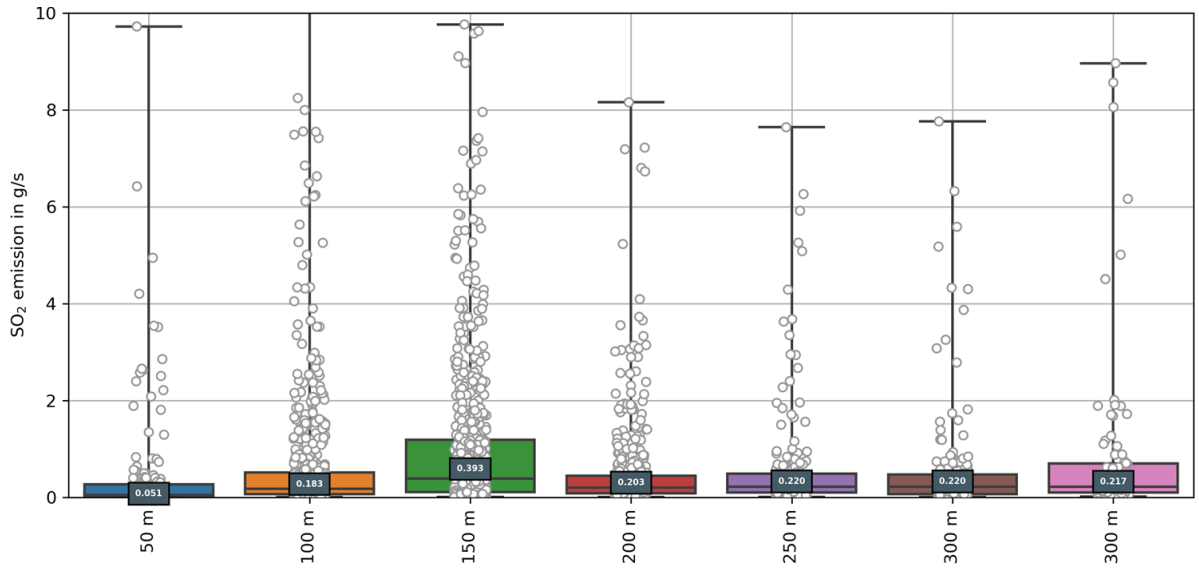

Figure 1-17: Absolute SO_2 emission rates depending on ship size. Similar to Figure 1-16 the dots represent single measurements and the box the range between the 9th and 91th percentile of the data. The indicated value is the median.

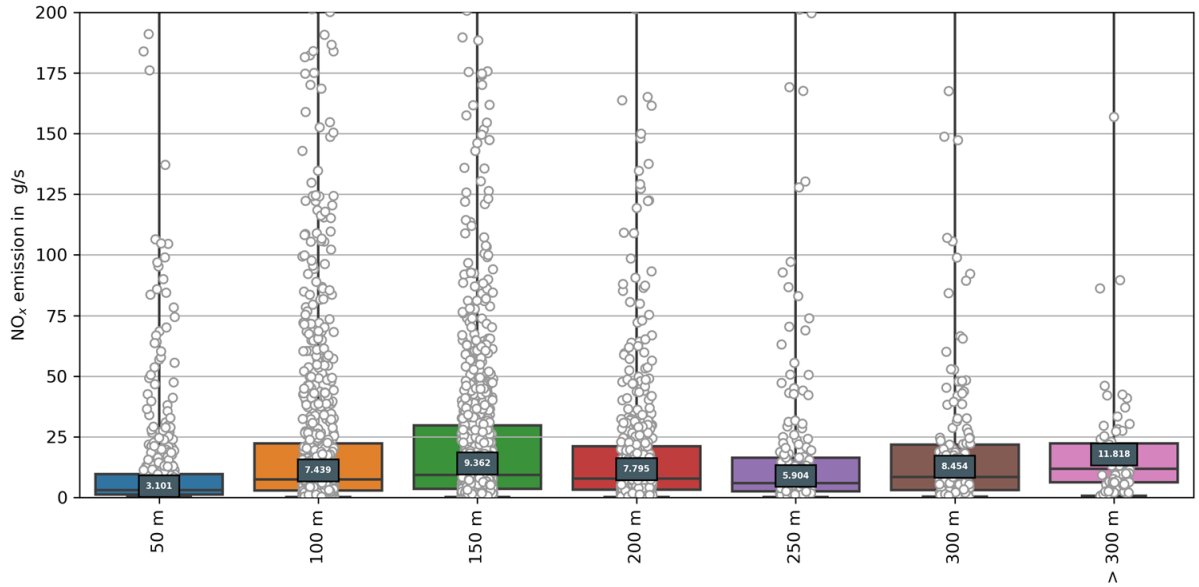

Figure 1-18: Absolute NO_x emission rates depending on ship size. Similar to Figure 1-16 the dots represent single measurements and the box the range between the 9th and 91th percentile of the data. The indicated value is the median.

Under favorable conditions the described method (Gaussian plume dispersion) can be used in a similar way for in situ measurements. This has been carried out using in situ data collected within the CLINSH (Clean Inland Shipping) project focusing on inland ships. First results are promising. The adaptation to data collected by the BSH in Bremerhaven and Kiel is therefore highly recommended.

WORK PACKAGE 1 SUMMARY

The results obtained in this work package have shown that the OP-DOAS technique has a high potential for near real-time monitoring of ship emission in harbor areas or across a river or channel. This method provides enhanced monitoring coverage and statistics of emission signatures compared to currently deployed in situ measurement stations which rely on meteorological transport of emission plumes or passive remote sensing with data coverage only during daytime and challenging monitoring conditions. The described system has a high automation level along with low maintenance.

However, to obtain reliable quantitative data for the fuel sulphur content emissions, the measurement of CO_2 is mandatory. Recent work by Griffith et al. (2018) showed first measurements of CO_2 using the long path technique in combination with a Fourier Transform Infrared spectrometer. We therefore propose a combination of UV-vis and IR long path measurements to achieve quantitative remote sensing emission measurements. The detection of NO to obtain on a direct way NO_x-emissions is desirable. However, the detection of NO (absorbing in the deep UV around 220 nm, Keller-Rudek et al. (2013), Luque and Crosley (1999)) along measurement paths of several hundred meters is quite challenging due to

limited radiance of available light sources and large light losses caused by scattering along the measurement path.

WORK PACKAGE 2 – IN SITU MEASUREMENTS AND PASSIVE REMOTE SENSING

IN SITU OBSERVATIONS

For a detailed description of the instruments and the retrieval methods used to obtain and interpret in situ data within this project we refer to the MeSmarT-I report and in particular to the PhD thesis by Lisa Kattner (2019). The latter one includes also a very comprehensive picture of the quality control measures to ensure the correct implementation of in situ instruments for compliance monitoring.

QUALITY CONTROL

It can be summarized, that a combination of different quality control measures offers the best assurance of the correct function of the instruments and a reliable data output. Regular zero and span gas measurements provided by permeation tubes are an easy applicable way of function control for the instruments and can help to determine possible drifts and malfunctions. They need to be monitored regularly over longer time spans. If drifts or offsets are observed, transfer standard measurements help to verify differences and provide the necessary validation for the calibration of instruments. For devices such as the CO_2 instrument, where no other function control is available, the measurements of transfer standards are especially important. Other publications report linearity problems with similar instruments (Beecken, 2015), which need to be calibrated regularly. General inspections of the instruments with transfer standards are recommended at least twice a year, or even more often if the instruments have been set up or modified recently. Temporal parallel measurement of comparable systems is highly recommended, not only to compare measurement values, but to test the reproducibility of the whole data acquisition and analysis process. If possible, inter-comparison campaigns of two or more measurement systems should be carried out regularly, ideally also including one scientific trace-level system as a reference.

As part of MeSmarT-II a trace-level system for SO_2 has been implemented in the mobile lab of the IUP Bremen. The Thermo Scientific™ Model 43i-TLE Enhanced Trace Level SO_2 Analyzer utilizes pulsed fluorescence technology to measure the amount of sulfur dioxide in the air down to 50 ppt (300 s averaging time). The standard setup has been slightly modified (higher pump throughput) to ensure a response time down to 30 s (80 s standard). A detailed description of the instrument and results from the evaluation campaign in Bremerhaven is given in Ochtmann, 2018. Figure 2-1 is showing one example for the comparison between the Airpointer system (which is the commonly used one within the BSH monitoring network) and the trace level system. The latter one exhibits a noise level around 10 times lower than the standard system which has a direct impact on the quality of retrieved FSC values (see Kattner, 2020).

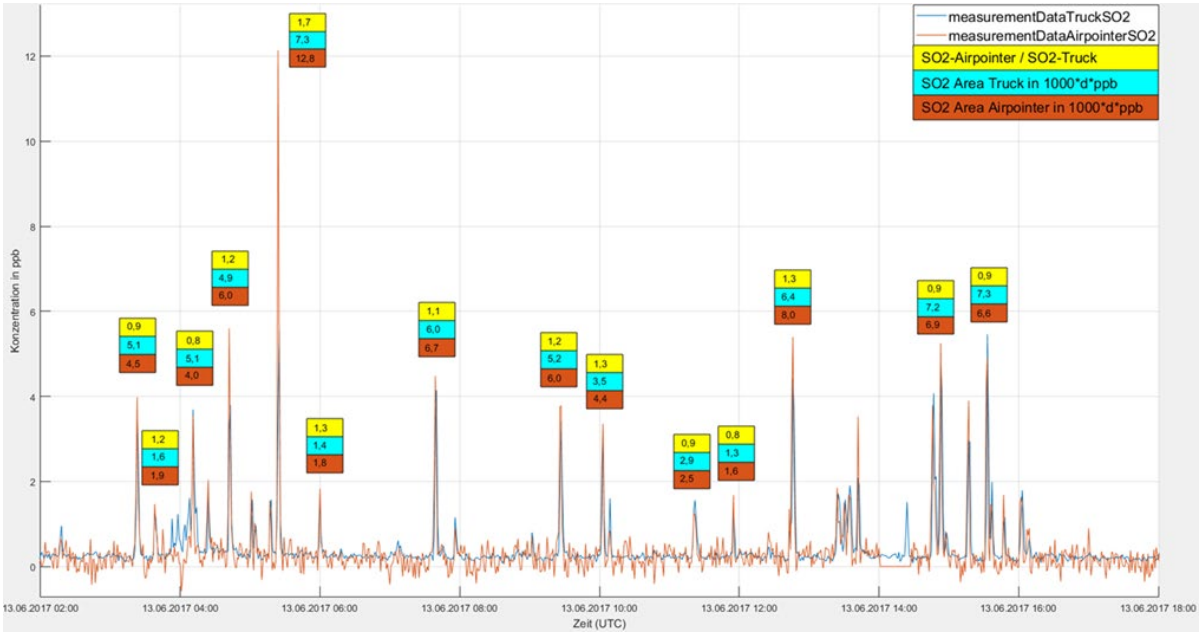

Figure 2-1: Comparison between standard in situ (Airpointer) and trace level system measurements of SO_2 in Bremerhaven. The general agreement is in average quite well. However, deviations in the calculated SFC were up to 30%. Obviously, the trace level system has a much lower zero noise (down to 50 ppt for 60 s averaging time).

ANALYSIS OF NO_X EMISSIONS

Similar to the calculation of the fuel sulfur content described e.g. in Kattner et al, 2015, NO_x emission factors can be calculated for the plumes that have been measured and allocated to individual ships. Although there was not yet a NO_x regulation in force for sea going ships in the North Sea and Baltic Sea ECA during the period of the MeSmarT-II project, it is possible to check for the potential compliance with future NO_x regulations, which will enter into force in 2021. For inland ships, regulations concerning allowed NO_x emissions are already active.

While the calculation of NO_x emission factors is quite simple, the comparison to MARPOL NOx limits is not straight-forward. The curves of NO_x emission limits for MARPOL Tiers I - III levels are shown in Figure 2-2. The limits are given as load-based emission factors, which relate the amount of emitted NOx to the generated crank shaft power, instead of the amount of fuel used.

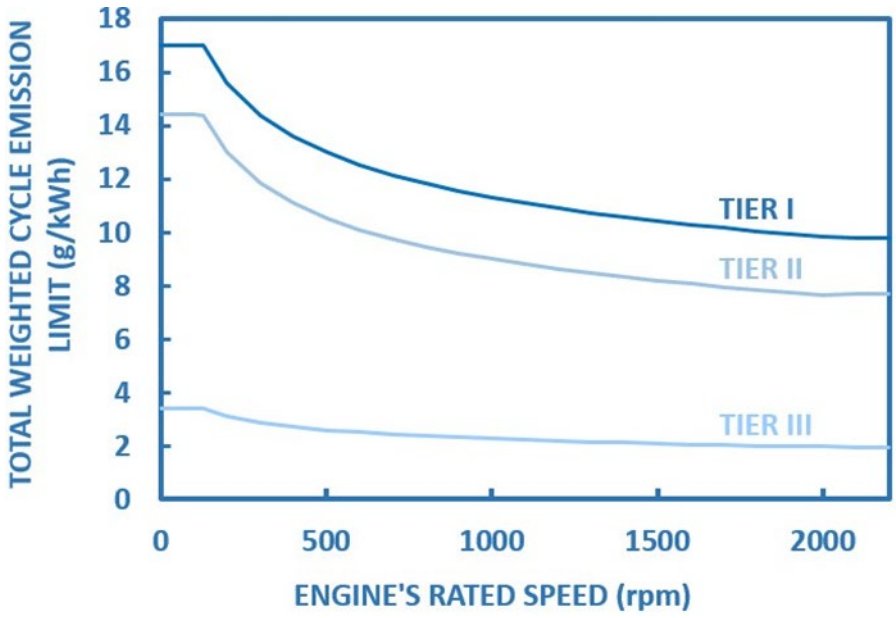

Figure 2-2: NO_x emission limits according to the year of ship construction: Tier I between 2000 and 2010, Tier II from 2010 and 2016 and Tier III from 2016 onwards.

This makes it difficult to compare instantaneous emission measurements to the limits and determine compliance with the regulations. To obtain values comparable to the limits, a specific fuel oil consumption (SFOC) factor would be needed, which is not available without knowledge about engine type and load for each ship of interest. Ship speed, as it is transmitted with the AIS signal, is not an useful indicator for engine load, especially for condition e.g. close to the pilot station Wedel at the Elbe river, which has a strong tidal current, which the ships either have to go against with higher engine work or go along with less work.

However, if the MARPOL limits are converted to an interval with the unit g/kg fuel with reasonable average SFOC and load values, it is possible to compare them in a qualitative way to the measured values. A broad range of 500 - 1500 rpm for the engines rated speed is used for the interval and converted to g/kWh according to the MARPOL NOx limit calculations.

Following the specification notes of ship engine manufacturers, typical SFOC values range between 160 to 180 g/kWh, for a variety of engine types and different operational conditions. With these values, the upper and lower limits of the different Tier regulations can be summarized as follows:

- Tier I (keeled on or after January 1st, 2000): 57.8 - 81.3 g/kg fuel
- Tier II (keeled on or after January 1st, 2011): 45.5 - 65.6 g/kg fuel
- Tier III (ships on or after January 1st, 2016): 11.6 - 16.3 g/kg fuel
  (see IMO)

These values are depicted in the following Figure 2-3. It shows that about 80% of the ships are within the upper limit of Tier I regulations for ships built after the year 2000. About 60% are within the upper limit of Tier II regulations. Although TIER III regulations are not yet in force in the North

and Baltic Sea ECA, many engine manufacturers promote their products as complying with these new limits for the US market or for ships to be deployed in the US ECA. However, less than 10% of the ships comply with the upper Tier III limit. A shift to smaller NO_x emission factors is expected in the future with the new Tier III regulations enter into force in the North and Baltic sea in 2021.

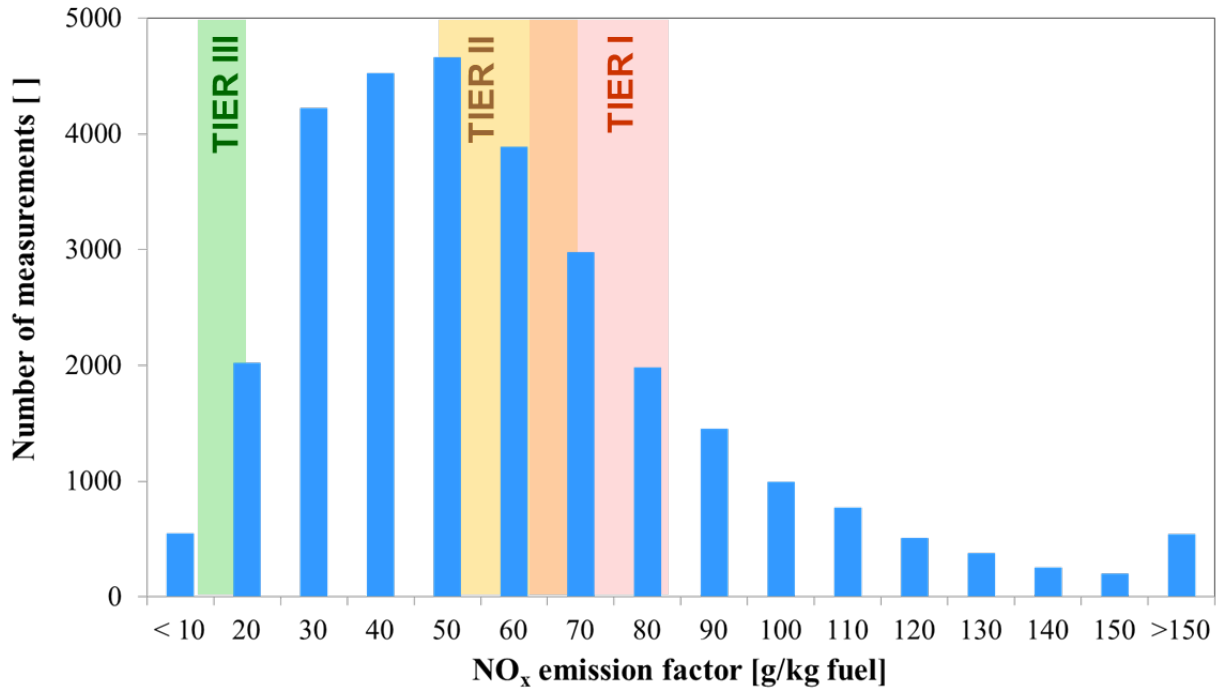

Figure 2-3: NO_x emissions calculated from the NOx/CO2 emission ratio for all sites of the BSH monitoring network (created by A. Weigelt, BSH) including ~30.000 single measurements.

PASSIVE REMOTE SENSING

MAX-DOAS NEUWERK: MEASUREMENT GEOMETRY AND ACQUIRED DATABASE

The quantity retrieved from MAX-DOAS measurements is the so-called slant column density (SCD), the concentration of an absorber integrated along the atmospheric light path. Figure 2-4 show how to measure the NO_2 and SO_2 absorption inside the ship plumes emitted on the shipping lane, the instrument is pointing towards the horizon (in 0.5° elevation). Taking a close-in-time zenith-sky measurement as a reference in a first assumption cancels out the absorption

higher up in the atmosphere and only the absorption along the horizontal part of the effective light path is retrieved (see Figure 2-4), yielding the differential slant column density (DSCD).

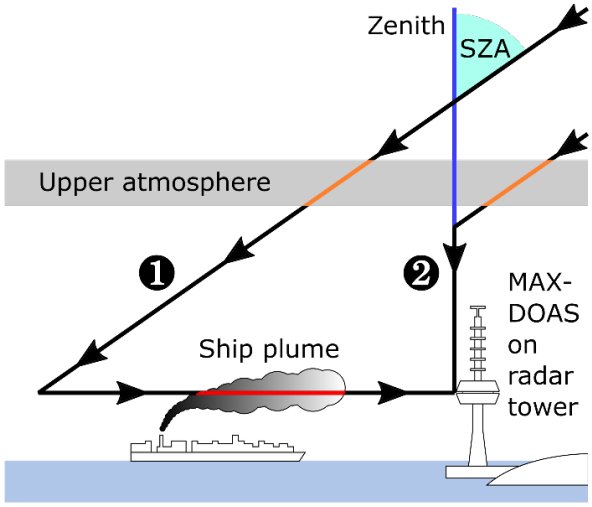

Figure 2-4. Measurement geometry for MAX-DOAS measurements on Neuwerk with schematic light paths for off-axis (1) and zenith sky reference measurements (2) for an exemplary solar zenith angle (SZA) of 55°. (Seyler et al., 2017)

The MAX-DOAS instrument, was installed on the radar tower of Neuwerk, 6–7 km south of the main shipping lane from the German Bight into the Elbe river (see Figure 2-5a). To sample a larger section of the shipping lane, the MAX-DOAS was measuring in five different azimuthal viewing directions: 310°, 335°, 5°, 35° and 65° with respect to north (see Figure 2-5b).

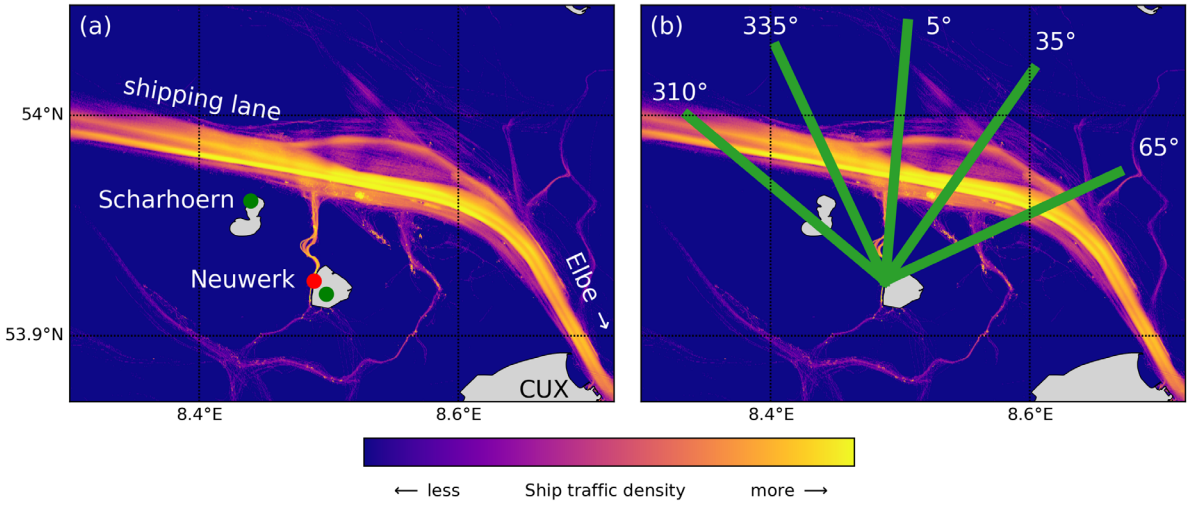

Figure 2-5. (a) Ship traffic density map calculated from all received AIS messages (2013-2016) showing the main shipping lane from the North Sea into the Elbe river close to the measurement site on the radar tower on the island Neuwerk (red dot). Wind measurements (HPA) are available on Neuwerk as well as the neighbouring island Scharhörn (green dots). (b) The five azimuthal viewing directions of the MAX-DOAS instrument (310°, 335°, 5°, 35°, 65°, with respect to north) towards the main shipping lane, passing the island in the north at a distance of 6–7 km. (Seyler et al., 2019)

An overview of the measurement data collected on Neuwerk from July 2013 until July 2016 by the various instruments is given in Figure 2-6, showing also the data availability.

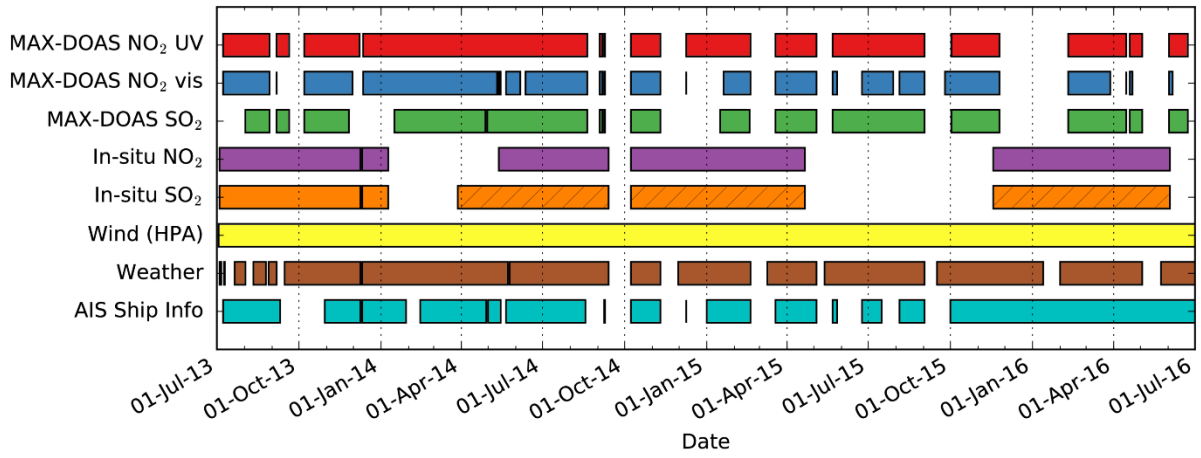

Figure 2-6. Data availability in the analyzed measurement period between July 2013 and July 2016. From March 2014 on (hatched), there were instrumental problems with the in situ SO2 instrument resulting in a strong oscillation of ± 0.5 ppb superimposing the data. (Seyler et al., 2017)

For further information on the MAX-DOAS instrument on Neuwerk and the Neuwerk site see Seyler et al. (2017). Therein, a detailed description of the measurement geometry and principle as well as data analysis can be found.

MAX-DOAS NEUWERK: SO_2 / NO_2 RATIOS IN SHIP PLUMES

This section is based on Seyler et al. (2017).

It is difficult to derive the absolute amounts (e.g. in mass units) of NO_x and SO_2 in the plumes with MAX-DOAS, as the width and height of the measured peaks does not only depend on the emitted amount of pollutants, but also strongly on the geometry. The highest values are measured alongside the plume, and much lower values when the plume is oriented orthogonally to the line-of-sight of the MAX-DOAS. Because of NO to NO_2 titration also the time span between emission and measurement influence the amount of measured NO_2. To determine in-plume mixing ratios and emission factors for the emitted gases, additional information on the length of the light path inside the plume is be needed, which auxiliary measurements can provide (see next section). Although the emission factors cannot be measured by MAX-DOAS directly, the NO_2 and SO_2 signals yield the ratio of both. These SO_2 to NO_2 ratios can be compared to other studies as well as measurements on other sites or with different instruments, bearing in mind possible deviations due to NO to NO_2 titration.

By comparing SO_2 to NO_2 ratios from different ships it is possible to roughly distinguish whether a ship is using high sulfur content or low sulfur content fuel (giving a high or low SO_2 to NO_2 ratio). Beecken and Mellqvist from Chalmers University (Sweden) use this relationship for airborne

DOAS measurements of ship exhaust plumes on an operational basis in the CompMon project (Mellqvist et al., 2017). Following the ships and measuring across the stack gas plume, they can discriminate between low (0.1%) and high (1%) fuel sulfur content ships with a probability of 80--90%. A more detailed analysis is then performed with in situ (sniffer) instrumentation inside the plume (Van Roy and Scheldeman, 2016).

From the spectra measured by the MAX-DOAS UV instrument both NO_2 and SO_2 columns can be retrieved at once. To separate ship related signals from smooth background pollution, first a running median filter was applied to the time series of SO_2 and NO_2 measurements with a large kernel size (e.g. over 21 points). If too many broad peaks are contained in the time series this is not sufficient and the resulting median might be systematically higher than the actual baseline. In this case, on the values in the lower 50% quantile again a running median with a smaller kernel size (e.g. 5) was applied, giving a good approximation of the real baseline. The adjustment of the kernel sizes is done manually. In the next step, this baseline is subtracted from the raw signal. A simple peak detection algorithm was used to identify the peaks in the baseline-corrected NO_2 signal, which allows to identify most peaks in the time series. Problematic are broad peaks or overlapping peaks from multiple plumes at once. Then the corresponding peaks in the SO_2 signal were assigned. This accounts for cases when no SO_2 enhancement is measured. The final selection of the peaks to be included in the statistics is done manually, filtering out for example all the cases when peaks are too close together to be separated and again fine-tuning the baseline detection algorithm parameters if necessary. To achieve a better signal-to-noise ratio, the integrals over both the NO_2 and SO_2 peak are calculated and the ratio of both values is computed in the last step. The differences in the resulting SO_2 to NO_2 ratios by taking the peak heights or peak areas are small, though.

Figure 2-7 shows NO_2 and SO_2 measurements for an example day in summer 2014, before the stricter fuel sulfur content limits were introduced. Both the NO_2 and SO_2 signal show sharp peaks, originating from ship plumes. Most of the peaks are of similar shape in NO_2 as well as SO_2 signal. The measured SO_2 to NO_2 ratios on this day in this direction range from 0.17 to 0.41. The SO_2 to NO_2 ratio can vary strongly for different ships. For example, the plume of the ship passing the line-of-sight around 12:00 UTC has a high NO_2 content, but low SO_2, whereas the opposite is true for the ship passing at 12:30 UTC, indicating that the second ship was using fuel with a considerably higher sulfur content than the first one.

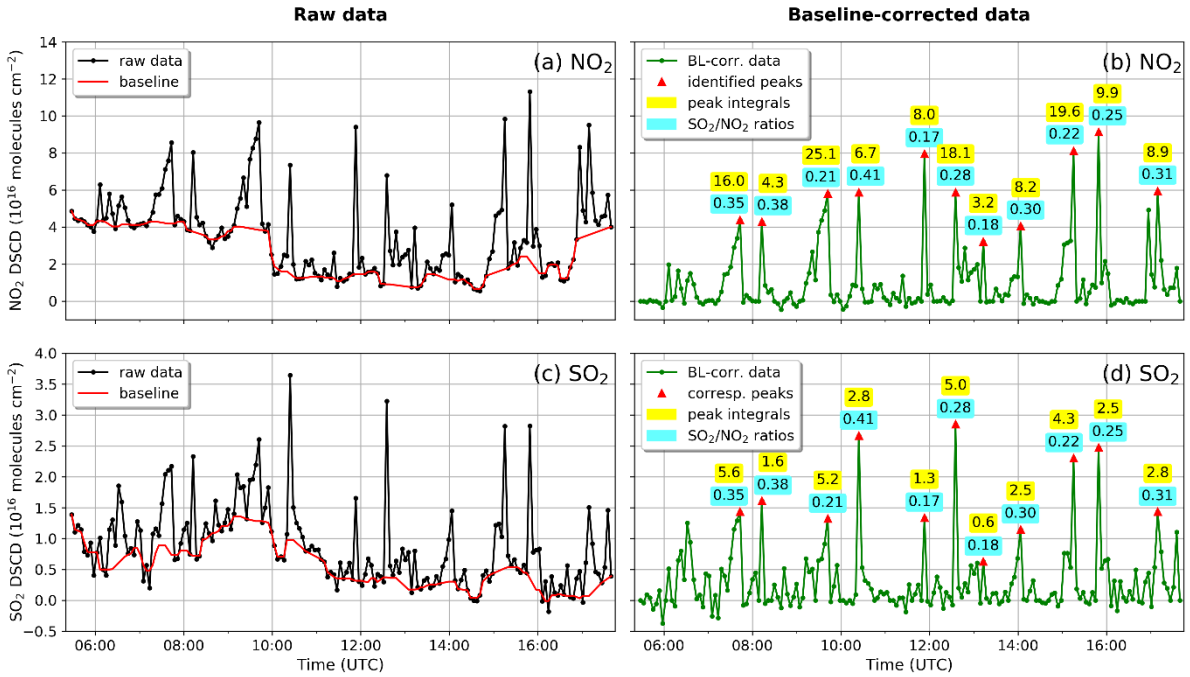

Figure 2-7. Example measurements and calculated SO_2-to-NO_2 ratios in ship plumes on 23 July 2014, before the change in fuel sulfur emission limits. Panel (a) shows the UV NO_2 DSCD raw data for 0.5° elevation and -25° azimuth and the determined baseline. Panel (b) shows the baseline-corrected NO_2 data for which the automatically identified peaks are highlighted with red triangles. Numbers close to the peaks denote the peak integrals in 10^{16} molecules/cm² (marked in yellow) and the SO_2-to-NO_2 ratios (marked in blue). Panels (c) and (d) show the corresponding plots for the SO_2 measurements. (Seyler et al., 2017)

Figure 2-8 shows one example day in summer 2015, after the establishment of stricter sulfur limits. For better comparison to Figure 2-7, the y-axis limits are the same. High NO_2 peaks also occur on this day. The SO_2 signal, however, shows no clearly distinguishable peaks anymore, a result of much less sulfur in the fuel. As a consequence, measured SO_2 to NO_2 ratios are much smaller on this day and range from 0 to 0.09. There might be some small peaks in the SO_2 signal, but with a very low signal to noise ratio. It cannot be determined if these are real enhancements or just noise fluctuations. The two peaks at 10:40 and 14:00 UTC, slightly above noise level but still very small, might be real SO_2 signals from ships with a higher than average fuel sulfur content.

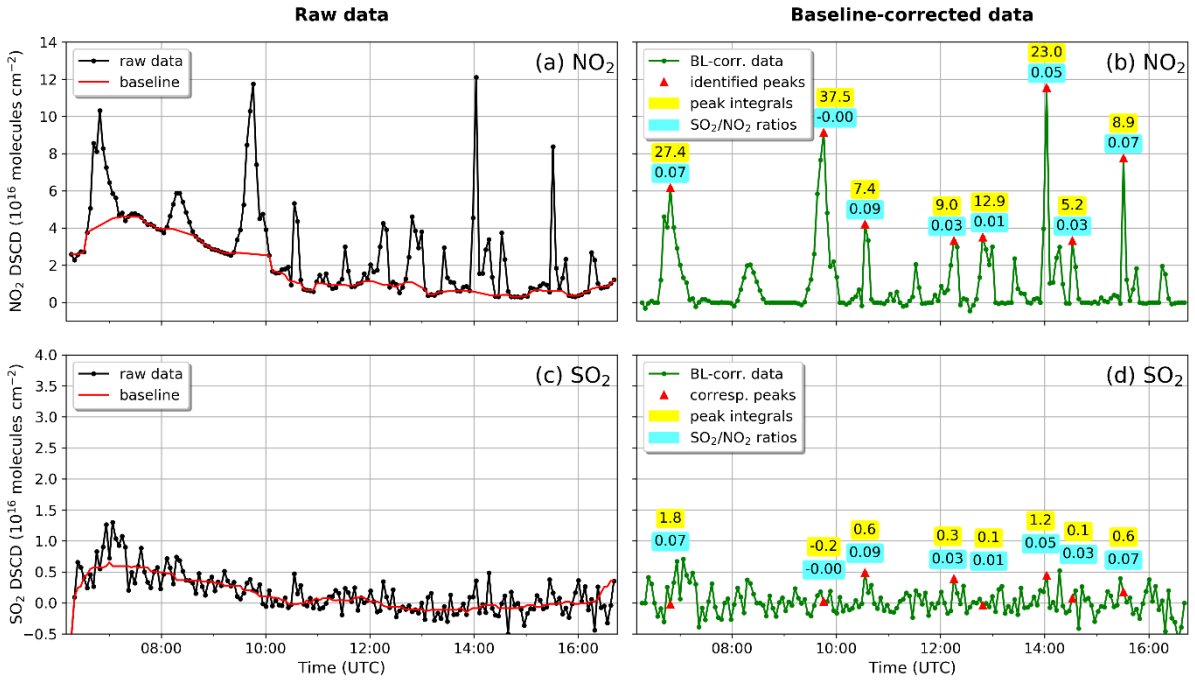

Figure 2-8. As Figure 2-7 but for an example day (3 July 2015) after the introduction of stricter fuel sulfur content limits. Measurements at 0.5° elevation and 65° azimuth are shown. Peak integrals are given in 10^{16} molecules/cm². (Seyler et al., 2017)

For a statistically meaningful comparison of both time periods, two representative samples of over 1050 ship emission peaks each have been selected by hand for days with good measurement conditions, which were identified by using the solar radiation measurement data of our weather station: one sample for 2013 and 2014 representing the state before introduction of stricter fuel sulfur content limits, the second one for 2015 and 2016, representing the situation afterwards. It cannot be ruled out that a certain fraction of ships were measured repeatedly on different days. It is also highly probable that the plumes of some ships were measured multiple times at different locations in the different MAX-DOAS azimuth directions while the ship was passing Neuwerk.

The distributions of in-plume SO_2 to NO_2 ratios derived from the peak integrals for the two samples is shown in Figure 2-9. It can be seen that SO_2 to NO_2 ratios were considerably higher in 2013 and 2014, with a mean of 0.30, a standard deviation of 0.13 and a median value of 0.28. In 2015 and 2016, after the change in fuel sulfur content limits, the SO_2 to NO_2 ratios became much lower with a mean of 0.007, a standard deviation of 0.089 and a median value of 0.013, showing a drastic reduction, which is statistically highly significant.

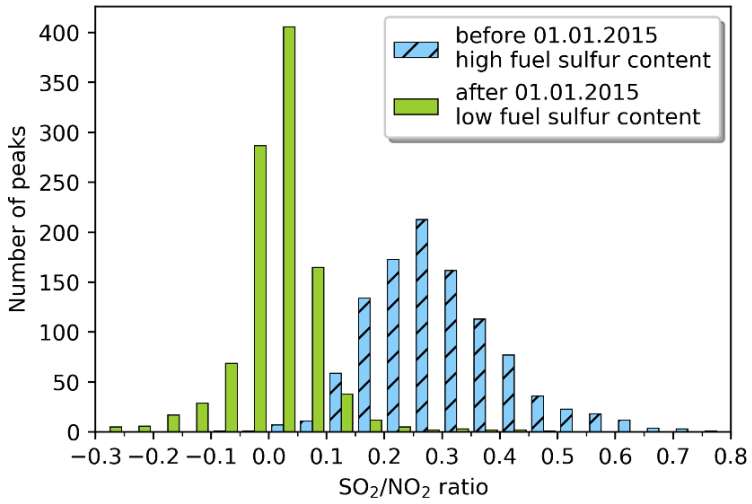

Figure 2-9. Histogram showing the distribution SO_2-to-NO_2 ratios in two samples (*N*=1055 for each) of ship emission plumes measured at 0.5° elevation and all azimuth angles for the time before (blue) and after (green) the change in fuel sulfur content regulation on 1 January 2015. (Seyler et al., 2017)

The overall average SO_2 to NO_2 ratios for all measurements for the days from which the peaks have been selected gives a mean value of 0.10 and a median of 0.17 for the time before 2015. As expected, these values are significantly lower than the in-plume SO_2 to NO_2 ratios as they include both plumes and background pollution, which contains much less sulfur.

It is also interesting to compare our results from 2013 and 2014 with those from other studies, bearing in mind possible systematic deviations due to different measurement geometries, techniques and sites and therefore different NO to NO_2 titration in the plumes.

McLaren et al. (2012) measured NO_2 to SO_2 emission ratios in marine vessel plumes in the Strait of Georgia in summer 2005. In a sample of 17 analyzed plumes, a median molar NO_2 to SO_2 ratio of 2.86 was found. Translated into a SO_2 to NO_2 ratio this yields a value of 0.35 which is, considering the small sample size, in good agreement with our findings for the time before 2015.

Another study was carried out by Diesch et al. (2013) measuring gaseous and particulate emissions from various marine vessel types and a total of 139 ships on the banks of the river Elbe in 2011. SO_2 to NO_2 emission ratios can also be derived from their reported NO_2 and SO_2 emission factors: For small ships (< 5000 tons) a ratio 0.13 and an average fuel sulfur content (FSC) of 0.22%±0.21% was found, for medium size ships (5000--30000 tons) a ratio of 0.24 and a FSC of 0.46%±0.40% and for large ships (> 30000 tons) a ratio of 0.28 and a FSC of 0.55%±0.20%. Especially the values for medium size and large ships fit quite well to our results, while plumes from very small vessels (if measurable at all) have often not been taken into account for the statistic because of the low signal-to-noise ratio.

The strict reduction after 2015 is in good agreement with other studies, for example the results of Kattner et al. (2015) and Yang et al. (2016).

MAX-DOAS NEUWERK: ONION PEELING MAX-DOAS APPROACH

This section is based on Seyler et al. (2019).

O_4 SCALING METHOD

The trace gas columns measured by a MAX-DOAS instrument can be converted to path averaged volume mixing ratios (VMRs) by using the O_4 scaling approach, which uses the oxygen collision complex O_4 as a tracer for the horizontal light path length. O_4 absorbs in similar wavelength ranges as NO_2 in the UV and visible and is retrieved as an essential additional absorber in the NO_2 DOAS fit. As its near surface concentration is known, dividing the measured O_4 DSCD by its number density yield the effective horizontal light path length:

$$L = \frac{\mathrm{SCD}_{\mathrm{O_4,\,horiz}} - \mathrm{SCD}_{\mathrm{O_4,\,zenith}}}{n_{\mathrm{O_4}}} = \frac{\mathrm{DSCD}_{\mathrm{O_4}}}{n_{\mathrm{O_4}}} \quad \text{with} \quad n_{\mathrm{O_4}} = (n_{\mathrm{O_2}})^2$$

Typical light path lengths under clear sky conditions are 10 km in the UV and 15 km in the visible spectral range (Seyler et al., 2017). Dividing the NO_2 DSCD by L gives the path averaged concentration (number density) of NO_2. Diving by the number density of air yields the path averaged volume mixing ratio of NO_2:

$$\mathrm{VMR}_{\mathrm{NO_2}} = \frac{\mathrm{SCD}_{\mathrm{NO_2,\,horiz}} - \mathrm{SCD}_{\mathrm{NO_2,\,zenith}}}{L \cdot n_{air}} = \frac{\mathrm{DSCD}_{\mathrm{NO_2}}}{L \cdot n_{air}}$$

ONION PEELING APPROACH

The wavelength dependence of Rayleigh scattering leads to the fact that the effective light path length in the atmosphere depends systematically on wavelength. Utilizing this, simultaneous measurements in the UV and visible spectral range can be used to separate NO_2 absorptions in different air masses at different horizontal distances to the instrument, making it possible to estimate the distance to the plumes.

The aforementioned O_4 scaling method provides two path-averaged VMRs for each two-channel measurement; one for the shorter UV and one for the longer visible effective

horizontal light path, which are shown in Figure 2-12 as a purple and green line, respectively. A third VMR can be calculated from the difference of the two DSCDs and path lengths

$$\mathrm{VMR}_{@\Delta L} = \frac{\mathrm{DSCD}_{\mathrm{vis}} - \mathrm{DSCD}_{\mathrm{UV}}}{(L_{\mathrm{vis}} - L_{\mathrm{UV}}) \cdot n_{\mathrm{air}}} = \frac{\Delta\mathrm{DSCD}}{\Delta L \cdot n_{\mathrm{air}}},$$

yielding the average VMR along the path difference ΔL, which is shown as an orange line in Figure 2-12b.

A condensed overview of the complete approach is given in the flow charts in Figure 2-10 and Figure 2-11. More detailed information on the approach, including underlying assumptions and uncertainties, can be found in Seyler et al. (2019).

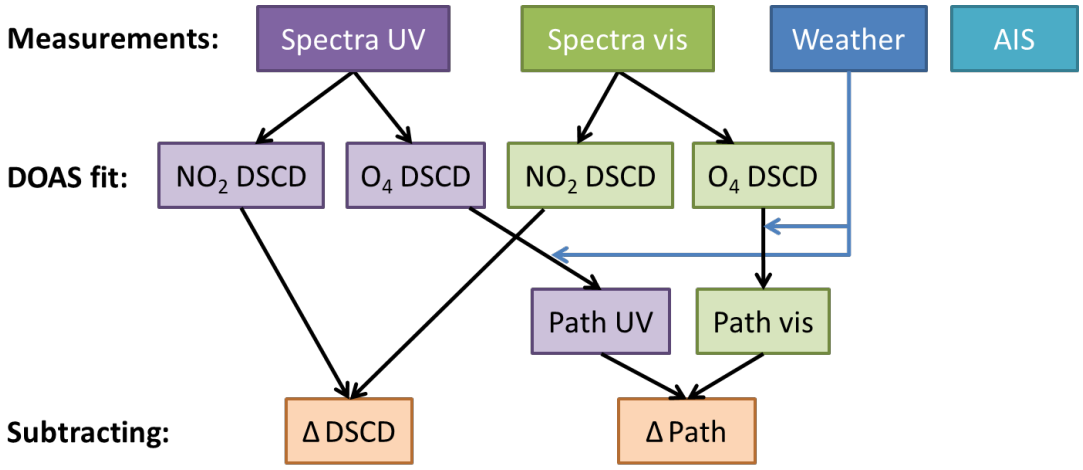

Figure 2-10. First steps of the onion peeling MAX-DOAS approach: One NO_2 DSCD and one O_4 DSCD is retrieved from the spectra measured in the UV and visible spectral range each. The O_4 DSCDs retrieved in the respective wavelength windows are used as a tracer for the light path lengths in UV and visible (so-called O_4 scaling method). ΔPath, in the following called ΔL, is the horizontal path difference. Subtracting the usually lower UV NO_2 DSCD (shorter light path) from the visible NO_2 DSCD delivers the column difference ΔDSCD. This horizontal column difference represents the NO_2 column along the path difference ΔL.

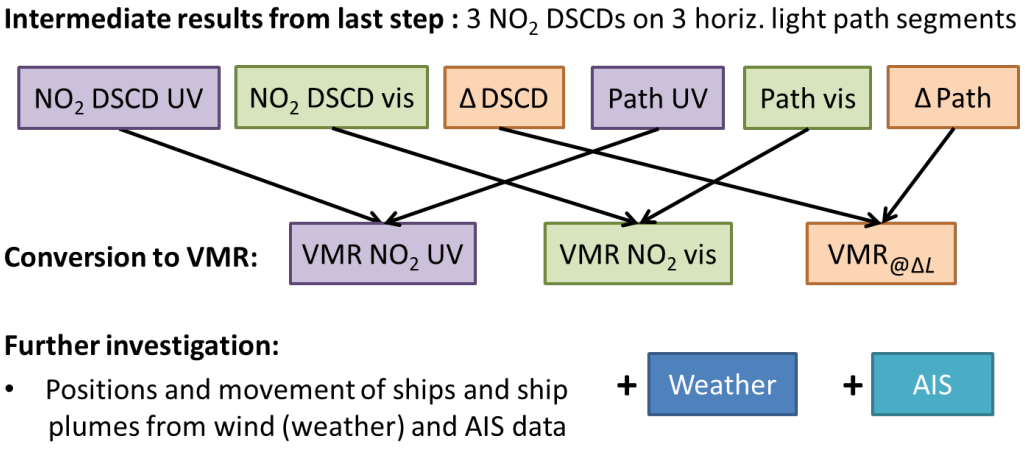

Figure 2-11. Final steps of the onion peeling MAX-DOAS approach: The intermediate results from Figure 2-10 are the NO_2 DSCDs along the UV and visible path as well as ΔDSCD along the path difference. Knowing the NO_2 column along a horizontal path, the average concentration or volume mixing ratio (VMR) along the path can be calculated. This is performed for UV, visible and the path difference Δ*L*, yielding three horizontal path-averaged NO_2 VMRs for the three different horizontal path segments.

PLUME LIGHT PATH GEOMETRY

Figure 2-12b shows the aforementioned horizontal light path segments as colored lines for typical path length values: in green the visible path, in purple the UV path and in orange the path difference Δ*L*. As can be seen from the map, the path segments probe different regions over and around the shipping lane. For example, the path difference Δ*L* (orange line) in the 5° azimuth direction probes an air mass in the north of the shipping lane. For southerly winds, one would not expect any NO_2 emitted from ships on the shipping lane in this air mass. Whereas the UV path in the 310° azimuth direction, for example, only probes air in the south of the shipping lane.

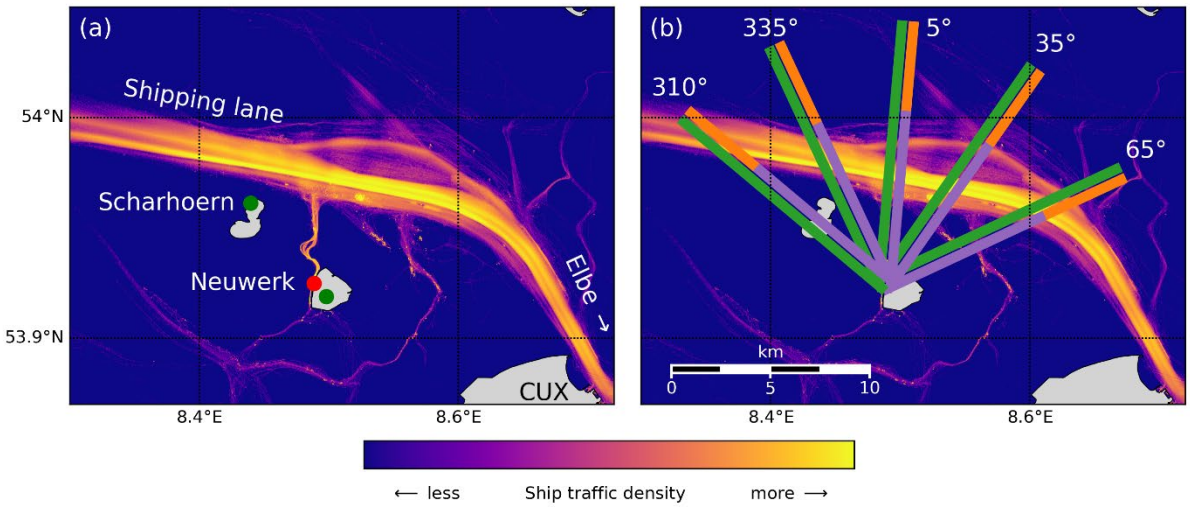

Figure 2-12. (a) as in Figure 2-5, but (b) showing the effective horizontal light paths in UV (purple line) and visible spectral range (green line) for the five azimuthal viewing directions of the MAX-DOAS instrument for typical light path lengths of 9km (UV) and 13km (vis), respectively. The difference between both paths, Δ*L*, is highlighted by the orange line. (Seyler et al., 2019)

As each ship represents a moving point source for NO_x emissions, the NO_2 field over the shipping lane and the whole region is strongly inhomogeneous and the NO_2 is usually not distributed evenly along the light paths. Figure 2-13 sketches the plume light path geometry and the expected NO_2 signal for three different scenarios: In case (a) the plume is close to the instrument and completely covered by both UV and visible path. Although both paths cover the same amount of NO_2, the retrieved path-averaged VMR is higher for the UV signal because of the higher relative contribution of the fraction of the light which probes the NO_2 plume. As there is no NO_2 on the path difference Δ*L*, no NO_2 enhancement is measured there, meaning the NO_2 VMR@Δ*L* is zero or stays on background level. As can be seen form the map in Figure 2-12b, this might occur for northerly wind directions.

Case (b) shows a contrary situation: The plume is far away from the instrument and only covered by the visible path (and therefore also Δ*L*). As a result, the UV instrument measures no NO_2 enhancement while the visible channel shows enhanced NO_2. The path averaged VMR retrieved for Δ*L* is even higher, because Δ*L* is only a small fraction of the complete visible path and therefore represents a shorter averaging length. As the map in Figure 2-12b shows, this might occur for southerly wind directions.

In case (c) the plume is close to the effective last scattering point in the UV, from which the light is scattered into the telescope of the MAX-DOAS. All three path segments measure enhanced NO_2, the relative peak heights depend on the situation.

This means that by comparing the NO_2 signal along the UV path (probing a region close to the instrument) and along ΔL (probing a region further away from the instrument), a rough estimate of the plume position and distance to the site can be obtained.

For the MAX-DOAS measurement geometry presented here, the measured trace gas columns and therefore also path-averaged VMRs depend not only on the emitted amount of NO_2, but also on the angle of intersection between the line of sight of the instrument and the plume. The measured NO_2 signal is larger, when measuring alongside the plume (more absorbing NO_2 molecules on the fixed path length) and much smaller, when the plume runs orthogonal to the line of sight (only a small fraction of the path contains NO_2 from the plume). As already mentioned above, NO to NO_2 titration and therefore the time span between emission and measurement plays also a role.

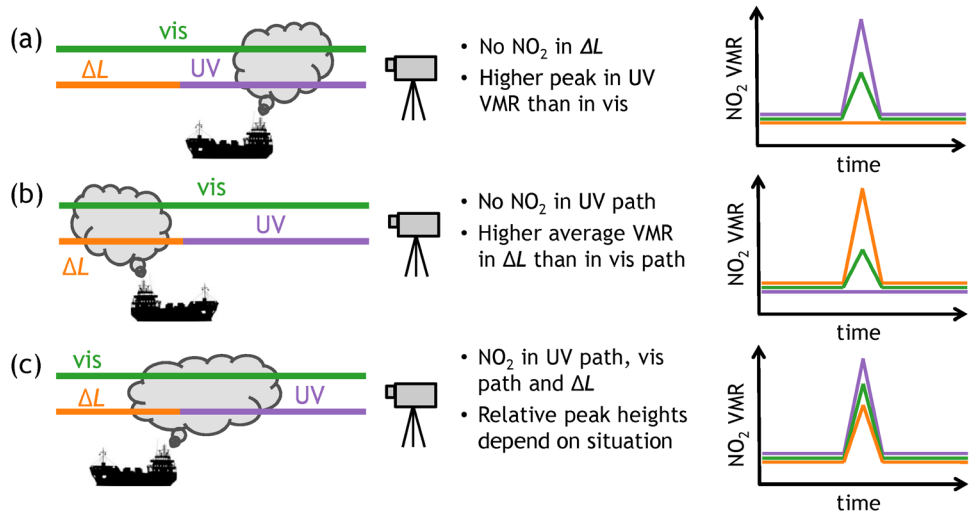

Figure 2-13. Plume–light-path geometry and the resulting path-averaged NO_2 VMRs for three possible cases: when the plume is close to the instrument and completely covered by the UV path (a), when the plume is further away from the instrument than the UV scattering point and is only covered by the visible path (and ΔL) (b) and when the plume is located around the UV scattering point (c). (Seyler et al., 2019)

PLUME TRAJECTORIES

Simple plume trajectories have been calculated as forward trajectories on a 10s time grid. The plumes consist of point shaped plume air parcels. Each time step each plume parcel is moved from its old position to a new position, calculated from wind speed and (horizontal) wind direction. Each ship emits a new plume air parcel at each time step at its respective position. Plume broadening and dilution over time as well as plume rise are neglected and the trajectories are calculated in a two dimensional space without height information. The width of

the plumes shown in the maps is not to scale and follows the simple relationship bigger ship – broader plume. The gray shading of the plumes (Figure 2-14) denotes the plume age.

NORTHERLY WIND SITUATIONS

As can be seen from Figure 2-12, northerly winds blow the ship plumes towards Neuwerk and the measurement site on the radar tower. As the wind is coming from the open North Sea, the ships on the shipping lane should be the only important NO_x emitters in such a case. NO_2 concentrations are expected to be low in the north of the shipping lane and enhanced in the region south of the shipping lane, towards the island.

Figure 2-14 shows a 12-minute sequence of consecutive MAX-DOAS measurements for such a case on 26 May 2014 starting at 12:46 UTC (14:46 local time), plotted as colored lines on a sequence of maps. Shown are the length and location of the UV path and ΔL as colored lines, with color representing the respective path averaged NO_2 VMR. In situ (Airpointer) NO_2 VMRs are shown as colored dots at the measurement site. Shown are also ship positions and course, taken from AIS data, plume trajectories and wind speed and direction.

The sequence shows two ships (magenta triangles) on the shipping lane, moving in opposite directions. The larger ship (351 m) moves westward, the smaller ship (151 m) moves eastward. The fact that the trajectories of the plumes of the two ships run in such different directions, is due to the different movement directions of the ships and the curved course of the shipping lane around the island. For two stationary point sources, like moored or anchoring ships, the plumes would run in parallel.

Panels 1 and 5 show low values on all path segments and also for the in situ measurements indicating that the ambient background NO_2 is homogeneously well-mixed in the boundary layer.

Panels 2 to 4 and Panels 6 to 10 show enhanced NO_2 along the UV path close to the site, likely due to the big ship's plume, and low NO_2 VMRs along ΔL further away from the island. In situ values stay low at first, but begin to rise as the plume reaches the radar tower. Starting with Panel 9 the in situ values are getting much higher than the long path-averaged MAX-DOAS VMRs, because the Airpointer instrument measures the NO_2 VMR directly inside the plume. This is not represented in the figure, as the color scale is saturated.

Panels 11 to 14 show low MAX-DOAS NO_2 VMRs on both path segments, as the plume moved out of the line of sight of the instrument, while the in situ measured VMR is still quite high.

Comparing Panel 6 and Panel 3 demonstrates the aforementioned dependence of the MAX-DOAS VMR on the angle of intersect between plume and line of sight of the instrument.

Figure 2-15 shows the measurements from Panel 6 to 10 in a condensed form, with ship and plume positions for the time of Panel 10. It highlights the strong horizontal gradient between enhanced NO_2 values close to the site and low values further away, right as expected for such a northerly wind situation.

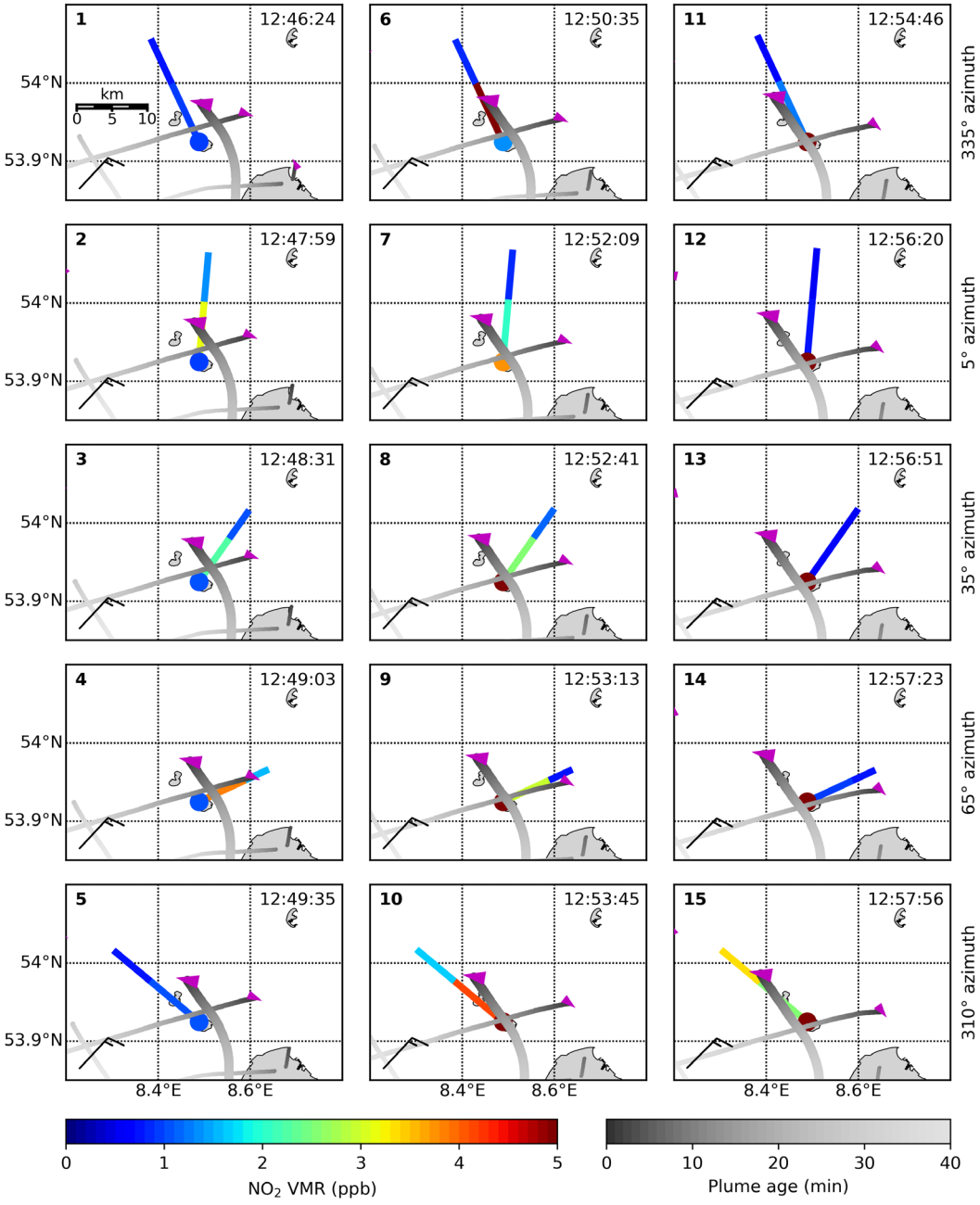

Figure 2-14. Sequence of maps showing 15 consecutive measurements in 0.5° elevation on 26 May 2014, starting at 12:46 UTC (14:46 local time): The extent of the UV path and ΔL and corresponding path-averaged NO_2 VMRs are shown as colored lines. In situ NO_2 VMRs are shown as a colored dot at the location of the measurement site. Magenta triangles show the ship position and course (sharp tip), with larger triangles for larger ships. Grey point clouds show forward trajectories of the emission plumes calculated from wind speed and direction for the moving ship. Wind direction and speed is shown with meteorological wind barbs. (Seyler et al., 2019)

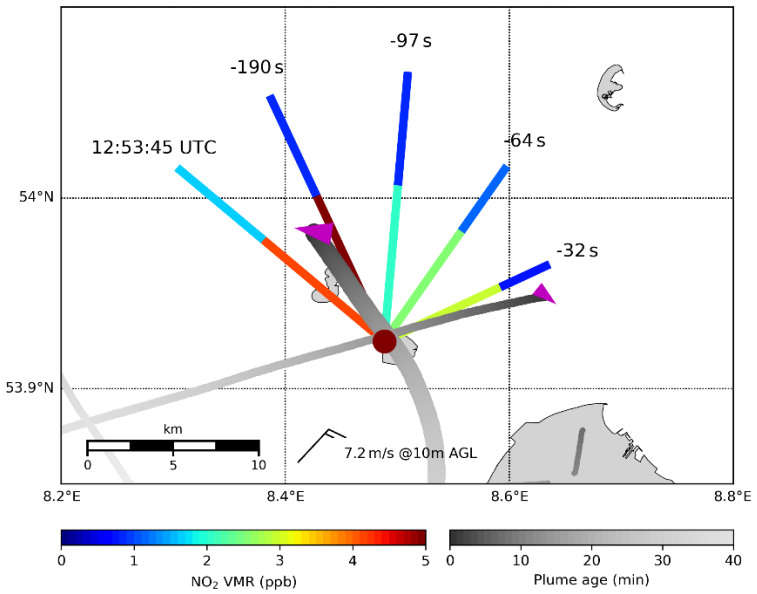

Figure 2-15. As Panel 10 of Figure 2-14, but including the four previous MAX-DOAS measurements, being measured between 30 seconds and 3 minutes before the current observation. Please keep in mind that ship and plume position were different for the additionally shown earlier measurements. (Seyler et al., 2019)

SOUTHERLY WIND SITUATIONS

A reverse situation occurs for southerly winds, which blow the ship plumes to the north of the shipping lane, further away from the measurement site. NO_2 values south of the shipping lane, close to the instruments, should be lower than in the north of the shipping lane. How low, depends on the ambient background pollution from land-based sources, which is present on this site for such wind directions.

Figure 2-16 shows the MAX-DOAS and in situ NO_2 measurements as well as ship positions and plume trajectories on 13 August 2014 at 12:47 UTC (14:47 local time), in a similar way to Figure 2-15. Not only the current MAX-DOAS measurement, but also the 4 previous measurements in the other azimuthal viewing directions are shown, taken between 30 seconds and 4 minutes before.

The map shows three ships on the shipping lane, two big ships (336m and 365m) and one smaller ship (100 m). As all ships move in the same, eastward, direction, the plume trajectories run almost parallel. The additional broad plume in the west of Scharhörn originates from the two coal-fired power plants in Wilhelmshaven, approximately 50 km southwest of Neuwerk, which crosses the measurement region for this prevailing wind direction. Taking into account the 10 m above ground layer (agl) wind speed of (7.5 ± 1.0) m/s, the plume age is approximately 110 minutes, even less taking into account that wind speed increases with height.

As can be seen from the map, enhanced NO_2 VMRs are measured along ΔL, far away from the instrument, northward of the shipping lane, where the plumes of the two big ships are

located. The slightly enhanced NO_2 values along ΔL in the northwestward viewing directions indicate that the plume of the Wilhelmshaven power plants can still be measured in this distance from the plants and has an influence on the air quality in this region for such wind conditions. Low NO_2 VMRs are measured along the UV path, close to the site, representing ambient background NO_2 levels. In this situation, the Airpointer in situ instrument measured constantly low NO_2 values, agreeing very well with ambient NO_2 VMRs from the MAX-DOAS retrieved south of the shipping lane along the UV path. Under such southerly wind conditions the Airpointer cannot detect ship emission plumes at this site, because the plumes are blown away to the north of the shipping lane.

This demonstrates that with MAX-DOAS it is well feasible to detect ship emission plumes under conditions unfavorable for in situ measurements.

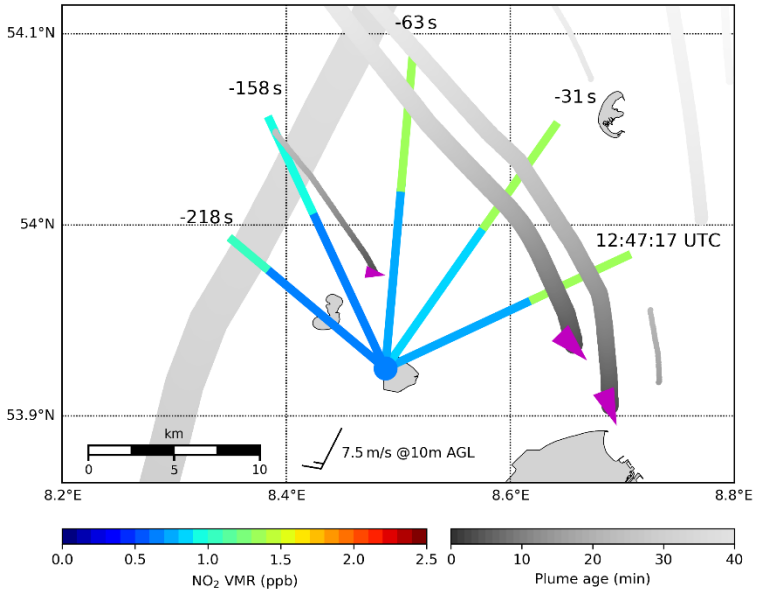

Figure 2-16. Map showing the MAX-DOAS measurements in 0.5° elevation on 13 August 2014 at 12:47 UTC (14:47 local time). The extent of the UV path and ΔL and corresponding path-averaged NO_2 VMRs are plotted as colored lines. The four previous MAX-DOAS observations, being measured between 30 seconds and 3.5 minutes before, are also included. In situ (Airpointer) NO_2 VMRs are shown as a colored dot at the location of the instrument. Magenta triangles show the ship position and course, with larger triangles for larger ships. Gray stripes show forward trajectories of the emission plumes calculated from wind speed and direction for the moving ship. The broader plume in the eastern part of the map originates from the Wilhelmshaven power plants. Please keep in mind that ship and plume position were different for the past measurements. Wind direction and speed is shown with a meteorological wind barb. (Seyler et al., 2019)

COMPARISON TO AIRBORNE IMAGING DOAS MEASUREMENTS

The plume position derived from the onion peeling MAX-DOAS can be validated with a comparison to air-borne imaging DOAS measurements, which map the NO_2 field of the plume from above. As the spatial resolution of satellite instruments is not sufficient to resolve individual

ship plumes, airborne imaging DOAS measurements as a middle ground between satellite and ground-based measurements are the ideal method to compare to, at least on a campaign base, since they can deliver high resolution NO_2 maps of the plumes. Such measurement have been performed with the AirMAP instrument onboard a Cessna from the FU Berlin during the NOSE (Nord-Ost-See-Experiment) campaign on 21 August 2013. The AirMAP measurements provide the vertical NO_2 column below the airplane, as it is sketched in Figure 2-17 comparing the different measurement geometries.

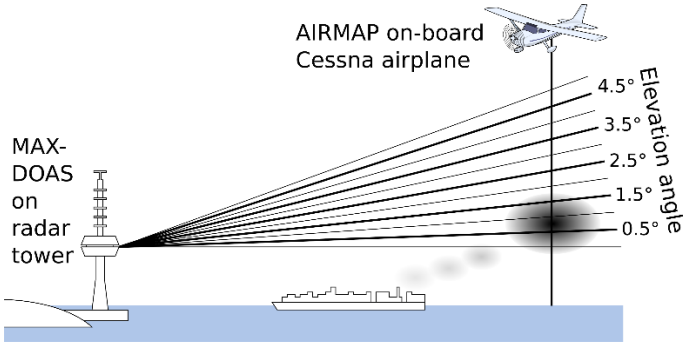

Figure 2-17. Sketch of the different measurement geometries of ground-based MAX-DOAS and airborne imaging DOAS instrument when measuring a ship plume. The MAX-DOAS instrument measures (slightly slanted) horizontal transects of the plume. The AirMAP instrument, measuring in nadir direction downward from the aircraft, observes vertical transects of the plume. Distances, heights and sizes are not to scale.

Two example results are shown in Figure 2-18 a and b.

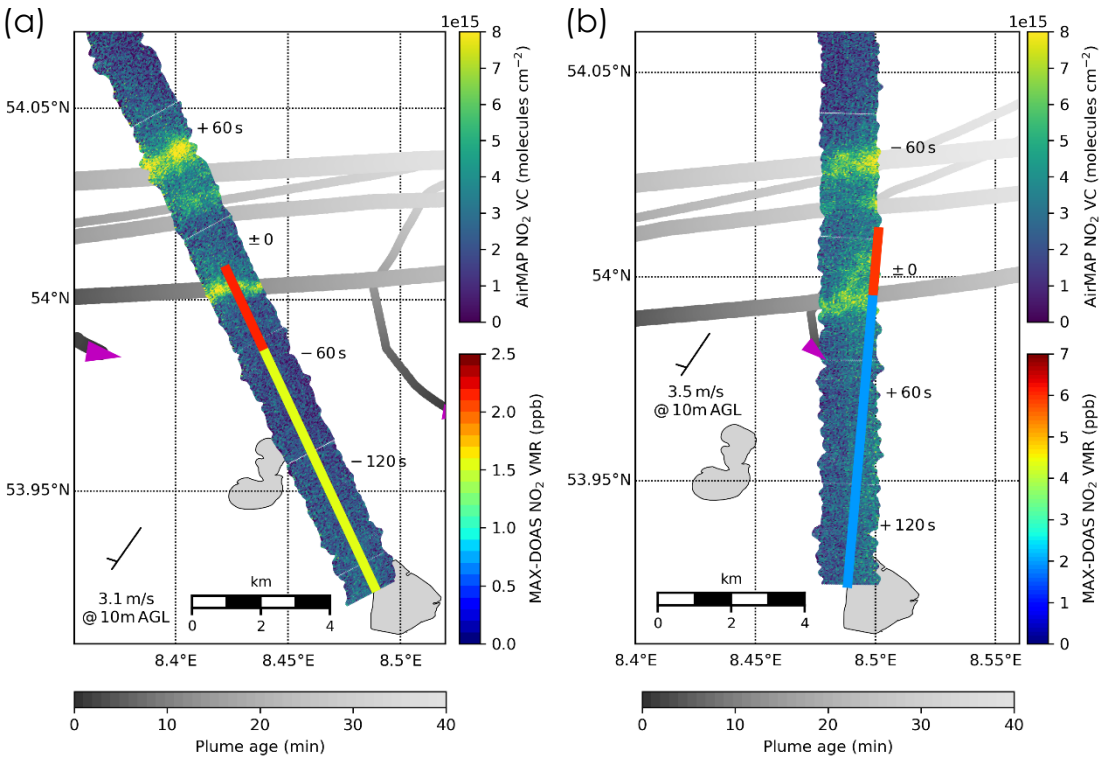

Figure 2-18. Map showing the MAX-DOAS path averaged VMRs (colored lines) and AirMAP vertical columns of NO_2 (broad image stripe beneath) on 21 August 2013 around 9:53 UTC (11:53 local time) (a) and 9:43 UTC (11:43 local time) (b). Magenta triangles show current ship positions and course. Grey stripes show forward trajectories of the ship emission plumes calculated from wind speed and direction for the MAX-DOAS measurement time. The time difference between AirMAP and MAX-DOAS measurements and therefore the time difference between AirMAP and plume locations is indicated in the map at specific parts of the flight track. Wind direction and speed is shown with a meteorological wind barb. (Seyler et al., 2019)

As can be seen from the figures, AirMAP measured enhanced NO_2 values at the projected location of the plumes, confirming the approximate plume position derived from the onion peeling MAX-DOAS.

The good agreement of AirMAP measured and MAX-DOAS derived plume positions shows that MAX-DOAS measurements can be used to detect and derive the approximate position of the emission plumes. The very good agreement of plume trajectories calculated from wind and AIS data with the AirMAP measurements shows that the simple forward trajectories already provide a good accuracy to model the two-dimensional NO_2 field over the shipping lane.

For a more detailed analysis of the MAX-DOAS and AirMAP comparison including the retrieved in-plume NO_2 VMRs see Seyler et al. (2019).

MAX-DOAS WEDEL

A detailed description of the MAX-DOAS used in Wedel can be found in Seyler, 2014. Since May 2013 the instrument is measuring NO_2 and SO_2 at this site. The same instrument has been used in particular within MeSmarT-I during several ship cruises (see report on MeSmarT-I) which leads to several data gaps in the time series. However, in total on 1387 from 2373 days the MAX-DOAS was fully operational in Wedel. The plan is to continue this time series for the next years in order to monitor possible trends e.g. due to future regulation activities on shipping emissions. These activities are then carried out by the IUP Bremen with financial support of related projects like CLINSH and with logistical support of the BSH and the WSA Hamburg.

One of the main objectives of MeSmarT was to find out whether the MAX-DOAS observations could be used to support compliance monitoring of single ships. As pointed out in the description for the MAX-DOAS measurements from Neuwerk, in principle the SO_2/NO_2 ratio holds information on the Sulphur content. Beside all the difficulties and assumptions needed to conclude from the ratios on possible violations of SFC regulations for single ships already described above, the situation in Wedel is even more challenging.

These difficulties are described best by discussing the following two figures.

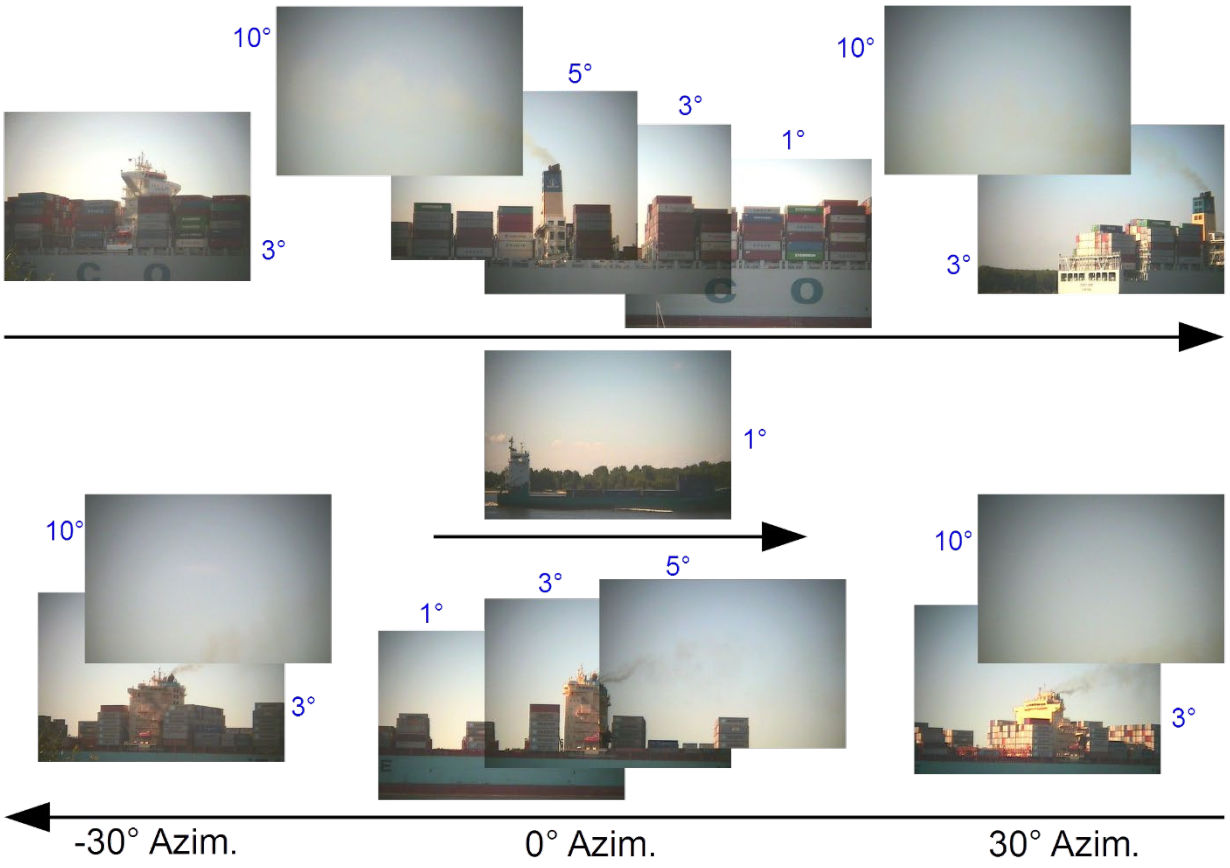

Figure 2-19: Snapshots from three different ships taken at various azimuth and elevation angles with the video camera included in the MAX-DOAS telescope in Wedel.

Figure 2-19 shows some images taken from the video camera included in the MAX-DOAS telescope in Wedel. These pictures illustrate how close the ships are passing the instrument. It also demonstrates that the line of sight (LOS) for large ships in the lowermost elevation angles is covered by the hull and superstructures of the ships and therefore the light path is blocked and significantly shortened. Exhausted ship plumes are also clearly visible in the images, which means that with this short distance the MAX- DOAS instrument measures frequently through the recently emitted plumes when most of the emitted NO_x is still not titrated to NO. Therefore, one can expect a huge range of SO_2/NO_2 values from the same plume depending on the exact light-path. A detailed statistical analysis has been carried out, taking into account meteorological parameters like wind speed and direction, solar intensity, temperature, but none of them could be used to get a reliable and clear correlation of calculated ratios to the SFC.

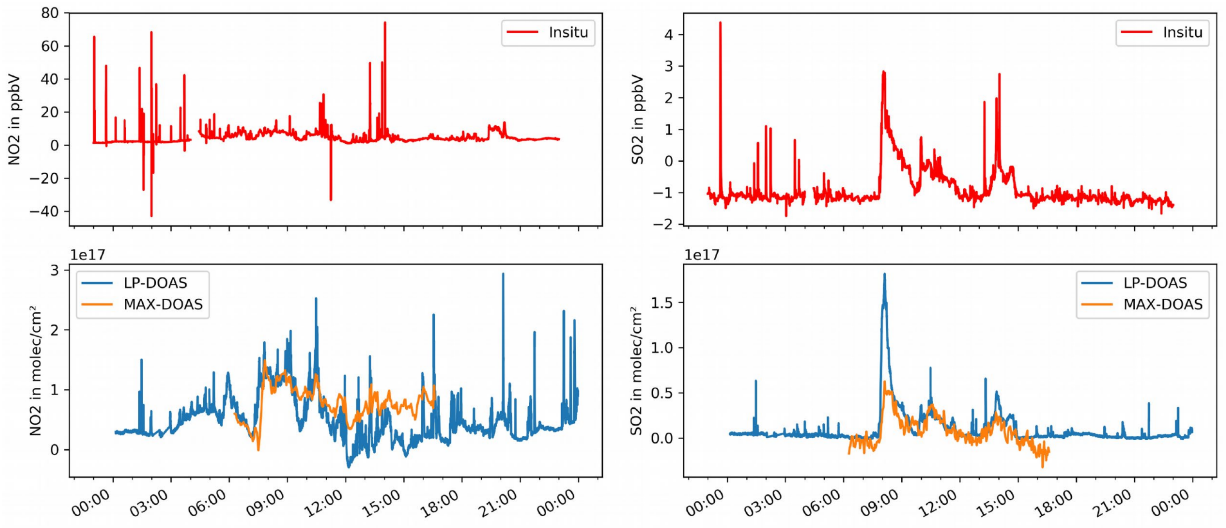

Figure 2-20: Comparison of measurements for NO_2 (left panels) and SO_2 (right panels) from in situ, LP-DOAS and MAX-DOAS instruments in Wedel.

Figure 2-20 illustrates another reason that for the station Wedel a simple ratio of SO_2/NO_2 cannot be used to get an indication for the Sulphur content in fuel. While the SO_2 measurements agree quite well between the different instruments, the NO_2 values of the MAX-DOAS show smoother peaks but a much higher variability in the baseline. This is due to the fact that in this case the in comparison to the OP-DOAS much longer light-path of the MAX-DOAS is affected by other NO_x sources nearby (local traffic, industry,…).

SATELLITE-DOAS

UV-visible satellite instruments in low earth orbits can provide global observations of a number of trace gases including key species for tropospheric pollution from ships: nitrogen dioxide, sulphur dioxide and formaldehyde. They also can provide measurements of aerosol optical depth, which is linked to the atmospheric abundance of aerosols and their optical properties. Satellite observations are therefore at least in principle interesting tools for monitoring of ship

emissions in areas where there are no or not enough ground-based measurements available such as remote oceanic regions.

POTENTIAL AND LIMITATIONS OF SATELLITE OBSERVATIONS

The measurement principle of UV-visible satellite observations is the same as for other passive remote sensing methods such as MAX-DOAS: Scattered sunlight is used as the light source, trace gas specific absorption structures are used for the identification and quantification of absorption, and the length of the light path needs to be corrected by using radiative transfer modelling. Compared to the MAX-DOAS measurements used for quantification of ship emissions in this project, there are however three significant differences in satellite data: a shorter measurement time, a different observation geometry, and a larger measurement volume.

Because of the rapid movement of a satellite, the measurement time of a space-borne instrument needs to be short in order to limit the amount of averaging along track. Typical integration times are 1 second, which limits the signal to noise ratio of an individual satellite observation in spite of the high throughput and quantum efficiency of the instruments. Thus, averaging over larger areas or longer time periods is needed to detect small signals. As low earth orbit satellites provide only one measurement of a certain location per day (at least for low and mid-latitudes), averaging reduces time resolution quickly to monthly or seasonal values.

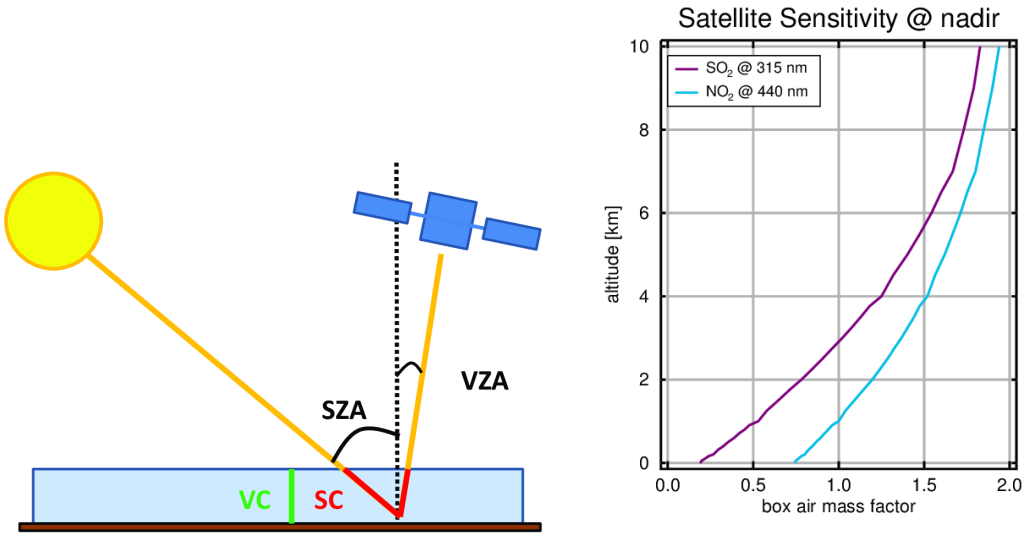

Figure 2-21: Left: Sketch of satellite viewing geometry. Right: Example for sensitivity of satellite observations of NO_2 and SO_2 as a function of altitude. The sensitivity in the lowest 200 m is in case of SO_2 less than 25%!

Satellite measurements of tropospheric composition are performed in nadir viewing geometry, and with this set-up, the geometric light path through a ship plume is relatively short even under ideal conditions where all light is reflected at the surface. In practice, the ocean surface is very dark, absorbing most of the photons, and light detected by a satellite is to a large fraction scattered on air molecules, partly above the ship plume. This leads to a reduction in

the sensitivity of the measurement towards the surface as shown in Figure 2-21. The effect is stronger towards the UV as Rayleigh scattering increases, resulting in low sensitivity of satellite observations of SO_2 close to the surface. The sensitivity further decreases in the presence of aerosols and clouds, the latter effectively blocking any view on pollution below them from the satellite view.

Because of the observation geometry from space, and with the need for global coverage, the foot print of satellite observations on the Earth's surface is large compared to ground-based measurements. Pixel sizes are of the order of 40 x 80 km^2 for the GOME2 instruments and 3.5 x 7 km^2 for the most recent TROPOMI instrument on Sentinel 5 precursor (S5P). When trying to measure local emissions such as from a ship, the size of the averaging volume leads to a large reduction in signal. As an estimate for the order of magnitude, an idealised ship plume extending for 7 km in the across-track direction of the satellite pixel and having an average width of 200 m fills only 6% of an S5P pixel. In combination with the dilution of the signal in the widening plume, this currently prevents the detection of individual ship plumes from satellite data.

As result of the viewing geometry, satellite measurements integrate over the signal from the full atmosphere. It is therefore not straight forward to separate signals from the stratosphere, the background troposphere, transport from land-based sources and ships. One approach to separate the signals is to apply spatial high-pass filtering. With this method, shipping signals can be extracted where ships travel along narrow, well defined routes. However, the cut-off selected for the filtering impacts on the magnitude of the shipping signal retrieved. As a result, such maps are well suited for the detection of shipping signals but less so for the quantification of emissions.

SUMMARY OF SATELLITE MEASUREMENTS OF SHIP EMISSIONS IN THE LITERATURE

The first satellite detection of NO_2 from ships was reported for the region between India and Indonesia in GOME data (Beirle et al., 2004) and for the Red Sea in SCIAMACHY data (Richter et al., 2004). Also for the Indian Ocean, formaldehyde (HCHO) could be detected over shipping lanes in GOME data (Marbach et al., 2009). Combining GOME and SCIAMACHY data, a link could be established between changes in shipping transport volume and NO_2 levels over shipping lanes (de Ruyter and de Wildt, 2012). An increase in shipping NO_2 had earlier already been reported for the Indian Ocean region using GOME, SCIAMACHY and GOME-2 data (Franke et al., 2009). In GOME2 observations, additional NO_2 shipping signals in the Mediterranean, around the Iberian Peninsula and around the African continent could be identified (Richter et al., 2011). The OMI instrument provides data with much better spatial resolution than that obtained by GOME, SCIAMACHY and GOME2. In OMI data, NO_x ship emissions along the coast of China could be determined (Mijling et al., 2012), ship emissions in European Waters were quantified (Vinken et al., 2014), ship emission in the Baltic Sea were detected (Ialongo eA det al, 2014) and a link was drawn between slow steaming of ships in the Mediterranean and the amount of NO_x emitted (Boersma et al., 2015). In long-term averages of OMI data, even indication for enhancements in SO_2 signals in the Strait of Gibraltar and in the Red Sea could be found where also NO_2 is enhanced (Theys et al., 2015).

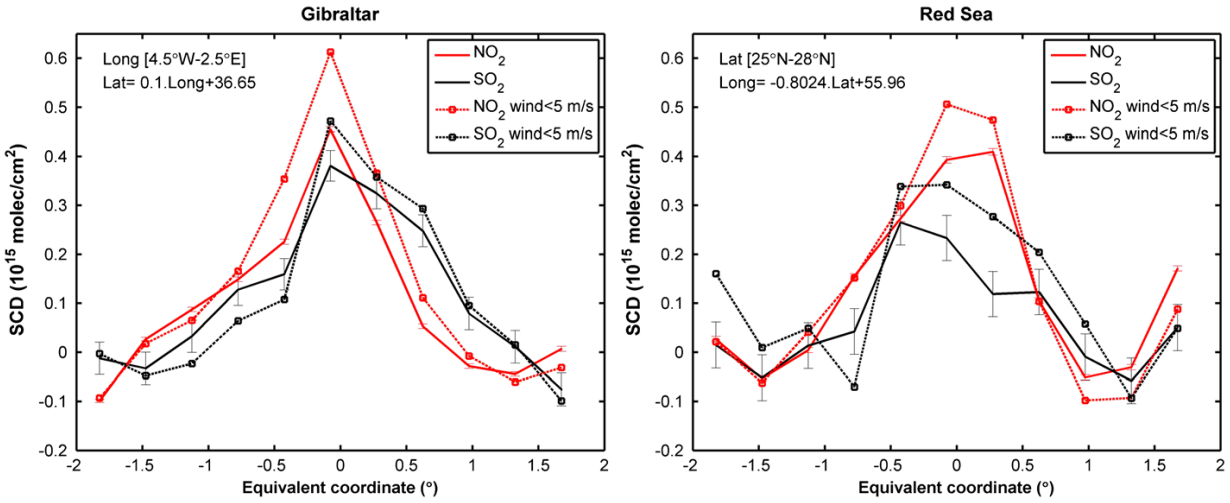

Figure 2-22: Adapted from Theys et al., 2014. OMI multiannual-averaged (2005 to 2009) slant columns of SO_2 (black) and tropospheric NO_2 (red) along ship tracks ((left)strait of Gibraltar and (right) Red Sea). The slant columns are shown as a function of the equivalent coordinate (distance in degree from the shipping lane), and first-order polynomial fits are subtracted from the averages. The error bars represent the errors on the mean SCDs, i.e., the standard deviation divided by the square root of the number of observations. Note that the error bars for the low wind speed values are not shown for better readability.

THE TROPOMI INSTRUMENT ON SENTINEL-5 PRECURSOR

In October 2017, the European Sentinel 5 precursor satellite was launched with its only payload TROPOMI on board. The TROPOMI instrument (Veefkind et al., 2012) is in many respects similar to the OMI instrument. It is a nadir viewing imaging grating spectrometer with a wide swath (2600 km) and an early afternoon orbit, resulting in near global coverage every day. The instrument covers the UV and visible spectral ranges up to 490 nm for O_3, SO_2, NO_2, HCHO, H_2O, BrO and other trace gases and addition small channels in the NIR and SWIR for clouds, CO and CH_4 retrievals. The main advantages of the TROPOMI instrument are its very good signal to noise ratio and the small ground pixel size, which for NO_2, HCHO, and SO_2 is 3.5 x 7 km^2, much smaller than for any other passive UV-vis instrument. In August 2019, the ground-pixel size was further decreased to 3.5 x 5.5 km^2. Data from TROPOMI is freely available via the Copernicus Open Access Hub (https://scihub.copernicus.eu/).

SOME TROPOMI NO_2 RESULTS

The standard IUP-UB DOAS NO_2 retrieval was applied to 7 months of TROPOMI nadir observations. The resulting data were filtered for clear-sky scenes applying a cloud threshold of 20%. In order to account for the light path length, a simple air mass factor was applied assuming a surface reflectance of 5% and a well-mixed boundary layer of 600 m depth containing all the NO_2. On the resulting average NO_2 map, the continental regions were masked out and a high pass filter with a 1° threshold was applied to extract the shipping signal. The resulting map for Europe is shown in Figure 2-22. The shipping lane through the Mediterranean, passing the Strait of Gibraltar and around the Iberian Peninsula towards the

English Channel can clearly be seen. There are also smaller signals through the Baltic Sea and the Black Sea. All these shipping lanes have already been detected in earlier measurements from SCIAMACHY, GOME2 and OMI, but not in this clarity and not using only little more than half a year of data.

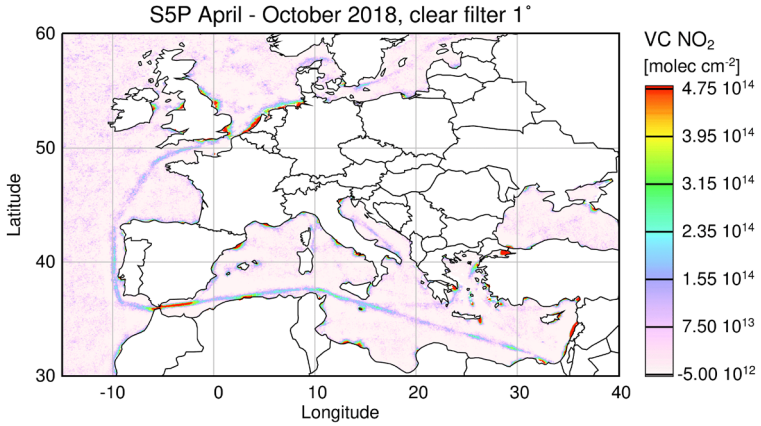

Figure 2-23: High pass filtered 7 month average of tropospheric NO_2 columns from TROPOMI over Europe. Only clear-sky observations were used and a spatial filter of 1° was applied.

Using a lower threshold of 0.3° for the spatial filter, additional shipping lanes become visible in the Mediterranean as shown in Figure 2-23. However, this reduces the magnitude of the signal and increases noise levels. NO_2 from ferries to Corsica and Sardinia as well as from ships servicing harbours in Italy and heading to and from the Bosporus can be identified. This level of detail is unprecedented in satellite data.

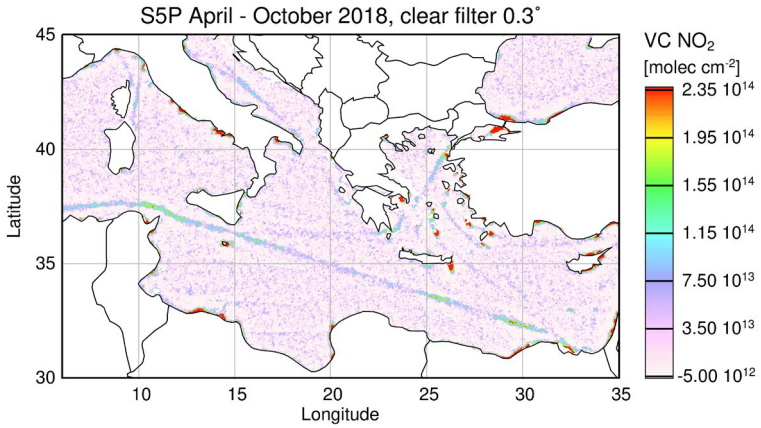

Figure 2-24: High pass filtered 7 month average of tropospheric NO_2 columns from TROPOMI over the Mediterranean. Only clear-sky observations were used and a spatial filter of 0.3° was applied, revealing additional ship tracks when compared to Figure 2-22.

As briefly discussed above, the sensitivity of satellite observations is limited by the degree to which light from the boundary layer is scattered back to the satellite. It is also limited by dilution in the relatively large measurement volume. In order to investigate options to improve the

signal by selection of advantageous measurement situations, a sensitivity study was performed on the shipping lane between the southern tip of India and Indonesia, the strongest shipping signal worldwide. Four different data sets were created and are compared in Figure 2-24: an analysis using all data (red), a data set using only clear-sky observations (blue), a data set limited to measurements having a sun-glint geometry where much more light is reflected from the surface than normally (green) and finally a data set including only measurements at relatively low wind speeds (< 7m/s in ECMWF surface wind speed; brown). The results show that in all cases a clear NO_2 enhancement can be detected in the shipping lane. The small negative overshooting to the sides of the shipping lane is a result of the spatial filtering. The difference between using all data and only cloud free data is surprisingly small, a result already found in data of other satellite instruments. This is probably caused by vertical mixing of NO_2 into and above clouds where it is highly visible for satellite instruments. Limiting the analysis to situations where sun-glint increases the sensitivity to NO_2 close to the ocean surface, leads to a higher signal as expected. At the same time, the noise increases due to the reduced number of measurements contributing to the average. Selecting for calm wind situations further increases the signal, but also results in even larger noise levels.

The methods tested for improving detection sensitivity thus have proven to be all effective as expected. However, the increase in noise limits the usability for smaller signals where more averaging is needed. Also, neither the sun glint geometry nor calm wind situations are often found in Northern European waters and therefore this approach cannot be extended to the German Bay or the Baltic Sea.

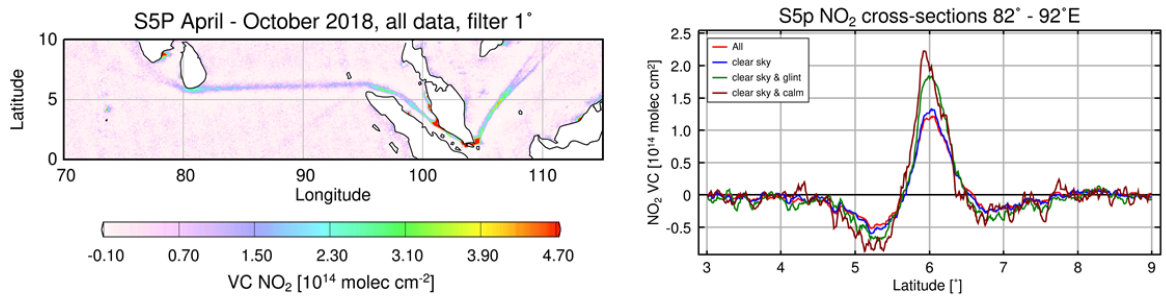

Figure 2-25: Change in shipping signal for the region between India and Indonesia (left) when using all data (red), only clear-sky data (blue), only data with sun-glint geometry (green) and using only data under calm wind conditions (brown) (right).

SUMMARY OF SATELLITE MEASUREMENTS

In summary, satellite measurements show shipping signals in maps of NO_2, HCHO and to some degree also SO_2. The signal is best for NO_2, where many shipping lanes can be identified in monthly and annual averages. The new TROPOMI instrument with its much improved spatial resolution can detect additional shipping lanes and needs much less averaging than previous satellite data sets, resulting in impressive maps of ship emissions of NO_x. However, fundamental limitations such as the low temporal sampling (once per day), relatively low sensitivity towards

pollution close to the surface and the large ground pixel size limit the usability of satellite data for quantitative emission control.

WORK PACKAGE 3 – NETWORK FOR COMPLIANCE MONITORING

TRANSFORMATION TO OPERATIONAL FSC MONITORING STATIONS

A major aspect of the MeSMarT-I project was the assessment of measurement techniques with respect to establish a permanent monitoring station for the operational FSC compliance monitoring. This could be realized based on the work within MeSMarT-II and was mainly carried out as part of the PhD thesis by Lisa Kattner (2019).

In Germany, the BSH is the responsible authority for all matters in the maritime sector, including the implementation of IMO regulations and legal prosecution of minor offences like violations according MARPOL Annex VI (limitation of FSC). Therefore, the development of a monitoring station for FSC was part of the joint research projects MeSMarT-I and MeSMarT-II.

With their ability to directly assess the FSC by measuring SO_2 and CO_2 in a plume, in situ instruments are usually the most suitable measurement option. However, it is crucial to have a location for the measurement station, which is located downwind the shipping lane in a distance shorter than 1 km to the ships of interest. A low background pollution is important for the correct analysis of peaks and to separate ship plumes from background variability and other combustion sources. With this study, both the suitability of the in situ instruments and the measurement site of Wedel could be thoroughly proved. The next step to a permanent monitoring station was the automation of the analysis, the allocation of measured plumes and the reporting of possible non-compliant ships.

AUTOMATION OF NON-COMPLIANT SHIP IDENTIFICATION

The automation of the analysis has been developed for the usage of the BSH alongside with the data accumulation for MeSMarT. In February 2017 the software was completely transferred to the BSH for their own further use and further development (e.g. adaptation to new sites).

From the Horiba instrument at the measurement station in Wedel, a file with all the measurement data is generated every hour. It is transferred automatically via internet connection to a BSH server. The MATLAB analysis code continuously checks the availability of a new file via the timer function by comparing the existing files with an internally generated list of already analyzed files. If a new file is available, it is analyzed together with the two previous files for peaks as described in detail in Kattner (2019). Using the two previous files generates an overlap, which is important to avoid the cut off of peaks at the end of a file. If a peak is found, its time stamp is compared to previously found peaks to avoid double analysis within that overlap time. The FSC is calculated for each peak form the measured SO_2 to CO_2 mixing ratio. If an exceedance is found and the ship allocation was successful, an automatically generated E-mail is sent to the responsible BSH scientist for a manual check of both the FSC and the ship assigning. This ensures an additional step of quality control, before the E-mail is forwarded to the responsible authorities (Port State Control and waterways police). In the next step the authorities use this information as initial suspicion (clear ground) for further inspection related to a minor offence or a criminal act of the responsible ship. The time it takes for the hourly analysis, the subsequent manual check and the notification of the police is typically between

two and 20 hours. This is usually enough time for the police to be able to access and check the ship during its berth duration of 24 to 72 hours, but it is not always enough time to acquire a sample of the same fuel which was used while passing the measurement station. This could result in false positive notifications, since the legal prosecution can only take place based on exceedances in fuel samples.

The procedure described with notification of the waterways police is of course only feasible for ships entering Hamburg harbor. If a ship is measured with an exceeding FSC while leaving Hamburg harbor, the responsible authority of the destination harbor is informed, if this destination is within the European SECA.

NEW MEASUREMENT SITES

Based on the successful operation of the measurement station in Wedel and supported by the experience and practical knowledge acquired during the MeSMarT projects, two additional ship emission monitoring stations have been set up by the BSH. The identification of possible measurement locations was supported by preceding test measurements with a laboratory van of the University of Bremen (see next section).

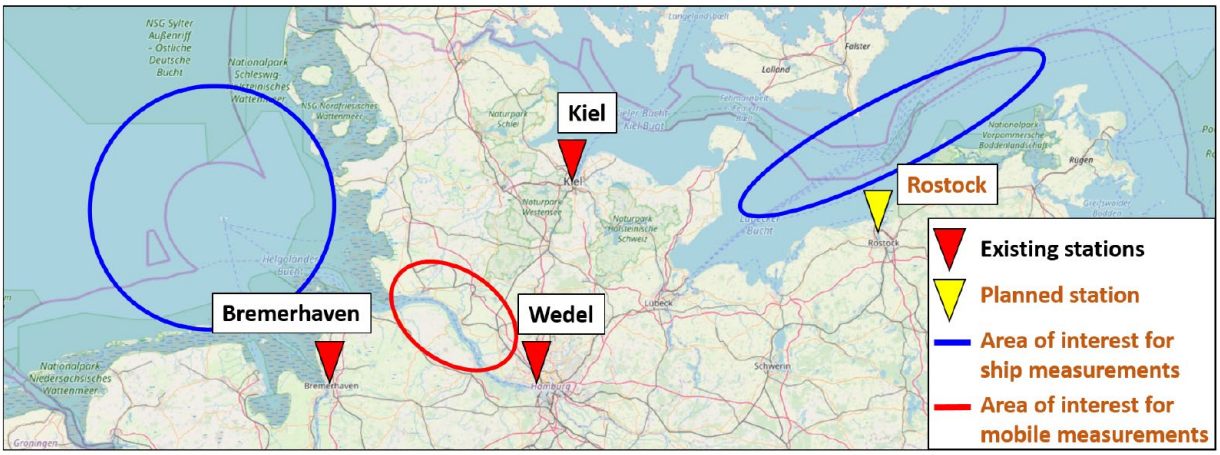

Figure 3-1: German ship emission monitoring network operated by BSH. While red triangles show locations of existing land based measurement sites, the yellow triangle and blue circles indicate potential locations of new measurement stations.

In June 2017, a station in Bremerhaven, the second largest harbor of Germany, was set up at the northernmost edge of the container terminal, where all ships entering the harbor and the Weser river in general are passing by. The implementation of this site was supported with parallel measurements of the IUP Bremen mobile lab (detailed report in Ochtmann, 2017, in german). The third German measurement station was set up in May 2018, in a military area at the east coast of the Kiel Fjord. The station is located about 4 km north of the entrance to the Kiel Canal, which is one of the world's busiest canals. With favorable wind conditions all ships entering or leaving the Kiel Canal and the harbor of Kiel can be measured.

In 2020, the new BSH research vessel "Atair" will also be equipped with a measurement station to be able to perform compliance monitoring in the open North Sea and Baltic Sea. Prior to

that, a short term campaign in the German Baltic Sea was carried out on board a vessel of the German coast guard. These measurements are based on the experiences gained during the ship cruises of the MeSMarT projects.

Since the transition of the measurement station in Wedel to a permanent monitoring station operated by the BSH, the on-going measurements showed a decreasing number of FSC exceedances. Figure 3-2 shows the distribution of measured FSC and the fraction of probably non-compliant ships until 2019, provided by courtesy of the BSH. The pink trend line in the back-ground shows the clear reduction of exceedance measurements until a compliance rate of about 99% is reached in 2017.

The measurement stations in Bremerhaven and Kiel show a similar trend in the data. While Bremerhaven has a very low number of possible non-compliant cases from the beginning, the non-compliance rate in Kiel decrease significantly after the installation of the monitoring station. This trend was already visible in 2018. An explanation can be the improved acceptance of the FSC regulation and the awareness of the shipping industry of the monitoring stations and the increased possibility of an inspection.

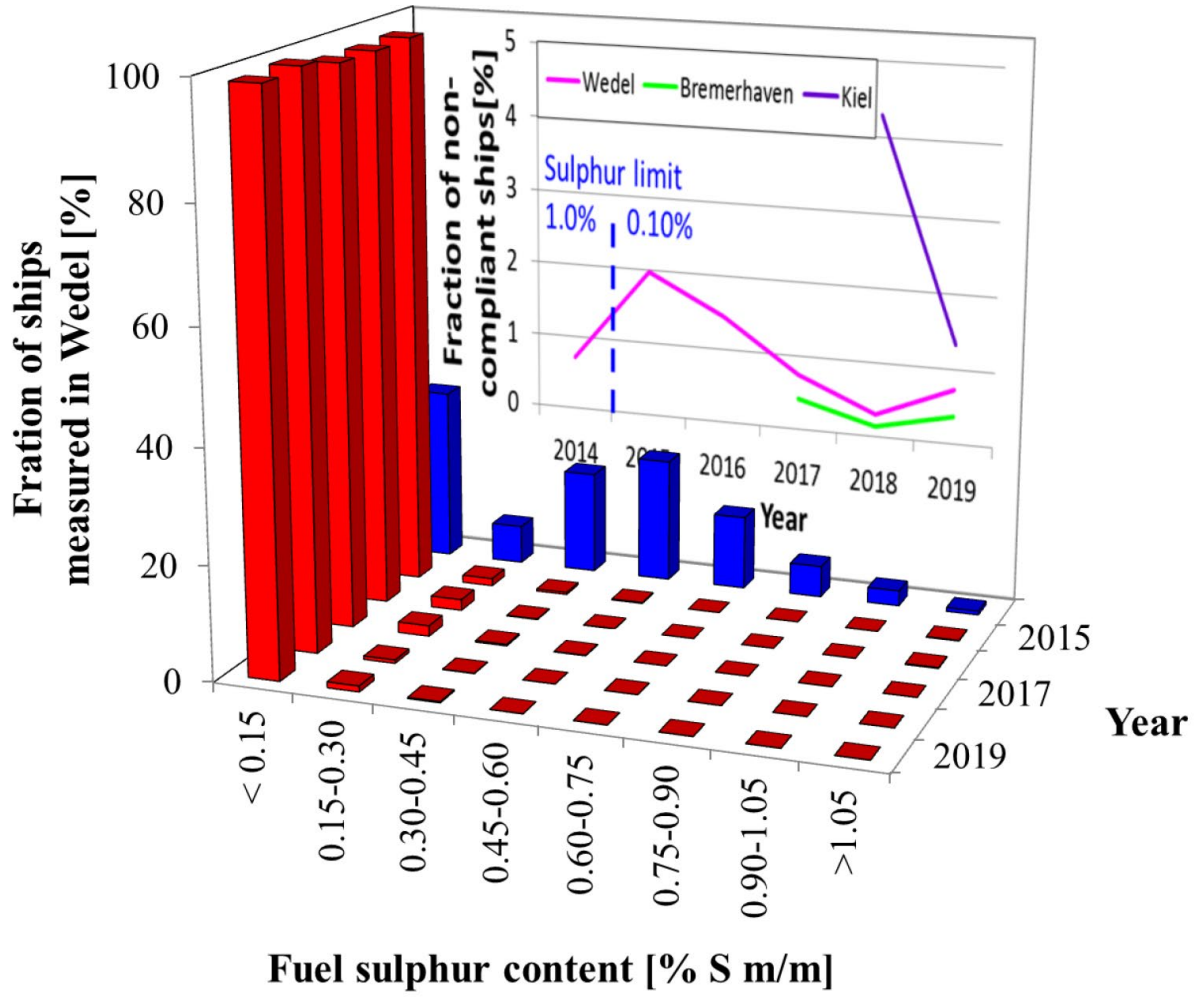

Figure 3-2: Distribution of calculated FSC and trends for all German permanent ship emission monitoring sites (by courtesy of A. Weigelt, BSH)

A similar trend has been observed and published in a report about compliance measurements in Gothenburg, Sweden, and on the Oresund Bridge, Denmark, (Mellqvist et al., 2017). Although the explanation in this report for the trend is an assumed technical effect of the measurement system, it could also be caused by the deterrence effect of remote compliance monitoring.

It can be concluded that the initial compliance with the MARPOL VI regulations was already high since the beginning. The last few percent of non-compliance can be prevented by establishing a more dense monitoring system in combination with a good cooperation with the executive authorities and distribute this information to the shipping industry. The high compliance rates enable modelling studies to correctly assess the reduction of SO_2 pollution in ECAs and provide a promising outlook on the implementation of future sulfur regulations as well as new regulation on NO_x emissions.

SITE ASSESSMENT

One important task within MeSMarT-II was the assessment of potential new monitoring sites in particular in the area of the Baltic Sea. These sites should fill the gap in the monitoring network of the BSH. Due to the prevailing wind direction in this region (Southwest) only locations east of main shipping lanes are of interest. Since authorities in other countries reported higher non-compliance rates for ships in the open sea, one idea was to find a monitoring location close to the Kadettrinne where the ship density is very high and all ships coming from or going to the Eastern part of the Baltic Sea including big harbors like Stockholm, Helsinki, Tallinn and St. Petersburg are passing.

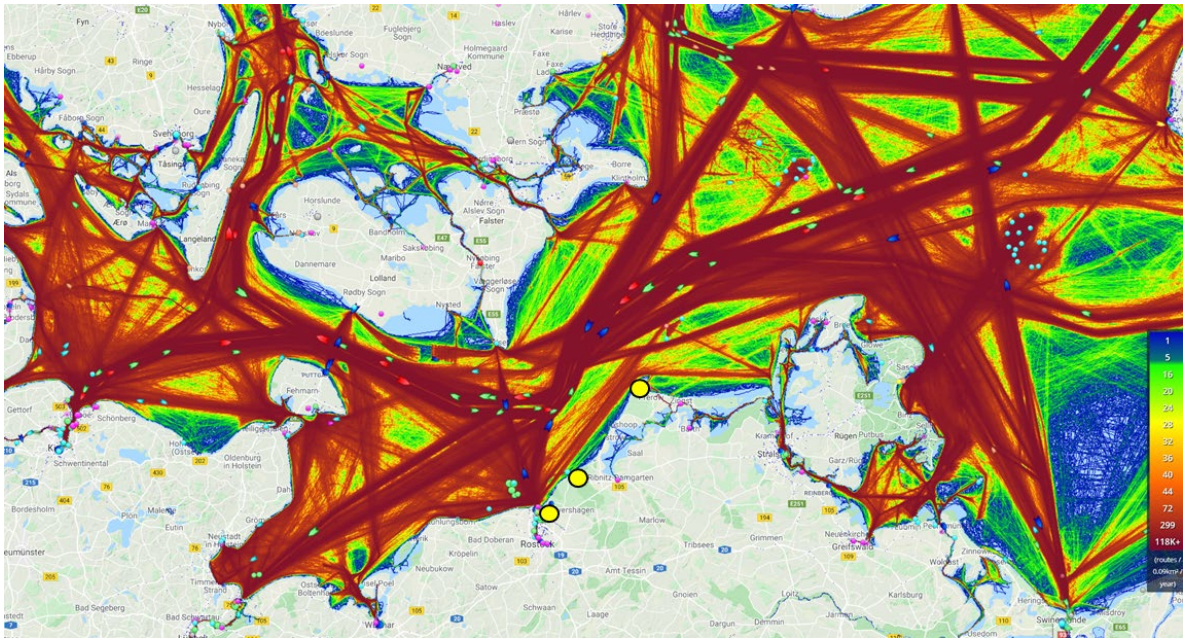

Figure 3-3: Ship density map taken from marinetraffic.com for the Baltic Sea covering the area from Kiel to Swinemünde (data from 2017). Sites, where test measurements have been carried out in June 2019, are indicated with yellow dots.

In June 2019 three sites at the coast of the Baltic Sea have been examined with the IUP Bremen mobile lab (see Figure 3-3 and 3-4). The truck is equipped with both, in situ and passive remote sensing techniques. High capacity batteries and an emergency generator enable measurements without external power for at least 24 hours.

Unfortunately for the sites Graal-Müritz and Darßer Ort only background values for both SO_2 (< 1 ppbv) and NO_2 (< 3 ppbv) were found, even meteorological conditions were quite favorable with wind blowing from Southwest with 3 to 5 m/s. According to recorded AIS data the distance to passing ships was about 18 km in case of Darßer Ort and 11 km in case of Graal-Müritz, causing a very high dilution of possible ship plumes. According to Seyler et al. (2019) the maximum horizontal effective path length for MAX-DOAS observations is 15 km in the UV and 25 km in the visible, with typical values around 9 and 13 km respectively. This means that only under very good viewing conditions measurements from shipping emissions at

Graal-Müritz and Darßer Ort are possible, which was not the case on these days. In summary, we cannot recommend the two sites for FSC monitoring. However, MAX-DOAS observations in particular at Darßer Ort could help to monitor the general impact of new regulations on future reduction of NO_x on background concentrations, similar to what was found in Neuwerk for sulfur (see e.g. the MeSMarT-I report and Seyler et al., 2017)

In contrast, the site Hohe Düne was found to be a useful location for the monitoring of ship emissions. Maximum values of about 10 ppb_v for SO_2 and 50 ppb_v for NO were measured in diluted ship plumes. In total 51 peaks of single ships could be analyzed, two of them possibly non-compliant (Figure 3-5).

Figure 3-4: Picture of the IUP Bremen mobile lab in Hohe Düne close to the harbor Warnemünde/Rostock.

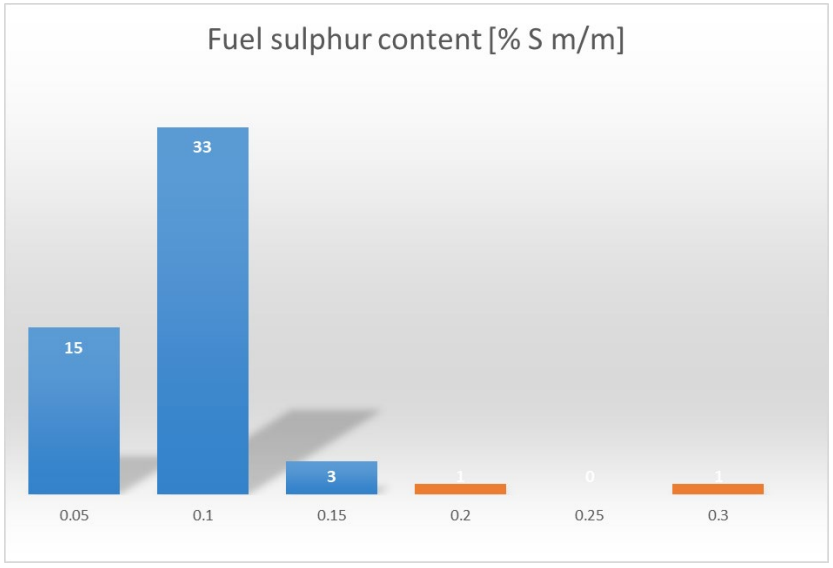

Figure 3-5: Distribution of FSC derived from ship plume measurements at the potential site Hohe Düne on June 19 to June 21.

SUMMARY AND OUTLOOK

WORK PACKAGE 1

- In July and August 2016 a measurement campaign (suitability study) has been carried out with an scientific open-path DOAS instrument from the IUP Heidelberg.
- In total more than 5000 peaks related to ship emissions were clearly identified, providing an enhanced monitoring coverage compared to in situ and passive remote sensing observations.
- Based on the experience of the campaign, a robust and easy to handle OP-DOAS system was developed and installed in November 2018.
- Absolute emission factors for SO_2 and NO_x have been derived, providing valuable input for air quality models.
- The lack of direct CO_2 measurements prevents the calculation of FSC with the OP-DOAS method. This should be solved with upcoming techniques using FTIR spectrometer.
- The OP-DOAS technique is a promising tool for monitoring ship emissions but it is limited to harbour or river areas.

WORK PACKAGE 2

- A trace-level SO_2 system has been implemented in the IUP Bremen mobile lab, providing an additional tool for the quality assurance of FSC monitoring.
- In preparation of future regulations, NO_x emission factors have been retrieved from in situ data. Currently (2019) less than 10% of the ships comply with Tier-III limits.
- SO_2/NO_2-ratios have been calculated from passive remote sensing (MAX-DOAS) data in Neuwerk and Wedel, showing a clear reduction after implementation of the new SECA limit in 2015. However, the ratio cannot be used for compliance monitoring of single ships.
- An onion-peeling MAX-DOAS approach has been developed to study horizontal inhomogeneities in the NO_2 distribution above shipping lanes.
- New satellite instruments (TROPOMI onboard S5p) with its much improved spatial resolution can detect additional shipping lanes and needs much less averaging than previous satellite data sets, resulting in impressive maps of ship emissions of NO_2 However, fundamental limitations such as the low temporal sampling (once per day), relatively low sensitivity towards pollution close to the surface and the large ground pixel size (3.5 x 5.5 km^2) limit the usability of satellite data for quantitative emission control.

WORK PACKAGE 3

- The FSC analysis, the identification, and notification of possible non-compliant ships has been automated.
- The setup of the monitoring site in Bremerhaven was supported and an assessment of potential new sites at the coast of the Baltic Sea was carried out. Hohe Düne was found to a very promising site for compliance monitoring.

In summary, the MeSMarT-II project has shown that remote sensing techniques can complement but not supersede in situ measurements. The passive remote sensing is due to its high sensitivity and robustness an ideal tool for observations of long-term trends as shown in Seyler et al., 2017 and for monitoring horizontal distributions of trace gases (Seyler et al., 2019). The open path DOAS technique impresses with its high monitoring coverage and again a very high sensitivity (Schmitt et al. and Krause et al., 2020). However, the lack of direct CO2 measurements prevents the direct calculation of the FSC and therefore compliance monitoring without any additional information. For the OP-DOAS this might be solved in the future by the means of observations in the infrared.

OUTREACH

POSTER PRESENTATIONS

Behrens, L.K., Hilboll, A., Richter, A., Peters, E., Alvarado, L. M. A., Hedegaard, A. B. K., Wittrock, F., Burrows, J.P., Vrekoussis, M., On the detection of African pollution outflow over the Atlantic Ocean using passive DOAS, *AGU 2018,* Washington, D.C., USA, December 2018

Behrens, L.K., Hilboll, A., Richter, A., Peters, E., Dörner, S., Burrows, J.P., Vrekoussis, M., Imaging DOAS NO_2 measurements during the AQABA ship campaign, *EGU General Assembly,* Vienna, Austria, April 2018

Seyler, A., Wittrock, F., Kattner, L., Mathieu-Üffing, B., Peters, E., Richter, A., Schmolke, S., Weigelt, A., Burrows, J.P., Monitoring shipping emissions in the German Bight using MAX-DOAS, *EGU General Assembly,* Vienna, Austria, April 2017

Behrens, L.K., Hilboll, A., Peters, E., Richter, A., Alvarado, L., Wittrock, F., Burrows, J.P., Vrekoussis, M., MAXDOAS measurements of atmospheric composition over the Atlantic Ocean, *EGU General Assembly,* Vienna, Austria, April 2017

Seyler, A., Wittrock, F., Kattner, L., Mathieu-Üffing, B., Peters, E., Richter, A., Schmolke, S., Burrrows, J.P., Monitoring shipping emissions in the German Bight using MAX-DOAS measurements, *DPG Spring Meeting, Bremen, Germany*, March 2017

Seyler, A., Wittrock, F., Kattner, L., Mathieu-Üffing, B., Peters, E., Richter, A., Schmolke, S., Weigelt, A., Burrows, J.P., Impact of sulfur content regulations of shipping fuel on coastal air quality, *EGU General Assembly, Vienna, Austria,* April 2016

TALKS

Wittrock, F., Schadstoffemissionen durch die Schifffahrt, 14. Master Class Course Conference "Renewable Energies" Noch zu klein - Die große Transformation, Eberswalde, Germany, Dezember 2019

Richter, A., Probing tropospheric composition with SCIAMACHY, SCIA4Future meeting, Bremen, Germany, December 2019

Wittrock, F., Messung von Schiffsemissionen in der marinen Troposphäre, 40. Duisburger Kolloquium Schiffstechnik/Meerestechnik, Duisburg, November 2019.

Krause, K., Comparative measurements for detection of ship emissions, EGU General Assembly, Vienna, Austria, April 2019

Krause, K., Comparative measurements of two Long Path-DOAS for detection of ship emissions, DPG Frühjahrstagung, München, Germany, March 2019

Krause, K., Integration of an active remote sensing system in the surveillance of traces gases in the maritime environment, Seminar on Physics and Chemistry of the Atmosphere, University of Bremen, Germany, December 7, 2018

Wittrock, F., Optische Fernerkundung von Schiffsemissionen, Nationales Forum für Fernerkundung und Copernicus, Berlin, Germany, November 29, 2018

Wittrock, F., New developments in the DOAS technique, SORBETTO summer school, July 4, Rome, Italy

Seyler, A., What can we learn about marine air pollution from MAX-DOAS measurements?, Seminar on Physics and Chemistry of the Atmosphere , University of Bremen, Germany, June 1, 2018

Wittrock, F., Measurements of Shipping emissions in the marine Troposphere, International Workshop on Emission Control Area Enforcement, Shenzhen, China, May 3, 2018

Seyler, A. et al., Monitoring air quality in North and Baltic Sea with ship-borne MAX-DOAS, DPG Frühjahrstagung, Erlangen, Germany, March 2018

Kattner, L. et al., Comprehensive study of NOx and SO2 from shipping emissions measured with on-shore in-situ instruments, DPG Spring Meeting, Bremen, Germany, March 2017

Seyler, A. et al., MAX-DOAS Measurements of Shipping Emissions, Air Quality Conference 2016, Milan, Italy, March 14 – 18, 2016

Kattner, L. et al., Monitoring Shipping Emission Regulations with In-situ Measurements, Air Quality Conference 2016, Milan, Italy, March 14 – 18, 2016

WEBSITE

www.mesmart.de

PEER-REVIEWED PUBLICATIONS

Seyler, A., Meier, A. C., Wittrock, F., Kattner, L., Mathieu-Üffing, B., Peters, E., Richter, A., Ruhtz, T., Schönhardt, A., Schmolke, S., and Burrows, J. P.: Studies of the horizontal inhomogeneities in NO2 concentrations above a shipping lane using ground-based multi-axis differential optical absorption spectroscopy (MAX-DOAS) measurements and validation with airborne imaging DOAS measurements, Atmos. Meas. Tech., 12, 5959–5977, https://doi.org/10.5194/amt-12-5959-2019, 2019.

Seyler, A., Wittrock, F., Kattner, L., Mathieu-Üffing, B., Peters, E., Richter, A., Schmolke, S., and Burrows, J. P.: Monitoring shipping emissions in the German Bight using MAX-DOAS measurements, Atmos. Chem. Phys., 17, 10997-11023, https://doi.org/10.5194/acp-17-10997-2017, 2017

PHD, BACHELOR AND MASTER THESIS

A. Seyler, Investigating air quality in the marine environment of the North and Baltic Sea with MAX-DOAS measurements – long term trends and new approaches, PhD thesis, University of Bremen, 2020

L. Kattner, Measurements of shipping emissions with in-situ instruments, PhD thesis, University of Bremen, December 2019

A.C. Meier, Measurements of horizontal trace gas distributions using airborne imaging differential optical absorption spectroscopy, PhD thesis, University of Bremen, February 2018

S. Ochtmann, Monitoring of the compliance with ship emission regulations for sulfur in Bremerhaven, Bachelor thesis, University of Bremen, April 2018

BIBLIOGRAPHY

Alföldy, B., Lööv, J. B., Lagler, F., Mellqvist, J., Berg, N., Beecken, J., Weststrate, H., Duyzer, J., Bencs, L., Horemans, B., Cavalli, F., Putaud, J. P., Janssens-Maenhout, G., Csordás, A. P., Van Grieken, R., Borowiak, A., and Hjorth, J. (2013). "Measurements of Air Pollution Emission Factors for Marine Transportation in SECA". In: Atmospheric Measurement Techniques 6.7, pp. 1777–1791. ISSN: 18671381. DOI: 10.5194/amt-6-1777-2013.

Andersson, K., Brynolf, S., Lindgren, F., and Wilewska-Bien, M. (2016). Shipping and the Environment: Improving Environmental Performance in Marine Transportation. Springer Berlin Heidelberg. ISBN: 978-3-662-49045-7. URL: https://books.google.de/books?id=XGqhCwAAQBAJ.

Arndt, E.-H. (2018). "Grünes Schiff Im Dienste Des Klimaschutzes". In: Tägliche Hafenbericht (THB - Deutsche Schiffahrts-Zeitung), p. 3. ISSN: 2190-8753.

Aulinger, A., Matthias, V., Zeretzke, M., Bieser, J., Quante, M., and Backes, A. (2016). "The Impact of Shipping Emissions on Air Pollution in the Greater North Sea Region – Part 1: Current Emissions and Concentrations". In: Atmospheric Chemistry and Physics 16.2, pp. 739–758. DOI: 10.5194/acp-16-739-2016. URL: http://www.atmos-chem-phys.net/16/739/2016/.

Azzara, A., Rutherford, D., and Wang, H. (2014). "Feasibility of IMO Annex VI Tier III Implementation Using Selective Catalytic Reduction". In: The International Council on Clean Transportation 4, pp. 1–9.

Balzani Lööv, J. M., Alfoldy, B., Gast, L. F. L., Hjorth, J., Lagler, F., Mellqvist, J., Beecken, J., Berg, N., Duyzer, J., Westrate, H., Swart, D. P. J., Berkhout, A. J. C., Jalkanen, J. P., Prata, A. J., Van Der Hoff, G. R., and Borowiak, A. (2014). "Field Test of Available Methods to Measure Remotely

SOx and NOx Emissions from Ships". In: Atmospheric Measurement Techniques 7.8, pp. 2597–2613. ISSN: 18678548. DOI: 10.5194/amt-7-2597-2014.

Beecken, J., Mellqvist, J., Salo, K., Ekholm, J., and Jalkanen, J. P. (2014). "Airborne Emission Measurements of SO2, NOx and Particles from Individual Ships Using a Sniffer Technique". In: Atmospheric Measurement Techniques 7.7, pp. 1957–1968. ISSN: 18678548. DOI: 10.5194/amt-7-1957-2014.

Beecken, J., Mellqvist, J., Salo, K., Ekholm, J., Jalkanen, J. P., Johansson, L., Litvinenko, V., Volodin, K., and Frank-Kamenetsky, D. A. (2015). "Emission Factors of SO2, NOx and Particles from Ships in Neva Bay from Ground-Based and Helicopter-Borne Measurements and AIS-Based Modeling". In: Atmospheric Chemistry and Physics 15.9, pp. 5229–5241. ISSN: 16807324. DOI: 10.5194/acp-15-5229-2015.

Berg, N., Mellqvist, J., Jalkanen, J. P., and Balzani, J. (2012). "Ship Emissions of SO 2 and NO 2: DOAS Measurements from Airborne Platforms". In: Atmospheric Measurement Techniques 5.5, pp. 1085–1098. ISSN: 18671381. DOI: 10.5194/amt-5-1085-2012.

Bovensmann, H., Burrows, J. P., Buchwitz, M., Frerick, J., Noël, S., Rozanov, V. V., Chance, K. V., and Goede, A. P. H. (1999). "SCIAMACHY: Mission Objectives and Measurement Modes". In: Journal of the Atmospheric Sciences 56, pp. 127–150.

Burrows, J. P., Hölzle, E., Goede, A. P. H., Visser, H., and Fricke, W. (1995). "SCIAMACHY - Scanning Imaging Absorption Spectrometer for Atmospheric Chartography". In: Acta Astronautica 35, pp. 445–451.

Burrows, J. P., Weber, M., Buchwitz, M., Rozanov, V., Ladstatter-Weissenmayer, A., Richter, A., DeBeek, R., Hoogen, R., Bramstedt, K., Eichmann, K. U., and Eisinger, M. (1999). "The Global Ozone Monitoring Experiment (GOME): Mission Concept and First Scientific Results". In: Journal of the Atmospheric Sciences 56.2, pp. 151–175.

Burrows, J. P., Platt, U., and Borrell, P. (2011). The Remote Sensing of Tropospheric Composition from Space. Physics of Earth and Space Environments. Berlin ; Heidelberg [u.a.]: Springer. XXXII, 549 S. ISBN: 978-3-642-14790-6 978-3-642-14791-3.

C˘ampara, L., Hasanspahi´c, N., and Vuji˘ci´c, S. (2018). "Overview of MARPOL ANNEX VI Regulations for Prevention of Air Pollution from Marine Diesel Engines". In: SHS Web of Conferences 58. Ed. by Notteboom, T., Peeters, C., Maria Gregorio Pina Calado, H., and Czermánski, E., p. 01004. ISSN: 2261-2424. DOI: 10.1051/shsconf/20185801004. URL: https://www.shs-conferences.org/ 10.1051/shsconf/20185801004 (visited on 06/09/2020).

Chen, G., Huey, L. G., Trainer, M., Nicks, D., Corbett, J., Ryerson, T., Parrish, D., Neuman, J. A., Nowak, J., Tanner, D., Holloway, J., Brock, C., Crawford, J., Olson, J. R., Sullivan, A., Weber, R., Schauffler, S., Donnelly, S., Atlas, E., Roberts, J., Flocke, F., Hübler, G., and Fehsenfeld, F. (2005). "An Investigation of the Chemistry of Ship Emission Plumes during ITCT 2002". In: Journal of Geophysical Research D: Atmospheres 110.10, pp. 1–15. ISSN: 01480227. DOI: 10.1029/2004JD005236.

Cheng, Y., Wang, S., Zhu, J., Guo, Y., Zhang, R., Liu, Y., Zhang, Y., Yu, Q., Ma, W., and Zhou, B. (2019). "Surveillance of SO₂ and NO₂ from Ship Emissions by MAX-DOAS Measurements and the Implications Regarding Fuel Sulfur Content Compliance". In: Atmospheric Chemistry and Physics 19.21, pp. 13611–13626. ISSN: 1680-7324. DOI: 10.5194/acp- 19- 13611- 2019. URL: https://www.atmos- chem- phys.net/19/13611/ 2019/ (visited on 06/11/2020).

Chu Van, T., Ramirez, J., Rainey, T., Ristovski, Z., and Brown, R. (2019). "Global Impacts of Recent IMO Regulations on Marine Fuel Oil Refining Processes and Ship Emissions". In: Transportation Research Part D Transport and Environment 70, pp. 123–134. DOI: 10.1016/j.trd.2019.04.001.

Corbett, J. J. and Koehler, H. W. (2003). "Updated Emissions from Ocean Shipping". In: J. Geophys. Res. 108, p. 9. ISSN: 0148-0227. DOI: 10.1029/2003JD003751.

Corbett, J. J., Fischbeck, P. S., and Pandis, S. N. (1999). "Global Nitrogen and Sulfur Inventories for Oceangoing Ships". In: Journal of Geophysical Research 104.D3, pp. 3457–3470. ISSN: 0148-0227. DOI: 10.1029/1998JD100040.

Corbett, J. J., Winebrake, J. J., Green, E. H., Kasibhatla, P., Eyring, V., and Lauer, A. (2007). "Mortality from Ship Emissions: A Global Assessment". In: Environmental Science and Technology 41.24, pp. 8512–8518. ISSN: 0013936X. DOI: 10.1021/es071686z. pmid: 18200887.

Diesch, J. M., Drewnick, F., Klimach, T., and Borrmann, S. (2013). "Investigation of Gaseous and Particulate Emissions from Various Marine Vessel Types Measured on the Banks of the Elbe in Northern Germany". In: Atmospheric Chemistry and Physics 13.7, pp. 3603–3618. ISSN: 16807316. DOI: 10.5194/acp-13-3603-2013.

Endresen, Ø., Sørgard, E., Sundet, J., Dalsøren, S., Isaksen, I., and Berglen, T. (2003). "Emission from International Sea Transportation and Environmental Impact". In: Journal of Geophysical Research 108.D17, pp. 1–22. ISSN: 0148-0227. DOI: 10.1029/2002JD002898.

EU (2005). "Directive 2005/33/EC of the European Parliament and of the Council". In: Official Journal of the European Union 1882, pp. 59–69. DOI: 10.3000/17252555.L_2009.140.eng. URL: http://eur-lex.europa.eu/LexUriServ/LexUriServ.do?uri=OJ:L:2005:191:0059:0069: EN:PDF.

Eyring, V., Bovensmann, H., Cionni, I., Dall'Amico, M., Franke, K., Khlystova, I., Klinger, C., Lauer, A., Paxian, A., Righi, M., and Schreier, M. (2010a). Impact of Ship Emissions on Atmosphere and Climate, SeaKLIM Final Report. DLR, p. 23. URL: http://www.pa.op.dlr.de/SeaKLIM/SeaKLIM%5C%7B_%5C%7DNachwuchsgruppe%5C%7B_%5C%7DSchlussbericht%5C%7B_%5C%7DFINAL.pdf.

Eyring, V., Köhler, H. W., Lauer, A., and Lemper, B. (2005a). "Emissions from International Shipping: 2. Impact of Future Technologies on Scenarios until 2050". In: Journal of Geophysical Research 110.D17, p. D17306. ISSN: 0148-0227. DOI: 10.1029/2004JD005620. URL: http://doi.wiley. com/10.1029/2004JD005620.

Eyring, V., Köhler, H. W., van Aardenne, J., and Lauer, A. (2005b). "Emissions from International Shipping: 1. The Last 50 Years". In: Journal of Geophysical Research 110.D17, p. D17305. ISSN: 0148-0227. DOI: 10 . 1029 / 2004JD005619. URL: http:// doi. wiley . com / 10 . 1029 / 2004JD005619.

Eyring, V., Isaksen, I. S., Berntsen, T., Collins, W. J., Corbett, J. J., Endresen, O., Grainger, R. G., Moldanova, J., Schlager, H., and Stevenson, D. S. (2010b). "Transport Impacts on Atmosphere and Climate: Shipping". In: Atmospheric Environment 44.37, pp. 4735–4771. ISSN: 13522310. DOI: 10.1016/j.atmosenv.2009.04.059. URL: http://linkinghub.elsevier.com/retrieve/pii/S1352231009003379.

Hönninger, G., von Friedeburg, C., and Platt, U. (2004). "Multi Axis Differential Optical Absorption Spectroscopy (MAX-DOAS)". In: Atmos. Chem. Phys. 4, pp. 231–254.

IMO (2008a). Resolution MEPC.176(58) - Amendments to the Annex of the Protocol of 1997 to Amend the International Convention for the Prevention of Pollution from Ships, 1973, As Modified By the Protocol of 1978 Relating Thereto (Revised MARPOL Annex VI). International Maritime Organi- sation (IMO). URL: http://www.imo.org/en/OurWork/Environment/PollutionPrevention/AirPollution/Documents/176%2858%29.pdf (visited on 06/09/2020).

IMO (2008b). Resolution MEPC.177(58) - Amendments to the Technical Code on Control of Emis- sion of Nitrogen Oxides from Marine Diesel Engines (NOx Technical Code 2008). International Maritime Organisation (IMO). URL: http : / / www . imo . org / en / OurWork / Environment / PollutionPrevention/AirPollution/Documents/177%2858%29.pdf (visited on 06/09/2020).

IMO (2009). Revised MARPOL Annex VI: Regulations for the Prevention of Air Pollution from Ships and NOx Technical Code 2008. 2nd ed. London: International Maritime Organization. 212 pp. ISBN: 978-92-801-4243-3.

IMO (2013). MARPOL: Annex VI and NTC 2008 with Guidelines for Implementation. International Maritime Organisation (IMO). ISBN: 978-92-801-1560-4. URL: https://books.google.de/books?id=G-tVmwEACAAJ.

IMO (2015). Resolution A.1106(29) - Revised Guidelines for the Onboard Operational Use of Shipborne Automatic Identification Systems (AIS). SN / Circ . 227. London: International Maritime Organisa- tion (IMO), p. 19. URL: http://www.imo.org/en/KnowledgeCentre/IndexofIMOResolutions/Assembly/Documents/A.1106%2829%29.pdf (visited on 06/27/2020).

IMO (2017). Resolution MEPC.286(71) - Amendments to MARPOL Annex VI (Designation of the Baltic Sea and the North Sea Emission Control Areas forNOXTierIII Control)(Information to Be Included in the Bunker Delivery Note). International Maritime Organisation (IMO). URL: http://www.imo.org/en/OurWork/Environment/PollutionPrevention/AirPollution/Documents/Res_MEPC_286%2871%29_Tier%20III%20ECA%20and%20BDN.pdf (visited on 06/09/2020).

IMO (2018). Resolution MEPC.305(73) - Amendments to MARPOL Annex VI (Prohibition on the Carriage of Non-Compliant Fuel Oil for Combustion Purposes for Propulsion or Operation on Board a Ship). International Maritime Organisation (IMO). URL: http://www.imo.org/en/OurWork/Environment/PollutionPrevention/AirPollution/Documents/Air%20pollution/MEPC.305%2873%29.pdf (visited on 06/09/2020).

IMO (2020). Emission Control Areas (ECAs) Designated under MARPOL Annex VI. URL: http://www.imo.org/en/OurWork/Environment/PollutionPrevention/AirPollution/Pages/Emission-Control- Areas-(ECAs)- designated- under- regulation- 13- of- MARPOL- Annex- VI-(NOx-emission-control).aspx (visited on 06/09/2020).

International Air Transport Association (IATA) (2015). "IATA Annual Review 2015". In: p. 62. URL:http://www.iata.org/about/Documents/iata-annual-review-2015.pdf.

IPCC (2013). Climate Change 2013: The Physical Science Basis. Contribution of Working Group I to the Fifth Assessment Report of the Intergovernmental Panel on Climate Change. Cambridge, United Kingdom and New York, NY, USA: Cambridge University Press, p. 1535. ISBN: ISBN 978-1-107-66182-0. DOI: 10.1017/CBO9781107415324. URL: www.climatechange2013.org.

Johansson, L., Jalkanen, J.-P., and Kukkonen, J. (2017). "Global Assessment of Shipping Emissions in 2015 on a High Spatial and Temporal Resolution". In: Atmospheric Environment 167, pp. 403– 415. ISSN: 13522310. DOI: 10.1016/j.atmosenv.2017.08.042. URL: https://linkinghub.elsevier.com/retrieve/pii/S1352231017305563 (visited on 06/11/2020).

Kattner, L., Mathieu-Üffing, B., Burrows, J. P., Richter, A., Schmolke, S., Seyler, A., and Wittrock, F. (2015). "Monitoring Compliance with Sulfur Content Regulations of Shipping Fuel by in Situ Measurements of Ship Emissions". In: Atmospheric Chemistry and Physics 15.17, pp. 10087–10092. ISSN: 1680-7324. DOI: 10.5194/acp-15-10087-2015. URL: http://www.atmos-chem-phys.net/15/10087/2015/.

Lack, D. A., Cappa, C. D., Langridge, J., Bahreini, R., Buffaloe, G., Brock, C., Cerully, K., Coffman, D., Hayden, K., Holloway, J., Lerner, B., Massoli, P., Li, S. M., McLaren, R., Middlebrook, A. M., Moore, R., Nenes, A., Nuaaman, I., Onasch, T. B., Peischl, J., Perring, A., Quinn, P. K., Ryerson, T., Schwartz, J. P., Spackman, R., Wofsy, S. C., Worsnop, D., Xiang, B., and Williams, E. (2011). "Impact of Fuel Quality Regulation and Speed Reductions on Shipping Emissions: Implications for Climate and Air Quality". In: Environmental Science and Technology 45.20, pp. 9052–9060. ISSN: 0013936X. DOI: 10.1021/es2013424. pmid: 21910443.

Lange, B. (2014). Auswirkungen von Abgasnachbehandlungsanlagen (Scrubbern) Auf Die Umweltsituation in Häfen Und Küstengewässern. 83/2014. Dessau-Roßlau: Umweltbundesamt (UBA), p. 94.

Lauer, A., Eyring, V., Hendricks, J., Jöckel, P., and Lohmann, U. (2007). "Global Model Simulations of the Impact of Ocean-Going Ships on Aerosols, Clouds, and the Radiation Budget". In: Atmospheric Chemistry and Physics 7.19, pp. 5061–5079. DOI: 10.5194/acp- 7-5061- 2007. URL: https://www.atmos-chem-phys.net/7/5061/2007/.

Lawrence, M. G. and Crutzen, P. J. (1999). "Influence of NOx Emissions from Ships on Tropospheric Photochemistry and Climate". In: Nature 402.6758, pp. 167–170. ISSN: 0028-0836. DOI: 10. 1038/46013.

Liu, F., Beirle, S., Zhang, Q., Dörner, S., He, K., and Wagner, T. (2016). "NO x Lifetimes and Emissions of Cities and Power Plants in Polluted Background Estimated by Satellite Observations". In: Atmospheric Chemistry and Physics 16.8, pp. 5283–5298. ISSN: 1680-7324. DOI: 10.5194/acp- 16 - 5283 - 2016. URL: https:// www . atmos - chem - phys . net/ 16 / 5283 / 2016/ (visited on 05/01/2020).

Masieri, S., Premuda, M., Bortoli, D., Kostadinov, I., Petritoli, A., Ravegnani, F., and Giovanelli, G. (2009). "Cruise Ships Flow Rate Emission Evaluated by Means of a Passive DOAS Instrument". In: SPIE Europe Remote Sensing 7478, 74781S—74781S—10. DOI: 10.1117/12.830309. URL: http://dx.doi.org/10.1117/12.830309.

Matthias, V., Aulinger, A., Backes, A., Bieser, J., Geyer, B., Quante, M., and Zeretzke, M. (2016). "The Impact of Shipping Emissions on Air Pollution in the Greater North Sea Region-Part 2: Scenarios for 2030". In: Atmospheric Chemistry and Physics 16.2, pp. 759–776. ISSN: 16807324. DOI: 10.5194/acp-16-759-2016. pmid: 26160423.

Meier, A. C. (2018). "Measurements of Horizontal Trace Gas Distributions Using Airborne Imaging Differential Optical Absorption Spectroscopy". phd thesis. Bremen: University of Bremen.

Meier, A. C., Schönhardt, A., Bösch, T., Richter, A., Seyler, A., Ruhtz, T., Constantin, D. E., Shaiganfar, R., Wagner, T., Merlaud, A., Van Roozendael, M., Belegante, L., Nicolae, D., Georgescu, L., and Philip Burrows, J. (2017). "High-Resolution Airborne Imaging DOAS Measurements of NO2 above Bucharest during AROMAT". In: Atmospheric Measurement Techniques 10.5, pp. 1831–1857. ISSN: 18678548. DOI: 10.5194/amt-10-1831-2017.

Moldanova, J., Fridell, E., Popovicheva, O., Demirdjian, B., Tishkova, V., Faccinetto, A., and Focsa, C. (2009). "Characterisation of Particulate Matter and Gaseous Emissions from a Large Ship Diesel Engine". In: Atmospheric Environment 43, pp. 2632–2641. DOI: 10.1016/j.atmosenv.2009.02. 008.

ISBN: 978-0-19-103075-8. URL: https://books.google.de/books?id=XTBdDgAAQBAJ.

Peters, E. (2013). "Improved MAX-DOAS Measurements and Retrievals Focused on the Marine Boundary Layer". Ph.D. thesis, University of Bremen. University of Bremen.

Platt, U. and Stutz, J. (2008). Differential Optical Absorption Spectroscopy. Physics of Earth and Space Environments. Berlin ; Heidelberg: Springer. XV, 597 S. ISBN: 3-540-21193-4 978-3-540-21193-8 978-3-540-75776-4.

Prata, A. J. (2014). "Measuring SO2 Ship Emissions with an Ultraviolet Imaging Camera". In: Atmospheric Measurement Techniques 7.5, pp. 1213–1229. ISSN: 18678548. DOI: 10.5194/amt-7-1213-2014.

Premuda, M., Masieri, S., Bortoli, D., Kostadinov, I., Petritoli, A., and Giovanelli, G. (2011). "Evaluation of Vessel Emissions in a Lagoon Area with Ground Based Multi Axis DOAS Measurements". In: Atmospheric Environment 45.29, pp. 5212–5219. ISSN: 13522310. DOI: 10.1016/j.atmosenv. 2011.05.067. URL: http://dx.doi.org/10.1016/j.atmosenv.2011.05.067.

Richter, A., Eyring, V., Burrows, J. P., Bovensmann, H., Lauer, A., Sierk, B., and Crutzen, P. J. (2004). "Satellite Measurements of NO2 from International Shipping Emissions". In: Geophys. Res. Lett. 31, p. L23110. ISSN: 0094-8276. DOI: 10.1029/2004GL020822.

Rozanov, V. V., Rozanov, A. V., Kokhanovsky, A. A., and Burrows, J. P. (2014). "Radiative Transfer through Terrestrial Atmosphere and Ocean: Software Package SCIATRAN". In: Journal of Quan- titative Spectroscopy and Radiative Transfer 133, pp. 13–71. ISSN: 00224073. DOI: 10.1016/j. jqsrt.2013.07.004. URL: http://dx.doi.org/10.1016/j.jqsrt.2013.07.004.

Schönhardt, A., Altube, P., Gerilowski, K., Krautwurst, S., Hartmann, J., Meier, A. C., Richter, A., and Burrows, J. P. (2015). "A Wide Field-of-View Imaging DOAS Instrument for Two-Dimensional Trace Gas Mapping from Aircraft". In: Atmospheric Measurement Techniques 8.12, pp. 5113–5131. ISSN: 1867-8548. DOI: 10.5194/amt- 8- 5113- 2015. URL: https://www.atmos- meas-tech.net/8/5113/2015/ (visited on 05/12/2020).

Seyler, A. (2014). "Retrieval of Shipping Emissions from MAX-DOAS Measurements – Ableitung von Schiffsemissionen Aus MAX-DOAS-Messungen". Master thesis. Bremen, Germany: University of Bremen. 107 pp.

Seyler, A., Meier, A. C., Wittrock, F., Kattner, L., Mathieu-Üffing, B., Peters, E., Richter, A., Ruhtz, T., Schönhardt, A., Schmolke, S., and Burrows, J. P. (2019). "Studies of the Horizontal In-homogeneities in NO_2 Concentrations above a Shipping Lane Using Ground-Based Multi-Axis Differential Optical Absorption Spectroscopy (MAX-DOAS) Measure-ments and Validation with Airborne Imaging DOAS Measurements". In: Atmospheric Measurement Techniques 12.11, pp. 5959–5977. ISSN: 1867-8548. DOI: 10.5194/amt- 12- 5959- 2019. URL: https://www.atmos-meas-tech.net/12/5959/2019/ (visited on 11/19/2019).

Seyler, A., Wittrock, F., Kattner, L., Mathieu-Üffing, B., Peters, E., Richter, A., Schmolke, S., and Burrows, J. P. (2017). "Monitoring Shipping Emissions in the German Bight Using MAX-DOAS Measurements". In: Atmospheric Chemistry and Physics 17.18, pp. 10997–11023. ISSN: 16807324. DOI: 10.5194/acp-17-10997-2017.

Stenersen, D. and Thonstad, O. (2017). GHG and NOx Emissions from Gas Fuelled Engines. OC2017 F-108. Trondheim: SINTEF Ocean AS, p. 52.

UNCTAD (2018a). 50 Years of Review of Maritime Transport, 1968–2018. New York; Geneva: United Nations. 97 pp. URL: https://unctad.org/en/PublicationsLibrary/dtl2018d1_ en.pdf (visited on 06/11/2020).

UNCTAD (2018b). Review of Maritime Transport 2018. Review of Maritime Transport. New York; Geneva: United Nations. ISBN: 978-92-1-112928-1. URL: https://unctad.org/en/PublicationsLibrary/ rmt2018_en.pdf (visited on 06/11/2020).

UNCTAD (2019). Review of Maritime Transport 2019. Review of Maritime Transport. New York; Geneva: United Nations. ISBN: 978-92-1-112958-8. URL: https://unctad.org/en/PublicationsLibrary/ rmt2019_en.pdf (visited on 06/11/2020).

Van Roy, W. (2016). "Best Practices Airborne MARPOL Annex VI Monitoring". In: URL: https:// www. trafi.fi/filebank/a/1482762219 / d80cdd7de80e58885ce5a4dd0af86c02 / 23541 - Best%5C%7B_%5C%7DPractices%5C%7B_%5C%7DAirborne%5C%7B_%5C%7DMARPOL%5C%7B_ %5C% 7DAnnex%5C%7B_%5C%7DVI%5C%7B_%5C%7DMonitoring.pdf.

Veefkind, J. P., Aben, I., McMullan, K., Förster, H., de Vries, J., Otter, G., Claas, J., Eskes, H. J., de Haan, J. F., Kleipool, Q., van Weele, M., Hasekamp, O., Hoogeveen, R., Landgraf, J., Snel, R., Tol, P., Ingmann, P., Voors, R., Kruizinga, B., Vink, R., Visser, H., and Levelt, P. F. (2012). "TROPOMI on the ESA Sentinel-5 Precursor: A GMES Mission for Global Observations of the Atmospheric Composition for Climate, Air Quality and Ozone Layer Applications". In: Remote Sensing of Environment 120.2012, pp. 70–83. ISSN: 00344257. DOI: 10.1016/j.rse.2011.09.027. URL:http://dx.doi.org/10.1016/j.rse.2011.09.027.

Vinken, G. C. M., Boersma, K. F., van Donkelaar, A., and Zhang, L. (2014). "Constraints on Ship NOx Emissions in Europe Using GEOS-Chem and OMI Satellite NO2 Observations". In: Atmospheric Chemistry and Physics 14.3, pp. 1353–1369. ISSN: 1680-7324. DOI: 10.5194/acp-14-1353-2014. URL: http://www.atmos-chem-phys.net/14/1353/2014/acp-14-1353-2014.html.

Wan, Z., Zhou, X., Zhang, Q., and Chen, J. (2019). "Do Ship Emission Control Areas in China Reduce Sulfur Dioxide Concentrations in Local Air? A Study on Causal Effect Using the Difference-in- Difference Model". In: Marine Pollution Bulletin 149. DOI: 10.1016/j.marpolbul.2019.110506.

Wan, Z., Zhu, M., Chen, S., and Sperling, D. (2016). "Pollution: Three Steps to a Green Shipping Industry". In: Nature 530, pp. 275–277. DOI: 10.1038/530275a.

Wang, Y., Li, A., Xie, P. H., Wagner, T., Chen, H., Liu, W. Q., and Liu, J. G. (2014). "A Rapid Method to Derive Horizontal Distributions of Trace Gases and Aerosols near the Surface Using Multi-Axis Differential Optical Absorption Spectroscopy". In: Atmospheric Measurement Techniques 7.6, pp. 1663–1680. ISSN: 18678548. DOI: 10.5194/amt-7-1663-2014.

Winebrake, J. J., Corbett, J. J., Green, E. H., Lauer, A., and Eyring, V. (2009). "Mitigating the Health Impacts of Pollution from Oceangoing Shipping: An Assessment of Low-Sulfur Fuel Mandates". In: Environmental Science and Technology 43.13, pp. 4776–4782. ISSN: 0013936X. DOI: 10.1021/es803224q. pmid: 19673264.

Winnes, H. and Fridell, E. (2009). "Particle Emissions from Ships: Dependence on Fuel Type". In: Journal of the Air & Waste Management Association 59.12, pp. 1391–1398. ISSN: 1096-2247, 2162-2906. DOI: 10.3155/1047-3289.59.12.1391. URL: https://www.tandfonline.com/doi/ full/10.3155/1047-3289.59.12.1391 (visited on 06/11/2020).

Winnes, H. and Fridell, E. (2010). "Emissions of NOX and Particles from Manoeuvring Ships". In: Transportation Research Part D: Transport and Environment 15.4, pp. 204–211. ISSN: 13619209. DOI: 10.1016/j.trd.2010.02.003. URL: http://dx.doi.org/10.1016/j.trd.2010.02.003.

Wittrock, F., Oetjen, H., Richter, A., Fietkau, S., Medeke, T., Rozanov, A., and Burrows, J. P. (2004). "MAX-DOAS Measurements of Atmospheric Trace Gases in Ny-Ålesund - Radiative Transfer Studies and Their Application". In: Atmos. Chem. Phys. 4, pp. 955–966.

Wittrock, F. (2006). "The Retrieval of Oxygenated Volatile Organic Compounds by Remote Sensing Techniques". Phd thesis. Bremen, Germany: University of Bremen. URL: http://www.iup.uni- bremen.de/doas/paper/diss_wittrock_06.pdf (visited on 05/12/2020).

Yang, M., Bell, T. G., Hopkins, F. E., and Smyth, T. J. (2016). "Attribution of Atmospheric Sulfur Diox- ide over the English Channel to Dimethyl Sulfide and Changing Ship Emissions". In: Atmospheric Chemistry and Physics 16.8, pp. 4771–4783. ISSN: 1680-7324. DOI: 10.5194/acp-16-4771-2016. URL: https://www.atmos-chem-phys.net/16/4771/2016/ (visited on 06/09/2020).

Zhang, F., Chen, Y., Tian, C., Lou, D., Li, J., Zhang, G., and Matthias, V. (2016). "Emission Factors for Gaseous and Particulate Pollutants from Offshore Diesel Engine Vessels in China". In: Atmospheric Chemistry and Physics 16.10, pp. 6319–6334. ISSN: 16807324. DOI: 10.5194/acp-16-6319-2016.

ACKNOWLEDGMENTS

This work was supported by the research group of John P. Burrows at the Institute of Environmental Physics.

The project MeSmarT-II thanks following institutions and persons for providing technical and logistical support:

- WSA Hamburg, Bauhof Wedel
- WSA Cuxhaven (Radar tower Neuwerk)
- HPA (Hamburg Port Authority: Transport with MS Nigewark, support and accommodation at Neuwerk; weather data)
- IHU Hamburg (Institut für Hygiene und Umwelt: calibration measurements, instrumental support and consulting; weather data)

ACRONYMS AND ABBREVIATIONS

AirMAP	Airborne imaging DOAS instrument for Measurements of Atmospheric Pollution
AIS	Automatic Information System (automatic tracking system for ships)
BSH	Bundesamt für Seeschifffahrt und Hydrographie, Federal Maritime and Hydrographic Agency, Germany
CCD	charge coupled device
DOAS	Differential Optical Absorption Spectroscopy
ECA	Emission Control Area
FOV	field of view
HPA	Hamburg Port Authority, Germany
iDOAS	imaging DOAS
IMO	International Maritime Organisation
IUP Bremen	Institute of Environmental Physics, University of Bremen, Bremen, Germany
IUP Heidelbg.	Institute of Environmental Physics, University of Heidelberg, Heidelberg, Germany
LOS	Line of Sight (during spectroscopic measurement)
LP-DOAS	Long-Path DOAS – active remote sensing system (similar to OP-DOAS)
MAX-DOAS	Multi-Axis DOAS
MeSmarT	Measurements of shipping emissions in the marine troposphere
MARPOL	International Convention for the Prevention of Marine Pollution from Ships (1973)
MLH	mixing layer height (MLH)
NECA	Nitrogen Emission Control Area
NME	normalized mean error
NO_x	Nitrogen Oxides (NO and NO_2)
N_{ox}	Oxidised Nitrogen compounds (NO, NO_2, NO_3, N_2O_5, HNO_3, and particle bound Nitrate)
NO_3^-	Nitrate

OP-DOAS	Long-Path DOAS – active remote sensing system (similar to LP-DOAS)
OSPAR	Oslo and Paris Convention for the Protection of the Marine Environment of the North-East Atlantic (1992)
SCD	Slant Column Densities (integrated number density of a trace gas along the light path)
SECA	Sulfur Emission Control Area
SFC	Sulfur fuel content
SZA	Solar zenith angle
VC, VCD	tropospheric vertical column density
VMR	Volume mixing ratio (volume ratio of trace gas to air)
WSA	Water and Shipping Authority, Germany